Controller Design of a Swift-shift Multi-speed Transmission for Electric Vehicles

Mehdi Roozegar

A Thesis Submitted in Partial Fulfillment of the Requirements for the
Degree of Doctor of Philosophy
in
Mechanical Engineering
McGill University, Montreal, Canada

August 2018

This thesis is dedicated to my family for their endless love, support and encouragement throughout my life.

Abstract

Internal-combustion-engine vehicles (ICEVs) entail various problems, first and foremost, pollution. Due to a much lower impact on the environment, electric vehicles (EVs) appear as proper substitutes for ICEVs. Nonetheless, EVs have failed to gain popularity because of an inherent problem, as the current energy-storage capacity of electric batteries is much lower than that of fossil fuels. Hence, the efficiency of EVs should be improved to make them viable. One step in this direction is the application of multi-speed transmissions (MSTs) in EVs. This way, the desired power is transmitted in more than one way, via several gear ratios included; therefore, by appropriate gear-shifting, a higher efficiency can be achieved. Compared to ICEVs, electric motors (EMs) are speed-controllable in an extensive range. Accordingly, it is not required to disconnect the motor from the transmission during gear-shifting. In fact, for a seamless gear-shifting in EVs, the drive torque supplied by the EM can be adopted as an autonomous control input. Since gear-shifting influences passenger comfort and vehicle drivability, the main objectives are smoothness, swiftness, and cancellation of output-torque interruption.

Firstly, the kinematics and dynamics models of the proposed MST designed for EVs, with the advantages of simplicity and modularity, are derived via a Lagrangian formulation. Next, the Kalman filter, the Luenberger observer and neural networks are used to estimate the unavailable states, the unknown arbitrary disturbance and the unknown clutch torque applied to the transmission. After defining the gear-shifting problem in the space of angular velocities, to guarantee velocity, acceleration and jerk continuity, the optimal trajectory for a swift and seamless shift is found based on variational calculus and polynomial blending functions.

From a control point of view, the formulation of the gear-shifting problem leads to an over-actuated system, i.e., the number of control inputs is greater than the number of states to be controlled. Furthermore, there are terminal constraints on both states and control inputs. Several control algorithms are proposed for this specific problem to satisfy all end control and state conditions,

while tracking the desired trajectory. The first algorithm, which includes two phases, approaching and coasting, is based on a genetic algorithm, a supervisory controller and PID gain-scheduling. In the second algorithm, one input is suggested to be changed independently, based on a 2-3 blending polynomial. Then, the new fully-actuated system is controlled using a linear quadratic integral controller, which is an extension of the linear quadratic regulator for tracking problems. Moreover, to find a continuous and smooth optimal control input, two different novel, non-standard optimal control problems are formulated, which allow us to apply soft or hard terminal constraints on the control input, both applicable to the gear-shifting problem in EVs. Lastly, to find the optimum trajectory, while satisfying both terminal control and state constraints, a control scheme is suggested based on Bellman's dynamic programming and the principle of optimality.

Résumé

Les véhicules à moteur à combustion interne (VMCI) posent divers problèmes, le principal étant la pollution. En raison d'un impact beaucoup plus faible sur l'environnement, les véhicules électriques (VE) s'avèrent être des substituts appropriés pour les VMCI. Néanmoins, les véhicules électriques n'ont pas réussi à gagner en popularité parce que la capacité actuelle de stockage d'énergie des batteries électriques est beaucoup plus faible que celle des combustibles fossiles. Par conséquent, il faut améliorer le rendement des VE pour les rendre viables. L'application de transmissions multi-vitesses (TMV) dans les véhicules électriques va dans cette direction. La puissance désirée est transmise de plusieurs manières, par des rapports de démultiplication portés, qui permettent d'améliorer l'efficacité grâce à un changement de vitesse approprié. La vitesse des moteurs électriques (ME) est réglable de diverses façons, contrairement à celles des VMCI; il n'est donc pas nécessaire de déconnecter le moteur de la transmission pendant le changement de vitesse. En fait, pour obtenir un changement de vitesse en douceur dans les véhicules électriques, le couple d'entraînement fourni par l'ME peut être adopté comme entrée de commande autonome. Puisque le changement de vitesse influe sur le confort des passagers et la maniabilité du véhicule, les principaux objectifs sont la fluidité, la rapidité et l'annulation de l'interruption du couple de sortie.

Les modèles cinématique et dynamique de la TMV proposée pour les véhicules électriques, avec les avantages de la simplicité et de la modularité, est obtenu d'une formulation Lagrangienne. Le filtre de Kalman, l'observateur de Luenberger et les réseaux neuronaux sont ensuite utilisés pour estimer les états non-mesurables, toute perturbation arbitraire inconnue et le couple d'embrayage inconnu appliqué à la transmission. Après avoir défini le problème du changement de vitesse dans l'espace des vitesses angulaires, afin de garantir la continuité de la vitesse, l'accélération et la suraccélération, la trajectoire optimale pour un déplacement rapide et continu se base sur le calcul variationnel et des fonctions polynomiales de transition.

En ce qui concerne la commande, la formulation du problème de changement de vitesse mène

à un système sur-actionné, c'est-à-dire que le nombre de signaux de commande est supérieur au nombre d'états à commander. De plus, il existe des contraintes terminales sur les états et les signaux de commande. L'auteur propose plusieurs algorithmes pour la synthèse de la commande pour ce problème spécifique afin de satisfaire toutes les conditions de commande et d'état, tout en suivant la trajectoire désirée. Le premier algorithme, qui comprend deux phases, en approche et en roue libre, se base sur un algorithme génétique, une commande de supervision et un réglage de type odométrique-intégral-tachymétrique. Dans le deuxième algorithme, l'auteur propose une excitation à modifier indépendamment, basée sur un polynôme de transition 2-3. Ensuite, le nouveau système entièrement actionné est commandé à l'aide d'une commande intégrale quadratique linéaire, soit une extension du régulateur quadratique linéaire pour les problèmes de suivi. De plus, pour trouver un signal de commande optimale continue et lisse, l'auteur formule deux nouveaux problèmes de commande optimale non standard, qui permettent d'appliquer des contraintes terminales souples ou dures sur les signaux de commande, applicables au problème de changement de vitesse dans les VE. Enfin, pour trouver la trajectoire optimale qui satisfait à la fois la commande terminale et les contraintes d'état, l'auteur propose un schéma de commande, basé sur la programmation dynamique de Bellman et le principe d'optimalité.

Contributions and Claims of Originality

This is a manuscript-based thesis consisting of seven journal papers, Chapters 2 to 8, which have been published in or submitted to the most appropriate journals in the field. The details of each paper, including the title, the journal, the authors, and the contributions of authors are given below. In all articles, Prof. J. Angeles supervised the entire procedure and guided the research, including presentation of the results and writing of the manuscripts.

- M. Roozegar, Y. D. Setiawan, and J. Angeles, "Design, modelling and estimation of a novel modular multi-speed transmission system for electric vehicles," *Mechatronics*, vol. 45, pp. 119–129, 2017.
  Mr. Y. D. Setiawan's participation was mainly on the experimental side. The main contributions include:
  - Development of the mathematical model of the proposed multi-speed transmission (MST) for electric vehicles (EVs) using a Lagrangian formulation.
  - Estimation of the unavailable states and loads applied to the transmission, based on the Kalman filter, the Luenberger observer and neural networks (NNs).
- M. Roozegar and J. Angeles, "The optimal gear-shifting for a multi-speed transmission system for electric vehicles," *Mechanism and Machine Theory*, vol. 116, pp. 1–13, 2017.
  The main contributions include:
  - Definition of the gear-shifting problem for a multi-stage planetary gear set in the space of angular velocities, based on the kinematic relations.
  - Synthesis of the optimum trajectory, including the schedules of the angular velocities, during gear-shifting for a swift, seamless operation using variational calculus and polynomial blending functions.

  - Synthesis of continuous angular velocity, acceleration and jerk, in the presence of limits on the power supply, besides the shifting time in determining the optimum trajectory among 2-3, 3-4-5 and 4-5-6-7 polynomials.

- M. Roozegar and J. Angeles, "A two-phase control algorithm for gear-shifting in a novel multi-speed transmission for electric vehicles," *Mechanical Systems and Signal Processing*, vol. 104, pp. 145–154, 2018.
  The main contributions include:

  - Establishment of a two-phase algorithm, with approaching and coasting phases, for gear-shifting in MSTs for EVs.
  - Design of various proportional-integral-derivative (PID) controllers for gear-shifting, based on trial-and-error and genetic algorithms (GAs), then selecting the proper PID gains by a supervisory controller, called PID gain-scheduling.

- M. Roozegar and J. Angeles, "Gear-shifting in a novel modular multi-speed transmission for electric vehicles using linear quadratic integral control," *Mechanism and Machine Theory*, vol. 128, pp. 359–367, 2018.
  The main contributions include:

  - Change of one of the inputs independently, based on a 2-3 blending polynomial, which, besides satisfying the input terminal constraints, guarantees the continuity of the velocity, acceleration and jerk at the ends of the gear-shifting interval.
  - Synthesis of a linear quadratic integral (LQI) controller, an extension of the linear quadratic regulator (LQR) for tracking problems, to control the new fully-actuated system.

- M. Roozegar, J. Angeles, and H. Michalska, "Optimal control with terminal control constraints and over-actuation," submitted.
  Prof. H. Michalska contributed to the formulation of the proposed scheme and to its presentation. The main contributions include:

  - Formulation of a non-standard optimal control problem to find the optimal control inputs for over-actuated systems, in the presence of control and state boundary conditions, applicable to gear-shifting in EVs.
  - Inclusion of a modified terminal penalty term, with terminal control input, within a novel Lagrange variational problem.
  - Allocation of control in an over-actuated linear quadratic tracking (LQT) problem for linear time-varying (LTV) systems.

- M. Roozegar and J. Angeles, "Optimal control of over-actuated systems applying smooth control inputs with terminal constraints," submitted.
  The main contributions include:
  - Definition of a novel optimal control problem to determine the smooth, continuous optimal control effort in a given time interval, for over-actuated systems, with control and state terminal constraints.
  - Inclusion of the time derivative of the control input in the functional, i.e., the performance index, to be minimized.
  - Narrowing of the results to an over-actuated LQT problem for LTV systems, applicable to a gear-shifting problem in MSTs for EVs.
- M. Roozegar and J. Angeles, "Gear-shifting control in electric vehicles with multi-speed transmissions via dynamic programming," submitted.
  The main contributions include:
  - Application of Bellman's dynamic programming (DP) and the principle of optimality to solve the optimal control problem of gear-shifting, i.e., finding the optimum trajectory for the states, while meeting both control and state boundary conditions.
  - Definition of various performance indices with different weights to find the optimal state trajectory and control input using DP.
  - Reduction of the computational complexity required to find the optimal control policy by means of the principle of optimality in DP.

Acronyms

AMT	automated manual transmission
APC	Automotive Partnership Canada
AT	automatic transmission
CLAM	clutchless automated manual transmission
CO	completely observable
CoV	calculus of variation
CVT	continuously variable transmission
DCT	dual-clutch transmission
dof	degree of freedom
DP	dynamic programming
ECU	electronic control unit
EM	electric motor
EV	electric vehicle
GA	genetic algorithm
HAMT	hybridized automated manual transmission
HEV	hybrid electric vehicle
I-AMT	inverse automated manual transmission
ICE	internal-combustion-engine
ICEV	internal-combustion-engine vehicle
LQI	linear quadratic integral
LQR	linear quadratic regulator
LQT	linear quadratic tracking
LTI	linear time-invariant
LTV	linear time-varying
MCU	microcontroller unit
MIMO	multi-input-multi-output
ML	machine learning
MST	multi-speed transmission
NN	neural network
NSERC	Natural Sciences and Engineering Research Council of Canada
PID	proportional-integral-derivative
RBFNN	radial basis function neural network
SAT	semi-automatic transmission
TGF	torque gap filler

Acknowledgements

Firstly, I would like to gratefully acknowledge and express my most sincere gratitude to Professor Jorge Angeles for being a wonderful supervisor during my PhD studies. This research would not have been possible without his great guidance, encouragement and support. I am proud to have worked under Prof. Angeles's supervision. I really appreciate Prof. Angeles for providing me with the opportunity to grow here, both professionally and personally. As well, I extend my appreciation to Prof. Arun K. Misra and Prof. Benoit Boulet, my PhD Committee members, for their valuable comments and support.

I would like to thank the financial support of the Canadian funding agencies for making the research work behind this thesis possible. The financial support for this thesis came from the Natural Sciences and Engineering Research Council of Canada (NSERC) through the Automotive Partnership Canada (APC) Project at McGill University, Grant APCPJ418901-11, in 2013-2016, and the McGill Engineering Doctoral Award (MEDA). Also, I would like to acknowledge the support of our industrial partners: Linamar, TM4 and Infolytica.

More importantly, I would like to express my deepest thanks to my parents and my siblings for their unconditional and endless support, love and encouragement throughout my life, especially these recent years. As well, my amazing friends, who were like my family here and never let me feel away from home, deserve my highest acknowledgement.

Contents

List of Figures

List of Tables

Chapter 1

Introduction

Internal-combustion-engine vehicles (ICEVs) give rise to various problems, first and foremost, pollution. The need to find an appropriate substitute has thus notably increased in recent years. Hybrid electric vehicles (HEVs) and electric vehicles (EVs) are suitable substitutes of their internal-combustion-engine (ICE) counterparts, since they are capable of operating with a much lower impact on the environment. However, EVs have failed to gain popularity because of an inherent problem, as the current storage-capacity of electric batteries is much lower than that of fossil fuels. In other words, when the source of energy changes from ICE to electricity, for longer running time on a single charge of the battery, it is required to enhance the efficiency of the vehicle. This can be done in various ways, such as improvement of the electric motor (EM) performance and decreasing transmission losses. Such performance features are limited by current technology. Nonetheless, the efficiency of EVs can still be improved. Most EVs on the market are equipped with a single-speed gearbox that exhibits a trade-off between efficiency and dynamic performance. Research demonstrates that applying a multi-speed transmission (MST) in EVs and designing/tuning appropriate control algorithms for gear-shifting can not only reduce the size and cost of the EM used, but also provide an appropriate balance between efficiency and dynamic performance. However, employing MSTs with more than three gear ratios might not be justified due to the comparatively flatter energy efficiency curve of EMs and the energy losses brought about by the transmission. An EM equipped with an MST can provide the desired power in more than one way by means of gear ratios, and hence, reduce the energy consumption of the EV through proper gear-shifting. In fact, in this way, the EM can operate on the high-efficiency region for longer periods. However, the overall efficiency improvement depends on the gear ratio values, the number of gear ratios and the driving cycle [1, 2, 3, 4, 5, 6, 7].

The Automotive Partnership Canada (APC) Project at McGill University focused on developing MSTs in order to improve the efficiency of EVs. The APC Program is a joint effort between universities and industry partners with funding from the latter and the Natural Sciences and Engineering Research Council of Canada (NSERC). McGill University, in collaboration with three Canadian manufacturers, Linamar, TM4 and Infolytica, developed MSTs for EVs to enhance their efficiency. The McGill team worked on four different areas: EMs; new materials; EV drive systems; and transmissions. The research work reported here focuses on the latter. Several gear-shifting control algorithms were developed for the proposed transmission. An outline of this chapter follows. Section 1.1 is devoted to different types of transmission systems for EVs and provides an overview of the state of the art of MSTs for EVs. Gear-shifting in EVs with MSTs is discussed in Section 1.2. Finally, this chapter ends with conclusions, a brief description of the thesis materials and the main assumptions in Sections 1.3 and 1.4.

1.1 Multi-Speed Transmission Systems in EVs

Different types of MSTs can be applied in EVs, such as automated manual transmissions (AMTs), automatic transmissions (ATs), dual-clutch transmissions (DCTs), and continuously variable transmissions (CVTs). These transmissions were initially designed for ICEVs. Since these vehicles cannot operate below certain speeds and their speed control during gear-shifting is quite challenging, the presence of clutches or torque-converters is indispensable for startups, idle running and gear-changing. For EVs, however, this is not the case, because EMs are speed-controllable in a wide range of operating speeds. This difference provides an opportunity to design novel transmissions for EVs without any clutches or torque converters to disconnect the mechanical coupling during gear-shifting; as a result, the losses are minimized. In fact, to make seamless gear-shifting feasible, the EM is used as an independent control input in MSTs designed for EVs [8, 9, 10, 11].

1.1.1 Automated Manual Transmissions (AMTs)

AMTs are a kind of semi-automatic transmissions (SATs), which make gear-shifting easier when compared to manual transmissions, by dispensing with the need to press the clutch pedal during gear-shifting. In fact, AMTs do not include a clutch pedal, only accelerator and brake pedals. The purpose of applying AMTs is to make the powertrain automatic. This transmission system is widely used in the European car market. Compared to other types of transmissions, the advantages of this type are lower weight and higher efficiency. The AMT system is an enhanced version of the gearbox used by Ferrari since 1989, developed in association with Magneti-Marelli (another Italian automotive company) in its F355 F1 racing car in 1997. Apart from Ferrari, the German

transmission-maker Getrag, the world's largest supplier of transmission systems for passenger cars and commercial vehicles, was the first on the market with a sequential AMT, developed for the BMW M3 in 1996. An AMT generally includes a dry clutch and a multi-speed gearbox, which are equipped with electro-mechanical or electro-hydraulic actuators, driven by an electronic control unit (ECU) [12].

In AMTs, since the clutch affects the starting and shifting quality directly and the drive performance depends on their engagement process, the studies of AMT control mostly focus on clutch control, while engine control is usually neglected. Based on the kinematics and dynamics of the transmission system, Ge et al. [13] proposed a strategy for engine constant speed control in the starting-and-shifting process. A nonlinear multi-rigid body approach was developed by Zhang et al. [14] for modelling the automated clutch system in power transmissions during clutch engagement. An adaptive optimal controller was also designed for an ideal dynamic performance of the clutch engagement. In controller design, some significant factors such as throttle angle, engine speed, gear ratio, vehicle acceleration and road conditions were considered. Based on a novel design of the synchronizing rings and their actuation, Heath and Child [15] introduced an alternative design solution for the implementation of seamless gearshifts, called Zeroshift AMT. Zeroshift technology allows a manual transmission to change gears instantaneously. The main benefits lie in the areas of fuel economy, dynamic performance, shift quality and manufacturability. Moreover, the test data from a Ford Mustang demonstration vehicle was also reported [15]. Lucente et al. [12] developed detailed nonlinear models of the electro-hydraulic servo-actuated gearbox and clutch actuators of a car equipped with an AMT. Experiments were also conducted on a commercial car to verify the proposed model during gear-shifting. Miao et al. [16] applied a fuzzy-logic approach to control the gear-shifting process of AMTs with the engine running and considering clutch-engaging states. In other words, based on a radial basis function neural network (RBFNN), a wet clutch pressure "intelligent" control arithmetic was designed to realize accuracy control of the clutch pressure. RBFNNs are typically trained by a two-step algorithm. According to the error between the clutch target pressure and actual pressure value, the system under control learns the underlying dynamics, and hence, compensates for the clutch and solenoid valve model errors.

The main problems with AMTs lie in driving and passenger comfort, caused by torque interruption during gear-shifting. Gear-shifting and drivability-improvement of a clutchless AMT (CLAMT) for EVs was developed by means of a sliding-mode controller that reduces the gap of torque interruption during shifting. The main advantages of a CLAMT are high efficiency, low cost, and simple structure [17]. Zhu et al. [18] investigated the speed synchronization optimal controller design for CLAMT. To this end, a combination of state-feedback and H_∞ robust controllers was applied. Moreover, the linear quadratic cost function and the pole-placement technique were adopted to trade off between the transient response and the maximal control effort. Additionally, to accomplish the

traction interruption, Sorniotti et al. proposed a novel seamless transmission called inverse AMT (I-AMT) [19, 20]. In I-AMT, the dry clutch is located at the rear of the transmission so that the traction interruption of traditional AMT can be cancelled. Gao et al. [6] studied a two-speed transmission of this type. In fact, the gear ratios were optimized first, by minimizing the energy consumption under combined urban and suburban driving cycles, using Bellman's dynamic programming (DP). Then, after addressing gear-shift control, a smooth shift process without torque hole was achieved through feedforward and feedback control of the clutch and the motor. Furthermore, it was also shown that the two-speed AMT with a rear-mounted dry clutch performs much better than a fixed-ratio gear box in terms of acceleration time, maximum speed and energy consumption. Using optimal control techniques, reference trajectories of the clutch slip speed and motor torque were generated for improving the shift quality of a two-speed I-AMT of EVs. The off-line results were utilized for on-line implementation in a physical system, while using a PID controller to compensate for disturbances and errors [21]. Based on hybridized AMT (HAMT), a new type of hybrid powertrain system was designed by Wu and Dong [22], which, by applying the concept of torque gap filler (TGF), has the potential to overcome the torque gap issue during gear-shifting. A control scheme was also established to harmonically coordinate various powertrain components to realize the TGF function. Considering the angular-displacement sensor fault, a control method was proposed for AMT gear-shifting engaging process, based on updating the actuator current observer and the gear-shifting engaging torque table [23]. To realize power-on shifting without torque interruption and maximize the overall efficiency, a high-speed motor was adopted to connect to the input of a CLAMT, while a low-speed, high-torque EM was connected to the output shaft of the transmission with the fixed gear ratio [24].

1.1.1.1 Automatic Transmission Based on a Planetary Gear Set

In 1925, H. Rieseler designed an AT comprising a torque converter and a rear-mounted planetary gear set. In addition, Rieseler made an extraordinary contribution by replacing the dry clutches with a fluid clutch. The first mass-produced transmission of this kind was the General Motors Hydramatic in 1939 [10]. In fact, ATs with planetary gear sets have the advantage of eliminating the output-torque interruption during gear-shifting. Although the existence of a torque converter in this type of transmission increases passenger comfort and drivability, its efficiency is lower than in other types of transmissions because of the internal slippage inside the torque converter. Some researchers have worked on various aspects of this type of transmission, such as its dynamics modelling and analysis, closed-loop control of gear-shifting, and modelling and control of torque converters and clutches [25, 26, 27, 28].

1.1.2 Dual-Clutch Transmissions (DCTs)

ATs can change gear ratios automatically as the vehicle moves, freeing the driver from shifting gears manually. DCT is a kind of AT that uses two separate clutches for odd and even gear sets. It allows torque transfer from one clutch to another without interrupting traction. The clutches are engaged alternatively at different speed ratios, while power transmission continues during a shift through the control of clutch slippage. In fact, a shift process involves engaging the oncoming clutch and releasing the off-going clutch. Two important concerns in DCT, dynamic performance and the associated driver perception, are greatly dependent on the control system, which generates the reference signals for both synchronizers and clutches [29, 30].

A mathematical model for simulation, analysis and control of the launch and shift processes of DCT vehicles was proposed by Kulkarni et al. [29]. First, vehicle dynamics during shifting was modelled, then simulation results were analyzed. Afterwards, shift control was optimized using clutch-pressure profiles as control signals. For analysis of the powertrain overall performance and shift transient characteristics, Zhang et al. [31] modelled the kinematics, dynamics, and control of the transmission. The model was implemented in an object-oriented software tool, and mathematical formulations and look-up tables were both used to model the powertrain components. Synchronizer assemblies were modelled as switches for the power-flow paths at different speed ratios. Moreover, an integrated powertrain control for gearshifts was developed by Goetz et al. [32, 33]; in their algorithm, clutch slip for a smooth transfer of engine torque was controlled, with the aim of reproducing the operation of a one-way clutch. Furthermore, a closed-loop control of engine speed through a combination of engine controls and clutch pressure was implemented. Finally, dynamic effects of the gear preselection through conventional cone-type synchronizers on the overall shift quality was investigated . A detailed simulation model was built for the quantitative analysis of the vehicles equipped with a dry DCT during launch and shifts of the vehicle. The model provides a tool for DCT torque control and calibration. Based on calibration data, feedback control and open loop control were both used for the clutch torque during launch and shifts. Additionally, simulation results were compared with experimental data obtained from a Ford test vehicle [34]. The impact of pump selection on fuel economy in a DCT vehicle that lacks a torque converter and uses fewer clutches than conventional ATs, was investigated by Ahlawat et al. [35]. A reduced lumped-parameter model for DCTs was developed by treating the gear sets as modulated transformers with losses. Also, in this case, synchronizers were modelled as power-flow switches. The analysis provided insight into the pumping losses in a DCT, one of the areas where the greatest improvement can be achieved. A method was proposed for combined speed and torque control of vehicle powertrains with DCTs for both engine and clutches. In other words, the role of integrated power train control of both engine and clutches in reducing shift transient response for DCTs was demonstrated with the inclusion of detailed hydraulic system models. It was also concluded that the adoption of feedforward control of

engine torque has the potential to reduce the DCT transient response during shifting [36]. A full set of transmission kinematics and dynamics equations of a DCT was also reported, taking into account all the possible configurations that can take place in relation to the various power-flow paths [30]. An upshifting and downshifting open-loop control algorithm was proposed for a two-speed DCT [37]. A test rig was built at the powertrain lab of the University of Technology, Sydney (UTS). Further, both transient shifting and driving cycle control were implemented on the testbed. Results demonstrated that the vibration of the output torque was reduced and the torque interruption was almost eliminated. An optimization problem was formulated for gear-shifting in DCTs, in order to minimize the jerk and the energy losses in the clutches [38]. To this end, nonlinear constraints of the clutch friction were omitted by imposing linear constraints and dividing the time interval into two phases. To precisely describe the powertrain vibration, a control-oriented model was developed for DCT drivelines. Further, based on this model, a real-time torque observer was adopted to compensate for the absence of torque sensors [39].

1.1.3 Continuously Variable Transmissions (CVTs)

In contrast to other mechanical transmissions that offer a finite number of gear ratios, a CVT is capable of changing seamlessly through a continuous range of gear ratios between high and low extremes. This difference, flexibility of a CVT, provides the opportunity of operating at the most efficient point for the motor. As a result, a CVT improves the fuel economy and dynamic performance of the vehicle. Several vehicle manufacturers, such as Honda, Toyota, Ford, and Nissan, are working on exploiting the benefits of a CVT in a vehicle [40]. Among different types of CVTs, belt and chain CVTs are the most commonly used in automotive applications. A CVT includes two variable-diameter pulleys, kept at a fixed distance apart, connected by a power-transmitting device like a belt or a chain. The belt/chain can undergo both radial and tangential motions, depending on the torque loading conditions and the axial forces on the pulleys.

Extensive research has been conducted on different aspects of belt CVTs, such as dynamic modelling, performance, slip behavior, efficiency, configuration design, loss mechanisms, friction, vibrations, operating regime, and control [41, 42, 43]. For instance, Srivastava and Haque [44, 45] studied the effects of pulley flexibility, band-pack slip and lubrication-related friction characteristic in transient dynamic modelling of a metal pushing V-belt CVT. In addition to belt CVTs, significant research effort has been directed towards the dynamics and power transmission characteristics of chain CVTs. As an example, by developing a planar multibody model of a chain CVT, Srivastava and Haque [46, 47, 48, 49, 50] studied the influence of clearance and friction parameters on dynamic performance indices of chain CVTs for high torque applications. By inducing chaos and self-sustained vibration in the system, some models were developed to analyze the friction-induced nonlinear dynamics of a chain CVT drive. The dynamics model of a chain CVT was described

by a quite simple first-order nonlinear differential equation by Yildiz et al. [51], which makes the real-time control of a CVT easier.

The control aspect of CVTs includes achieving an appropriate gear-ratio profile, by means of pulley actuation forces, with the purpose of increasing the torque capacity of a CVT system, minimizing belt slip losses, and maximizing vehicle fuel economy and acceleration performance [40]. Based on a linearized slip model, Bonsen et al. [52, 53] developed a robust gain-scheduling PI controller to measure and control slip in a CVT while minimizing clamping forces and preventing destructive belt slip. Ryu et al. [54] developed a model-based control algorithm for the pressure-control type CVT using the steady-state characteristics of the ratio control valve. Applying a set-point feedforward and a linearizing feedback controller, a new ratio controller for a metal pushing V-belt CVT with a hydraulic clamping system was developed by Pesgens et al. [55]. Furthermore, Adachi et al. [56] employed a robust control method, l-synthesis, to design the controller and coupled it with a feedforward controller for better control performance. Considering the electrical and mechanical parameters of the EM, a fuzzy controller was designed for EVs equipped with CVTs to achieve the maximum efficiency of the motor during operation [57].

1.2 Gear-shifting in EVs

Gear-shifting is one of the most significant concerns in transmission systems, since it influences passenger comfort, dynamic performance and efficiency, besides drivability. The main difference between transmission systems in EVs and ICEVs is that, as mentioned before, EMs are speed-controllable in a wide range of operating speeds in the former. Consequently, instead of disconnecting the mechanical coupling by means of clutches or torque converters during gear-shifting, one can design novel transmissions for EVs, in which the drive motor is also an element to be controlled and, as a result, minimize the losses. The main purpose of gear-shift control is to make it as seamless and swift as possible. Additionally, there are some other goals which are also considerable, such as increasing drivability, eliminating vibrations, reducing power losses and improving efficiency, while eliminating output torque interruption. Extensive research has been conducted on each of the above-mentioned targets. Some of the remarkable ones were already discussed in Section 1.1, for different transmission systems. Further research in these areas is discussed below.

Generally speaking, one of the main conventional strategies for gear-shifting control is to separate the torque and inertia phases, and control each phase independently. This method is mostly employed for ATs and DCTs. As mentioned above, the control algorithm consists of two phases, i.e., the torque phase and the inertia phase. In the former, the clutches are switched by controlling the clutch torques. At the beginning of this phase, the off-going clutch is completely engaged and the on-going clutch is completely released. In the end, the off-going clutch is completely released and the on-going

clutch is slipping. In the inertia phase, the speed of the motor is matched with the speed of the driveline in the second gear set. At the same time, the output speed and torque of the transmission are controlled by means of the on-going clutch torque. At the end of the inertia phase, the on-going clutch is completely engaged. The point here is that during the torque phase, the angular velocities of gears and motor also need to be controlled [58, 33, 8].

In EVs, due to the perpetual connectedness of the power transmission paths, torques and speeds are always dependent on each other through the transmitted power. Hence, it is not required to separate the above-mentioned phases distinctly for control purposes. Rahimi et al. [7, 9] developed a control strategy based on this idea. With the purpose of keeping the output speed and torque of the driveline constant, the Pontryagin minimum principle was employed to design an optimum shifting controller for gear-shifting, while minimizing shifting time and energy dissipation. A back-stepping controller was also designed to provide a stabilizing feedback law based on the optimal control inputs. Experiments were conducted to validate the simulation results, thereby demonstrating a smooth shifting. Employing the time-optimum hybrid minimum principle, Pakniyat et al. [59] formulated the problem of the minimum acceleration time required for reaching the speed of 100 $\mathrm{km/h}$, from the stationary state, and found the optimal control inputs and the optimum gear-shifting instants. In addition, Pakniyat et al. [60] solved the problem of optimal gear selection for EVs and demonstrated the importance of gear selection on energy consumption. It was concluded that the minimum possible energy consumption was subject to several consecutive switchings in short periods. Since successive switchings are undesirable due to physical limitations and performance efficiency, restrictions were introduced on switching counts, which in general result in the dependence of the gear selection decision to the whole time interval of optimization. Rahimi et al. [61] designed a deterministic Luenberger observer and a stochastic Kalman-Bucy filter to estimate the unmeasured states for a seamless two-speed transmission for EVs. Under process noise, simulation and experimental results were compared. Thereafter, in order to provide a robust concurrent estimation of unavailable states and the unknown input, Rahimi et al. [62] combined the method of modelling the unknown input as a fictitious state variable with the fading-memory Kalman filter. The estimation results were compared to those of a conventional Kalman filter and a deterministic Luenberger observer. Using an unknown input observer, the estimation of the frictional torque of the synchromesh during the gear-shifting operation in an EV with a clutchless AMT was studied [63]. Similarly, a deterministic Luenberger observer and a stochastic Kalman-Bucy filter were designed to estimate the frictional torque of the synchromesh. The results demonstrated satisfactory performance of the stochastic observer when the system encounters process and measurement noise, which are likely to happen in the real world. Furthermore, an observer-based back-stepping controller was devised to provide seamless gear-shifting for an EV, while tracking the optimal trajectory corresponding to the minimum shifting time [64]. The input and output torques of the transmission and the angular velocities of the gears

were estimated based on measurements of the motor speed and the speed of the vehicle.

Other researchers have conducted studies on other aspects. For instance, Zhang et al. [58] simulated the transient torsional vibration for AT gear-shifting using the finite element method. In fact, a four-degree-of-freedom (dof) planetary gear set was considered to describe the dynamics of ATs during gear-shifting. Sorniotti et al. [65] studied the control system of a two-speed transmission system with focus on optimal gearshift dynamics. It was concluded that, in comparison to DCTs within ICEVs, the torque characteristics of typical EM drives require a different actuation for seamless gear-shifting. Hong et al. [66] proposed a gear-shifting control algorithm, to control two shift actuators and the driving motor, for an EV with a two-speed DCT. For the proposed control algorithm evaluation, based on MATLAB/Simulink, a shift performance simulator was developed by modelling a DCT-type EV with a two-speed transmission system. Without the algorithm, simulation showed drive shaft torque overshoot during gear-shifting. Results showed no overshoot in the drive shaft torque after using the proposed algorithm, which verified the shifting quality improvement. Similarly, Xu et al. [67] designed an automatic shifting controller for an EV with a five-speed transmission. Gear selection and gear-shifting were implemented using a pneumatic cylinder and shifting forks, driven by electromagnetic valves. Receiving data on vehicle velocity, motor speed, motor current, gear position, and accelerator position, a microcontroller unit (MCU) was applied to adjust the motor angular velocity accurately and rapidly as well as to control the electromagnetic valves. The controller was implemented in a converted electric Isuzu truck with AC induction motor. Results indicated that the controller improved the motor efficiency and shifting quality. Considering the DCT powertrain as an over-actuated system, a two-stage optimal control strategy was implemented for gear-shifting. In the first stage, an upper level controller determines the most proper torque trajectories of the clutches and engine, while in the second stage, a lower level controller is used to track the desired torque trajectories [68]. For achieving a swift and smooth shift in DCTs, Li and Gorges [69] proposed a new control algorithm to find the optimum trajectories for the clutch torque and input shaft torque. Moreover, to attain an appropriate friction torque for the two clutches, a finite-horizon linear quadratic regulator (LQR) was applied for the mutual engaging and disengaging control during the torque phase. Finally, an LQR-based integral controller was used to determine the optimal input for regulating the relative speed between the engine and the slipping clutch during the inertia phase.

1.3 Conclusions and Thesis Materials

This research work focuses on gear-shifting control algorithms for MSTs in EVs. A literature review on various types of EV transmissions and the state of the art were provided. Research on gear-shifting in MSTs was also discussed. Additionally, a review on modelling and control of

these transmissions was included. The literature review showed that implementation of MSTs for EVs has not been fully solved and is still controversial. Therefore, there is still much room for improvement; lack of knowledge warrants further work in this area. In this research, MSTs for EVs will be given due attention and consideration. Specifically, gear-shifting control schemes will be studied. Contribution to knowledge pertains to developing new gear-shifting algorithms for MSTs in EVs and establishing proper controllers for swift and seamless gear-shifting. An outline of the thesis materials follows.

Firstly, the mechanism of the proposed MST designed for EVs is briefly described. The main advantages of the proposed MST are simplicity and modularity, namely, depending on the application and the number of gear ratios required, the appropriate number of modules, including a planetary gear set and a clutch, can be added to the transmission. For effective gear-shifting, the model of the transmission is required. Moreover, reliable methods should be employed for estimation of the unmeasurable loads and states of the system, under model-based control. To this end, the kinematic relations, i.e., the constraints, and the dynamics model of the transmission are derived applying the Euler-Lagrange formulation. Next, after a brief description of the sources of the external disturbance applied to the output shaft and finding the process and measurement models, the Kalman-filter, the Luenberger observer and neural networks (NNs) are employed to estimate the states, the unknown arbitrary disturbance and the unknown clutch torque applied to the transmission. The estimation algorithms are evaluated by applying various disturbances to the system, such as linear, parabolic, sinusoidal, and arbitrary.

After defining the gear-shifting problem for a multi-stage planetary gear set in the space of angular velocities, based on the kinematic relations, calculus of variations (CoVs) is used to find the schedules of the angular velocities during gear-shifting for a swift, seamless operation, which leads to the optimum trajectory. To this end, we resort to polynomial transition functions in the time-domain. In fact, what we term 2-3, 3-4-5 and 4-5-6-7 polynomials are suggested for a swift and seamless shift. The continuity of the angular velocity, acceleration and jerk, the limitations of the power supply, and the shifting time are considered in comparing the results obtained with these polynomials. The corresponding input torques applied by the EM and the clutches are also determined based on inverse dynamics.

From a control point of view, the gear-shifting problem in the proposed transmission for EVs leads to an over-actuated system, i.e., the number of control inputs is greater than the number of states to be controlled. Furthermore, terminal constraints on both control inputs and states are included. Since these properties make the problem quite challenging, new algorithms should be developed for gear-shifting that, besides swiftness and smoothness, satisfy the end-point conditions on states and control inputs. Several control algorithms are proposed for this specific problem to meet all end control and state conditions, while tracking the desired trajectory.

The first control algorithm consists of two phases, the approaching phase and the coasting phase. During the former, the free clutch remains disengaged. In fact, the objective is to change gears artificially, namely, by changing the gear ratio without engaging the free clutch. At the end of this phase, the fixed clutch is engaged partially. Next, since the gear ratio has changed, we can readily engage the free clutch. Besides, we should start by disengaging the partially-engaged clutch completely, while controlling the drive torque to keep the input and output angular velocities constant. For each of the above-mentioned phases, a separate PID controller is designed based on trial-and-error and genetic algorithms (GAs). Depending on the phase and the gear-ratio values, the proper PID gains are selected by a supervisory controller, called PID gain-scheduling.

In the second algorithm, one of the inputs is changed independently, based on a 2-3 blending polynomial, which, besides satisfying the input terminal constraints, guarantees the continuity of the velocity, acceleration and jerk at the ends of the gear-shifting interval. Then, the new fully-actuated system is controlled employing a linear-quadratic-integral (LQI) controller, which is an extension of the LQR for tracking problems. In a real EV, some parameters, such as the mass of the vehicle, the vehicle speed, the forces between road and tires, the road slope and the aerodynamic drag force, influence significantly the size of the EMs used and the ranges of the applied power and torques. Hence, to assess the performance of the proposed approach in a real EV, unknown external disturbances and external loads are applied to the transmission system during gear-shifting, which include the effects of all parameters mentioned above. Compared to the first algorithm, this strategy is less complex and can be implemented on a physical MST more easily. Furthermore, the control inputs vary more smoothly than those of the previous scheme.

To find the smooth, continuous, optimal control inputs for this specific over-actuated system, with terminal-point control and state conditions, two different novel, non-standard optimal control problems are formulated. In other words, while the classical approaches only consider terminal time and state constraints in defining and solving optimal control problems (see e.g. [70, 71]), in the proposed approaches, besides the continuity and smoothness of the control effort, applying soft or hard terminal constraints on the control inputs is also included. This leads to the appearance of some new terms in most relations in the line of proof and deriving the necessary conditions for optimality. To this end, in the first scheme, a general Lagrange variational problem is considered with a modified terminal penalty term including the terminal control input, while in the second approach, the functional, i.e., the performance index to be minimized, includes the time derivative of the control input. The results are used to achieve control allocation in an over-actuated linear quadratic tracking (LQT) problem for linear time-varying (LTV) systems, which is applicable to the gear-shifting problem in MSTs for EVs. However, the application of the results extends to optimal control problems in which it is necessary to impose terminal constraints on the state, its time derivative, and/or its controls, to guarantee smooth system operation over extended periods,

or seamless blending of operation modes. Even if the system is not over-actuated, the proposed approaches can still be applied, as long as the constraints at the ends are reasonable and the solution exists.

Lastly, this specific optimal control problem is solved applying Bellman's DP and the principle of optimality: "An optimal policy has the property that, no matter what the previous decisions were, the remaining decisions must constitute an optimal policy with regard to the current state obtained from those previous decisions." In other words, to find the optimum trajectory for the states, while satisfying both terminal control and state constraints, a control scheme is suggested based on DP. The main advantage of DP is reducing the number of required calculations dramatically, as the number of decisions at each stage is restricted. In fact, instead of trying all admissible trajectories leading from each state to the target and choosing the one with the lowest cost, the principle of optimality is applied in DP. In using DP, depending on the control objectives, various performance indices with different weights can be defined to find the optimal state trajectory and control input.

1.4 Assumptions

The main assumptions are given below:

– The focus of the thesis is the development of gear-shifting control algorithms for the proposed MST designed for EVs. Hence, in establishing different approaches for gear-shifting, since the problem is mostly studied from a control point of view, only the gearbox is considered. In other words, the details of the electric powertrain system, EMs, clutches, differential and EV driving cycles lie beyond the scope of the thesis.

– The research work reported in the thesis hinges on the transmission testbed designed and prototyped in our laboratory. For this reason, the ranges of the torques and angular velocities are narrow. In an actual EV, these ranges are much broader.

– While DC motors are not used in EVs, our transmission is equipped with one such motor because of practical reasons, as DC motors are convenient for laboratory conditions.

– In the model derivation, all components are considered as rigid bodies without any nonlinearity, dissipation or flexibility, statically balanced and symmetrically laid out, the total potential energy of the system then being constant. As well, our models are based on the assumptions of pure-rolling relative motion, free of sliding and Coulomb friction. In fact, everything neglected in the model is included in the unknown external disturbance applied to the transmission system.

– In developing control algorithms for gear-shifting, the clutches are assumed to be active, not passive, i.e., they can apply the required torques in both directions regardless of the direction of the ring gear angular velocity. In fact, the torques applied by these clutches are provided by independent EMs. The reader is referred to the Appendix for more details.

Part I

Modelling, Estimation and Optimal Gear-shifting Trajectory in Multi-speed Transmissions for Electric Vehicles

Chapter 2

Design, Modelling and Estimation of a Novel Modular Multi-speed Transmission System for Electric Vehicles

Abstract

The efficiency of electric vehicles (EVs) should be improved to make them viable, especially in light of the current low energy-storage capacity of electric batteries. Research demonstrates that applying a multi-speed transmission (MST) in an EV can reduce the energy consumption of the vehicle through gear-shifting. However, for effective gear-shifting control in MSTs, first of all, the model of the transmission is required. Moreover, reliable methods should be employed for estimation of the unmeasurable loads and states of the system, under model-based control. This study establishes the mathematical model and estimation algorithms for a novel MST designed for EVs. The main advantages of the designed MST are simplicity and modularity. After devising the dynamics of our proposed transmission, the Kalman filter, the Luenberger observer and neural networks (NNs) are used to estimate the states, the unknown arbitrary disturbance and the unknown clutch torque applied to the system. Simulation results demonstrate that the proposed approach is suitable for estimation purposes. Experiments were conducted using an in-house prototyped transmission testbed, to validate the simulation results and assess the estimation algorithms.

2.1 Introduction

The main problem with internal-combustion-engine (ICE) vehicles is pollution. We thus need to find an appropriate substitute for them, with a much lower impact on the environment. Hybrid electric vehicles (HEVs) and electric vehicles (EVs) are two appropriate substitutes. Nonetheless, due to the current low energy-storage capacity of electric batteries, EVs have failed to gain popularity. Hence, it is required to improve the efficiency of EVs, to achieve longer running time on a single charge of the battery. Research demonstrates that by applying a multi-speed transmission (MST) in EVs, we can decrease the energy consumption of the vehicle, since the desired power is provided in more than one way in an MST. In fact, this way, the electric motor (EM) can operate on the high-efficiency regions for longer periods. However, the overall efficiency improvement depends on the gear ratio values and the number of gear ratios in the MST, as well as the chosen driving cycle [2, 1, 3, 4, 5, 6, 7].

Automated manual transmissions (AMTs) [12, 18, 21], automatic transmissions (ATs) [10, 72, 28], dual-clutch transmissions (DCTs) [30, 37, 73], and continuously variable transmissions (CVTs) [40, 50] are various kinds of MSTs. The above-mentioned MSTs were initially designed for ICE vehicles. However, EMs are speed-controllable in a wide range of speeds, compared to their ICE counterparts. Therefore, novel transmissions can be designed for EVs, without a clutch or torque converter to disconnect the motor from the transmission during gear-shifting; consequently, the losses are minimized. Instead, the EM is an element to be controlled to make gear-shifting swift and seamless [9, 10]. Gear-shifting affects drivability[1], passenger comfort, dynamic performance, and efficiency. Thus, the main objectives in gear-shifting are seamlessness, swiftness, increased drivability, vibration elimination, output-torque interruption cancelation, and improved efficiency. There has been extensive research on each of these targets [58, 65, 66, 67, 59, 60]. One of the main gear-shifting algorithms, mostly adopted in ATs and DCTs, is based on separating and controlling the torque and inertia phases distinctly [58, 33]. However, since the power transmission paths are permanently connected in EVs, torques and speeds are always related to each other. Accordingly, the above-mentioned phases should not be controlled independently [7, 9]. Using polynomial transition functions to guarantee the continuity of the velocity, acceleration and jerk, the optimal gear-shifting in MSTs for EVs was investigated, which led to a swift, seamless shift [74].

For appropriate gear-shifting, an accurate real-time monitoring of the unmeasurable states, the unknown disturbance and the unknown inputs of the transmission are required. Liu et al. [75] employed a combination of the auxiliary particle filter and the iterated extended Kalman filter (APF-IEKF) to estimate the tire-road friction coefficient using the existing sensors. Furthermore, a deterministic Luenberger observer, a stochastic Kalman-Bucy filter, and a fading-memory Kalman

[1] No generally acceptable definition of the term can be cited, but it usually includes the qualitative evaluation of a powertrain, such as the degree of smoothness and steadiness.

filter were designed by Rahimi et al. [62, 63, 76] to estimate the unmeasurable states and the unknown inputs for a seamless, two-speed clutchless AMT for EVs. Then, based on the estimation results, an observer-based back-stepping controller was established for a seamless gear-shifting in an EV, while following the optimal trajectory associated with the minimum shifting time [64]. Combining the model-based observer, the unknown input observers, and the adaptive output torque observer, a novel algorithm was developed to estimate the torque of the clutches during gear-shifts for a DCT [77]. Although there has been intensive research on MSTs, there are still lacunae in the design, mathematical modelling and estimation.

The mathematical modelling and estimation algorithms of a novel MST designed for EVs are developed in this paper. The main advantages of the designed MST are simplicity and modularity. Firstly, the kinematics and dynamics model of our proposed transmission system are established via a Lagrangian formulation. Then, after finding the process and the measurement models, the Kalman filter, the Luenberger observer and neural networks (NNs) are applied to estimate the unmeasurable states, the unknown arbitrary disturbance and the unknown clutch torque applied to the system. For the assessment of the estimation algorithms, various disturbances, such as linear, parabolic, sinusoidal, and arbitrary, are applied to the system. Results demonstrate that the Kalman filter has a better performance than the two other methods. In fact, compared to NNs, the Kalman filter is more precise, since it is based on a mathematical model. Also, compared to the Luenberger observer, the Kalman filter considers the covariances of the noise of both the process and the measurement models. Moreover, according to the error covariance, the Kalman gain is updated during the estimation, while the Luenberger gain remains constant. Using an in-house prototyped transmission testbed, some experiments are also conducted to validate the model and the estimation algorithms.

An outline of the paper follows. Section 2.2 is devoted to the mathematical model of the proposed MST designed for EVs. Estimation of the transmission is discussed in Section 2.3. Section 2.4 provides simulation results. Experimental work is reported in Section 2.5.

2.2 Mathematical Model of the Proposed MST for EVs

The proposed MST designed for EVs is depicted in Fig. 2.1. As shown in the figure, all sun gears are installed on the same shaft. As well, all planetary gear sets share the same carrier. In the overdrive gear train, the input shaft is connected to the carrier, while the output shaft is connected to the sun gears. The underdrive gear train operates the other way around. As mentioned, the main advantages of the proposed MST are simplicity and modularity. In other words, depending on the application and the number of gear ratios required, the appropriate number of modules, including a planetary gear set and a clutch, can be added to the transmission. The EM is connected to the input shaft. By engaging a clutch, the corresponding speed ratio is achieved in the output. In fact, for switching

between gears, the engaged clutch should be released and another one should be engaged. The resultant external disturbance is applied to the output shaft.

The overdrive and underdrive gear trains can also be combined to develop a single transmission, as represented in Fig. 2.2. In the new transmission, two friction clutches are required between the carrier and one of the planet or sun gears in both gear trains, C_f^i and C_f^o, in order to make the free overdrive or underdrive gear train act as a rigid body when the corresponding clutch is closed. In fact, depending on the operation mode required, i.e., underdrive or overdrive, one of the friction clutches is engaged, the other released. The new transmission supports $m + n$ main gear ratios, when one of the gear trains is operating and the other is disengaged, as well as $m \times n$ median gear ratios when both gear trains are controlled simultaneously. In median gear ratios, one ring clutch in engaged from each side and both friction clutches are released. Therefore, including the direct drive mode, the total number of speed ratios in the proposed transmission is

$$j = m + n + m \times n + 1 \tag{2.1}$$

The most significant benefit of the proposed transmission is that the designer can determine the numbers of the underdrive and overdrive modules independently, according to the application and the desired number of gear ratios. Note that in each gear ratio, the others can be treated as a rigid body. The kinematics and dynamics of a two-speed transmission, as well as the external disturbance applied to the transmission are investigated below. The parameters used here are defined in Table 2.1.

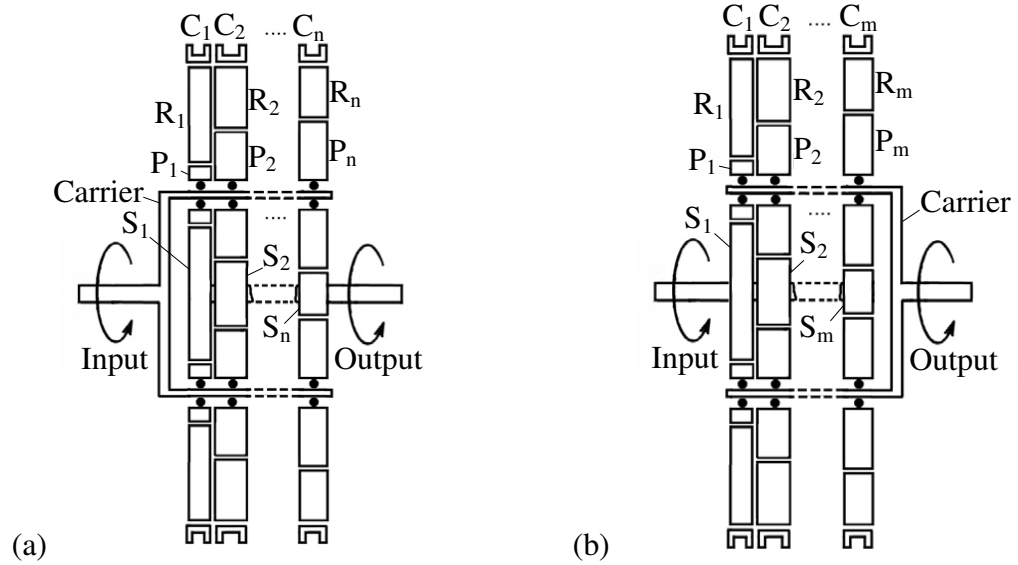

Figure 2.1: Multi-stage planetary gear sets: (a) overdrive gear train; and (b) underdrive gear train

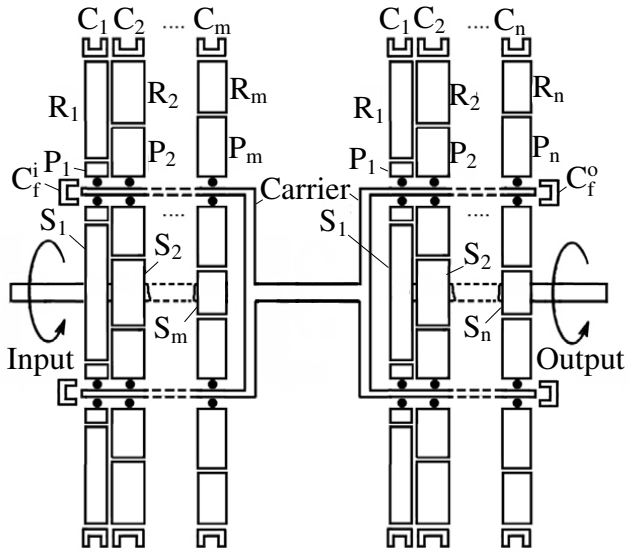

Figure 2.2: A combined multi-speed transmission system

Table 2.1: Definition of the system parameters

Parameter	Definition
r_s	pitch radius of the sun gear
r_r	pitch radius of the ring gear
r_p	pitch radius of the planet gear
r_c	centre-to-centre distance between sun and planet gears
r_{s_i}	pitch radius of the sun gear of the i^{th} planetary gear set
r_{r_i}	pitch radius of the ring gear of the i^{th} planetary gear set
r_{p_i}	pitch radius of the planet gear of the i^{th} planetary gear set
I_{s_i}	moment of inertia of the sun gear of the i^{th} planetary gear set
I_{r_i}	moment of inertia of the ring gear of the i^{th} planetary gear set
I_{p_i}	moment of inertia of the planet gear of the i^{th} planetary gear set
I_c	moment of inertia of the carrier
m_{p_i}	mass of the planet gear of the i^{th} planetary gear set

2.2.1 Kinematics of a Two-speed Transmission

The kinematic relations, i.e., the constraints, of the system are discussed in this subsection. These constraints will be used to formulate the dynamics equations.

A planetary gear set includes a sun gear, a carrier, a ring gear, and two to four planet gears, as illustrated in Fig. 2.3. Assuming ω_s, ω_c, ω_r and ω_p to be, respectively, the angular velocities of the sun, carrier, ring and planet gears, the kinematic relations below are obtained under the assumption of pure-rolling between the elements in contact.

$$r_r\omega_r = r_c\omega_c + r_p\omega_p, \quad r_c\omega_c = r_s\omega_s + r_p\omega_p \tag{2.2}$$

with

$$r_r = r_c + r_p, \quad r_c = r_s + r_p \tag{2.3}$$

Therefore, the system has two degrees of freedom (dof); four generalized coordinates, i.e., the angular displacements of the sun, carrier, ring and planet gears, and the two constraints of Eqs. (2.2). By eliminating ω_p from Eqs. (2.2) and (2.3), we obtain

$$(r_s + r_r)\,\omega_c = r_s\omega_s + r_r\omega_r \tag{2.4}$$

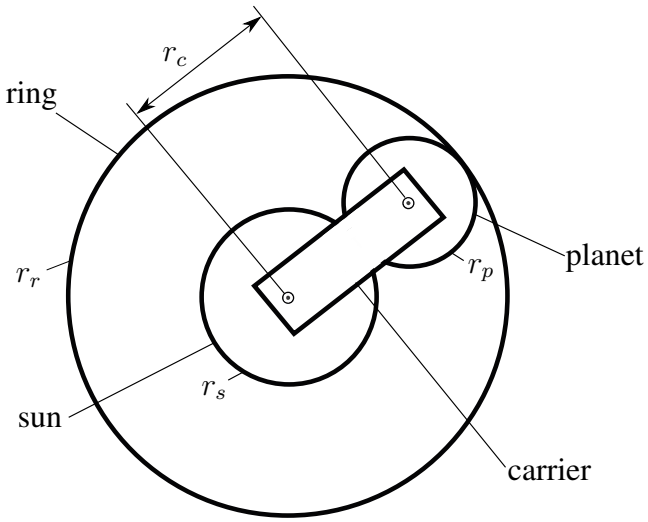

Figure 2.3: A planetary gear set

Assuming two planetary gear sets in the transmission, we have

$$\omega_c = \frac{\nu_1\omega_{r_1} + \omega_s}{\nu_1 + 1}, \quad \omega_c = \frac{\nu_2\omega_{r_2} + \omega_s}{\nu_2 + 1} \tag{2.5}$$

with

$$\nu_1 = \frac{r_{r_1}}{r_{s_1}}, \quad \nu_2 = \frac{r_{r_2}}{r_{s_2}} \tag{2.6}$$

Note that according to Fig. 2.1, in each gear train, all planetary sets share the same carrier rotating at ω_c. Further, all sun gears are installed on the same shaft rotating at ω_s.

2.2.2 Dynamics of a Two-speed Transmission

Applying the Lagrange equation, given below, the dynamics model of the transmission system is established in this subsection:

$$\frac{d}{dt}\left(\frac{\partial L}{\partial \dot{\mathbf{q}}}\right) - \frac{\partial L}{\partial \mathbf{q}} = \frac{\partial}{\partial \dot{\mathbf{q}}}\left(\Pi - \Delta\right), \quad L = T - V \tag{2.7}$$

with

$\mathbf{q}$: the vector of generalized coordinates
T : the total kinetic energy of the system
V : the total potential energy of the system
L : the Lagrangian
Π : the power supplied to the system
Δ : the dissipation function

Let T_c, T_s, T_r and T_p denote the kinetic energies of the carrier, the sun, the ring and the planet gears, respectively, and n the number of planet gears, the total kinetic energy of the system is given by

$$T = T_c + T_s + T_r + nT_p \tag{2.8}$$

where

$$T_c = \frac{1}{2} I_c \omega_c^2 \tag{2.9a}$$
$$T_s = \frac{1}{2}\left(I_{s_1} + I_{s_2}\right)\omega_s^2 \tag{2.9b}$$
$$T_r = \frac{1}{2} I_{r_1} \omega_{r_1}^2 + \frac{1}{2} I_{r_2} \omega_{r_2}^2 \tag{2.9c}$$
$$T_p = \frac{1}{2} m_{p_1} v_{p_1}^2 + \frac{1}{2} I_{p_1} \omega_{p_1}^2 + \frac{1}{2} m_{p_2} v_{p_2}^2 + \frac{1}{2} I_{p_2} \omega_{p_2}^2 \tag{2.9d}$$

with

$$v_{p_1} = v_{p_2} = r_c \omega_c \tag{2.10}$$

Since all elements are considered as rigid bodies in our model, the total potential energy of the system remains constant.[2] The external torques applied to the transmission include

[2]Note that all the nonlinearities, flexibilities and dry friction that have been neglected in the model are included in the disturbance applied to the transmission, which should also be estimated.

τ_d : drive torque of an EM applied to the input shaft

τ_l : external load applied to the output shaft

τ_{r_1} : torque of the first clutch applied to the first ring

τ_{r_2} : torque of the second clutch applied to the second ring

Therefore, under the assumption of an underdrive gear train, the power supplied to the system can be expressed as

$$\Pi = \tau_d \omega_s + \tau_l \omega_c + \tau_{r_1} \omega_{r_1} + \tau_{r_2} \omega_{r_2} \tag{2.11}$$

The dissipation function can also be written as

$$\Delta = \frac{1}{2} c_c \omega_c^2 + \frac{1}{2} c_s \omega_s^2 \tag{2.12}$$

with c_c and c_s denoting the resultant damping coefficients obtained from experiments, including the effects of all bearings and friction.

Finally, after substitution of Eqs. (2.8)–(2.12) into Eq. (2.7), and using Eqs. (2.2)–(2.4), the mathematical model of the transmission system is given below.

$$A_0 \dot{\omega}_c + B_0 \dot{\omega}_s = \tau_d - c_s \omega_s - \frac{r_{s_1}}{r_{r_1}} \tau_{r_1} - \frac{r_{s_2}}{r_{r_2}} \tau_{r_2} \tag{2.13a}$$

$$C_0 \dot{\omega}_c + D_0 \dot{\omega}_s = \tau_l - c_c \omega_c + \frac{2 r_c}{r_{r_1}} \tau_{r_1} + \frac{2 r_c}{r_{r_2}} \tau_{r_2} \tag{2.13b}$$

where A_0, B_0, C_0 and D_0 indicate the generalized inertias.

2.2.3 External Disturbance Applied to the Transmission

In this subsection, the external disturbance $\tau_l(t)$ applied to the output shaft of the transmission is studied. The external disturbance mostly originates from the road, aerodynamics and gravity. For the representation of the force between road and tire, there are semi-empirical models that are based on the measured data as well as the structures originating from physical models. In other words, tables of measured data have been applied together with interpolation schemes to improve the accuracy of the constitutive equations used for force modelling. Unlike a rigid, undeformable wheel, the tires of a vehicle deform due to the vertical load applied; the wheel contacts the road over a non-zero footprint area, called the contact patch. According to experimental results, the longitudinal tire force F_x depends on the slip ratio, which is defined below, the normal load F_z on the tire, and the friction coefficient of the tire-road interface. The tire normal load comes from a portion of the weight of the

vehicle. This normal force is influenced by fore-aft location of the mass centre, vehicle longitudinal acceleration, aerodynamic drag forces and grade of the road. The longitudinal force and the normal force are shown in Fig. 2.4. The longitudinal *slip ratio* is defined as

$$\sigma_x = \frac{r_w\omega_w - V_x}{V_x}; \quad \text{during braking} \tag{2.14a}$$

$$\sigma_x = \frac{r_w\omega_w - V_x}{r_w\omega_w}; \quad \text{during acceleration} \tag{2.14b}$$

Figure 2.4: Tire-road contact

where r_w and ω_w indicate the radius and the angular velocity of the wheel, respectively, and V_x is the longitudinal vehicle velocity. Assuming the friction coefficient of the tire-road interface and the normal force to be constant, if the longitudinal slip ratio is small, less than 0.1, the longitudinal tire force is proportional to the slip ratio, namely,

$$F_x = C_\sigma \sigma_x, \quad |\sigma_x| < 0.1 \tag{2.15}$$

where C_σ is the longitudinal tire stiffness. Note that F_x and C_σ have the same units, in Newtons, since σ_x is dimensionless. If the longitudinal slip ratio is not small enough or the road is slippery, a more sophisticated nonlinear tire model will be required to calculate the longitudinal tire force. In this case, the Pacejka "magic formula" for the tire model [78] can be used, i.e.,

$$F_x = y(x) + S_v \tag{2.16}$$

with

$$y(x) = D\sin\left\{C\arctan\left[Bx - E\left(Bx - \arctan Bx\right)\right]\right\}, \quad x = \sigma_x - S_h \tag{2.17}$$

where B, C, D, E, S_v and S_h denote the dimensionless stiffness factor, the shape factor, the peak value, the curvature factor, the horizontal shift and the vertical shift, respectively. Numerical values of these parameters have been found experimentally.

Furthermore, the equivalent aerodynamic drag force applied to a vehicle is given by [79, 77]

$$F_{aero} = \frac{1}{2}\rho C_d A_f V_{rel}^2, \quad V_{rel} = V_x + V_{wind} \tag{2.18}$$

with ρ, C_d, A_f, V_{rel} and V_{wind} denoting the density of the air, the aerodynamic drag coefficient, the frontal area of the vehicle (the projected area of the vehicle in the direction of travel), the relative velocity, and the wind velocity (positive for a headwind and negative for a tailwind), respectively.

Finally, the gravity force can be represented as [79, 77]

$$F_g = m_v g\sin(\theta_r) + K_r m_v g\cos(\theta_r) \tag{2.19}$$

where m_v, g, θ_r and K_r represent the mass of the vehicle, the gravity acceleration, the road inclination and the tire rolling resistance, respectively.

For control purposes, such as state-feedback, the unmeasurable states and inputs of the system should be estimated, which will be investigated in Section 2.3.

2.3 Estimation of the Transmission System

This section is devoted to the process of estimating the system. First, the process and measurement models are provided. Afterwards, a brief description of the Kalman-filter algorithm, the Luenberger observer and NNs are given. The methods are used to estimate the states, the unknown arbitrary disturbance and the unknown input to the system.

Upon letting $x_1(t) = \omega_c(t)$ and $x_2(t) = \omega_s(t)$ denote the state variables of the system, under no external load applied to the system, the process and measurement models are displayed below.

$$\dot{\mathbf{x}}(t) = \mathbf{A}\mathbf{x}(t) + \mathbf{B}(\mathbf{u}(t) + \mathbf{w}(t)) \tag{2.20a}$$

$$y(t) = \mathbf{c}^T\mathbf{x}(t) + v(t) \tag{2.20b}$$

where $\mathbf{w}(t)$ and $v(t)$ denote the process noise and the measurement noise, while the input is denoted by $\mathbf{u}(t) = \begin{bmatrix}\tau_{r_1}(t) & \tau_{r_2}(t) & \tau_d(t)\end{bmatrix}^T$. Herein, it is assumed that the only available measurement is $\omega_c(t)$, i.e. $\mathbf{c}^T = \begin{bmatrix}1 & 0\end{bmatrix}$. Also, $\mathbf{A}$ and $\mathbf{B}$ are constant, 2×2 and 2×3 matrices, namely,

$$\mathbf{A} = \begin{bmatrix} -0.3448 & -0.9196 \\ -0.9196 & -6.1311 \end{bmatrix}, \quad \mathbf{B} = \begin{bmatrix} 0.0336 & 7.6699 & 17.2394 \\ -110.2022 & -40.9364 & 45.9798 \end{bmatrix} \tag{2.21}$$

Note that the entries of $\mathbf{A}$ and $\mathbf{B}$ depend on the system parameters given in Eq. (2.13), such as the generalized inertias, damping coefficients and radii of the elements. Estimating the states of the system, i.e. $\omega_c(t)$ and $\omega_s(t)$, one can obtain the angular velocities of the rings from Eqs. (2.5).

Approximating $\dot{\mathbf{x}}(t_k) \approx (\mathbf{x}_k - \mathbf{x}_{k-1}) \,/\, T$, where T denotes the sampling time, the discrete-time state-space model is

$$\mathbf{x}_k = \mathbf{F}_{k-1}\mathbf{x}_{k-1} + \mathbf{G}_{k-1}\mathbf{u}_{k-1} + \mathbf{L}_{k-1}\mathbf{w}_{k-1} \tag{2.22a}$$

$$y_k = \mathbf{h}_k^T\mathbf{x}_k + M_k v_k \tag{2.22b}$$

where $\mathbf{F}_{k-1} = \mathbf{1} + T\mathbf{A}$, $\mathbf{G}_{k-1} = T\mathbf{B}$, $\mathbf{L}_{k-1} = T\mathbf{B}$, $\mathbf{h}_k = \mathbf{c}$ and $M_k = 1$.

2.3.1 Kalman Filter and Luenberger Observer

Assuming a constant sampling time T, the system can be proven to be completely observable (CO). Additionally, the system is linear and autonomous (or time-invariant). Hence, the Kalman filter, which is the best linear unbiased estimator (BLUE), is applied for estimation. Assuming $\mathbf{w}_k \sim \mathcal{N}(\mathbf{0}, \mathbf{Q}_k)$ and $\mathbf{v}_k \sim \mathcal{N}(\mathbf{0}, \mathbf{R}_k)$, i.e., Gaussian (normal) distributions with zero mean and covariances $\mathbf{Q}_k$ and $\mathbf{R}_k$, after initialization, the Kalman-filter algorithm for a multi-input-multi-output (MIMO) system with $\mathbf{y}_k = \mathbf{H}_k\mathbf{x}_k + \mathbf{M}_k\mathbf{v}_k$ is summarized in two steps:

- Prediction:

$$\hat{\mathbf{x}}_k^- = \mathbf{F}_{k-1}\hat{\mathbf{x}}_{k-1} + \mathbf{G}_{k-1}\mathbf{u}_{k-1} \tag{2.23a}$$

$$\mathbf{P}_k^- = \mathbf{F}_{k-1}\mathbf{P}_{k-1}\mathbf{F}_{k-1}^T + \mathbf{L}_{k-1}\mathbf{Q}_{k-1}\mathbf{L}_{k-1}^T \tag{2.23b}$$

- Correction:

$$\mathbf{V}_k = \mathbf{H}_k\mathbf{P}_k^-\mathbf{H}_k^T + \mathbf{M}_k\mathbf{R}_k\mathbf{M}_k^T \tag{2.24a}$$

$$\mathbf{K}_k = \mathbf{P}_k^-\mathbf{H}_k^T\mathbf{V}_k^{-1} \tag{2.24b}$$

$$\hat{\mathbf{x}}_k = \hat{\mathbf{x}}_k^- + \mathbf{K}_k(\mathbf{y}_k - \hat{\mathbf{y}}_k^-) \tag{2.24c}$$

$$\begin{aligned} \mathbf{P}_k &= (\mathbf{1} - \mathbf{K}_k\mathbf{H}_k)\mathbf{P}_k^-(\mathbf{1} - \mathbf{K}_k\mathbf{H}_k)^T + \mathbf{K}_k\mathbf{M}_k\mathbf{R}_k\mathbf{M}_k^T\mathbf{K}_k^T \\ &= \mathbf{P}_k^- - \mathbf{K}_k\mathbf{H}_k\mathbf{P}_k^- - \mathbf{P}_k^-\mathbf{H}_k^T\mathbf{K}_k^T + \mathbf{K}_k\mathbf{V}_k\mathbf{K}_k^T \end{aligned} \tag{2.24d}$$

where $\mathbf{P}_k$ is the covariance of the error and $\mathbf{K}_k$ denotes the Kalman gain.

The Luenberger observer for the discrete-time system is summarized as

$$\hat{\mathbf{x}}_k = \mathbf{F}\hat{\mathbf{x}}_{k-1} + \mathbf{G}\mathbf{u}_{k-1} + \mathbf{L}_l\left(\mathbf{y}_k - \hat{\mathbf{y}}_k\right) \tag{2.25a}$$

$$\hat{\mathbf{y}}_k = \mathbf{H}\hat{\mathbf{x}}_k \tag{2.25b}$$

where $\mathbf{L}_l$ is the Luenberger observer gain. The observer is asymptotically stable if the observer error $\mathbf{e}_k = \mathbf{x}_k - \hat{\mathbf{x}}_k$ converges to zero when $k \to \infty$. For the Luenberger observer, the error satisfies $\mathbf{e}_k = (\mathbf{F} - \mathbf{L}_l\mathbf{H})\,\mathbf{e}_{k-1}$. Therefore, the observer for the discrete-time system is asymptotically stable if and only if all the eigenvalues of the matrix $\mathbf{F} - \mathbf{L}_l\mathbf{H}$ lie inside the unit circle.

2.3.2 Disturbance and Clutch Torque Estimation

Now we assume that an unknown external load $\tau_l(t)$ is applied to the output shaft. In this case, the external load, i.e., the disturbance, should also be estimated, since it cannot be measured directly. Also, assuming the second clutch to be engaged, there is no sensor to measure the torque of the clutch; it should be estimated, too. Therefore, considering the disturbance and the clutch torque as states, the new process model can be written as

$$\dot{\mathbf{x}}(t) = \mathbf{A}\mathbf{x}(t) + \mathbf{b}u(t) + \mathbf{S}\mathbf{w}(t) \tag{2.26}$$

where

$$\mathbf{x}(t) = \begin{bmatrix} \omega_c(t) \\ \omega_s(t) \\ \tau_{r_2}(t) \\ \tau_l(t) \end{bmatrix}, \quad u(t) = \tau_d(t) \tag{2.27}$$

and

$$\mathbf{A} = \begin{bmatrix} -0.3448 & -0.9196 & 7.6699 & 45.9798 \\ -0.9196 & -6.1311 & -40.9364 & 306.5569 \\ 0 & 0 & 0 & 0 \\ 0 & 0 & 0 & 0 \end{bmatrix}, \quad \mathbf{b} = \begin{bmatrix} 17.2394 \\ 45.9798 \\ 0 \\ 0 \end{bmatrix}, \quad \mathbf{S} = \begin{bmatrix} 17.2394 & 0 & 0 \\ 45.9798 & 0 & 0 \\ 0 & 1 & 0 \\ 0 & 0 & 1 \end{bmatrix} \tag{2.28}$$

Herein, to write the process model, it is assumed that the disturbance and torque of the clutch are constant but noisy. For the system to be CO, angular velocities of both the input and the output shafts should be measurable directly. In other words, the output $\mathbf{y}(t)$ should be

$$\mathbf{y}(t) = \mathbf{C}\mathbf{x}(t) + \mathbf{v}(t) \tag{2.29}$$

with

$$\mathbf{C} = \begin{bmatrix} 1 & 0 & 0 & 0 \\ 0 & 1 & 0 & 0 \end{bmatrix}, \quad \mathbf{v}(t) = \begin{bmatrix} v_1(t) \\ v_2(t) \end{bmatrix} \tag{2.30}$$

2.3.3 Neural Networks

Machine learning (ML) is a branch of computer science. In fact, ML provides computers with the ability to learn without being explicitly programmed. Evolved from pattern recognition and computational learning theory in artificial intelligence (AI), ML focuses on the algorithms that can learn from collected data and make predictions or decisions on new data. An ML method that operates based on the way the brain solves problems, with large clusters of biological neurons connected by axons, is termed neural networks (NNs). In NNs, each individual neural unit, connected with many others, has a transfer function whose input is the weighted summation of the values of all the connected input neurons plus a bias. NNs typically include an input layer, some hidden layers and an output layer, as depicted in Fig. 2.5. Back propagation (BP) is a supervised learning technique in which the output error is applied to tune the weights and biases. BP is commonly used in conjunction with an optimization method, such as steepest descent. In BP, the gradient of the error function with respect to all the weights and biases in the network is calculated to update the weights and biases, in an attempt to minimize the loss function. The BP algorithm is now outlined, based on the nomenclature included below:

x_j^l : the input to node j of layer l
w_{ij}^l : the weight from node i of layer $l-1$ to node j of layer l
θ_j^l : the bias of node j of layer l
$\sigma(x)$: the transfer function
o_j^l : the output of node j of layer l
t_j : the target value of node j of the output layer

Given a set of training data, the loss function can be expressed as

$$E = \frac{1}{2}\sum_k (o_k - t_k)^2 \quad \rightarrow \quad \min_{\mathbf{w}_n} \tag{2.31}$$

with o_k and t_k indicating the output and the target values of node k of the output layer, respectively. The objective is to minimize the loss function w.r.t. the weights arrayed in vector $\mathbf{w}_n$. To this end, after simplification, for the output layer we have

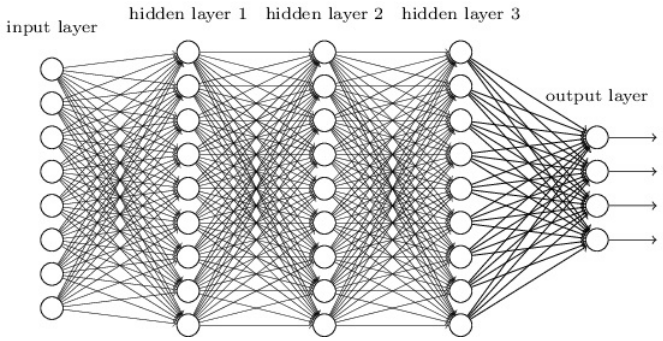

Figure 2.5: Schematic diagram of a multilayer neural network

$$\frac{\partial E}{\partial w_{jk}} = \frac{\partial}{\partial w_{jk}} \frac{1}{2} \sum_k (o_k - t_k)^2 = o_j \delta_k, \quad \delta_k = o_k(1 - o_k)(o_k - t_k) \tag{2.32}$$

Similarly, using the chain rule, for the hidden layers we obtain

$$\frac{\partial E}{\partial w_{ij}} = o_i \delta_j, \quad \delta_j = o_j(1 - o_j) \sum_k \delta_k w_{jk} \tag{2.33}$$

Finally, since $\partial o_k / \partial \theta = 1$, for the bias term θ in any layer l,

$$\frac{\partial E}{\partial \theta} = \delta_l \tag{2.34}$$

Hence, according to the steepest-descent algorithm [80], the weights and biases are updated according to

$$w \leftarrow w + \Delta w, \quad \theta \leftarrow \theta + \Delta \theta \tag{2.35}$$

with

$$\Delta w = -\eta \delta_l o_{l-1}, \quad \Delta \theta = -\eta \delta_l \tag{2.36}$$

where η is a small positive constant gain.

NNs can be applied to tune the weights and biases corresponding to the collected data, i.e., the measured output and the state values. Next, knowing the output values, one can find the unknown state values using the trained NNs. In our application, the input and target data to the network are the measured output values, i.e., $\omega_c(t)$ and/or $\omega_s(t)$, and the state values, respectively. The network is then trained using experimental data and the NN toolbox in MATLAB. The mean square error is applied to evaluate the performance of the trained network. About 75%, 15% and 10% of the samples are used as the training, validation and testing data, respectively. The number of hidden layers is chosen to be 15.

2.4 Simulation Results

This section includes simulation results obtained from the Kalman filter, the Luenberger observer and NNs for estimation of the system states, disturbances and clutch torques. The results are reported and compared for the methods.

Assuming no external load is applied to the system and the only measurable state is the first one, the results of the above techniques to estimate the states of the system are included in Figs. 2.6(a)–(d). The estimation results are compared in Figs. 2.6(a) and (b), while the estimation errors for the Kalman filter with the square root of their variance σ_k, $\pm 3\sigma_k$ bounds, are depicted in Figs. 2.6(c) and (d), which demonstrate the acceptability of the errors. As shown in the figures, the Kalman filter provides much better results, since, compared to the Luenberger observer, it considers the covariances of the noise of the process and measurement models. Moreover, according to the error covariance, the Kalman gain is updated during the estimation, while the Luenberger observer gain remains constant. As well, compared to the NNs, the Kalman filter is more accurate since it is based on the mathematical model. Nonetheless, the results of NNs are more accurate at the beginning. Note that, in simulation, the output values, i.e. $\mathbf{y}_k$, are generated artificially from Eqs. (2.22a) and (2.22b) using $\mathbf{w}_k \sim \mathcal{N}(\mathbf{0}, \mathbf{Q}_k)$ and $\mathbf{v}_k \sim \mathcal{N}(\mathbf{0}, \mathbf{R}_k)$, while in experiments, output values are measured directly. In other words, using measured outputs from the experiments, covariance matrices $\mathbf{Q}_k$ and $\mathbf{R}_k$ must be found to be used in the Kalman-filter algorithm.

Now, assuming a noisy constant disturbance applied to the output shaft, for a CO system, both angular velocities of the input and output shafts must be available. Simulation results to estimate the states, the unknown disturbance and the unknown clutch torque are depicted in Figs. 2.7(a)–(d).

Even if the disturbance is not constant, it can be estimated. The results of the above-mentioned algorithms to estimate various loads, such as linear, parabolic, sinusoidal, and arbitrary, are indicated in Figs. 2.8(a)–(d). Note that it is assumed that all loads are noisy.

2.5 Experimental Work

The system under study is a novel MST designed for EVs, consisting of a four-stage planetary gear set with spur gears[3]; two overdrive and two underdrive gear ratios. The ratios of the pitch diameters of the gears on the input and output sides are different in order to provide different gear ratios, i.e., different output speeds. Four clutches are used in the transmission, as control inputs, for engagement of the rings at each stage. The mechanism of the clutches designed for this purpose are represented in Figs. 2.9(a) and (b). The power of the motor is transmitted to the fingers through a double threaded rod acting as a power screw, converting the rotational motion into the translational motion. Hence,

[3]Spur, instead of helical gears, are used because of our own design constraints.

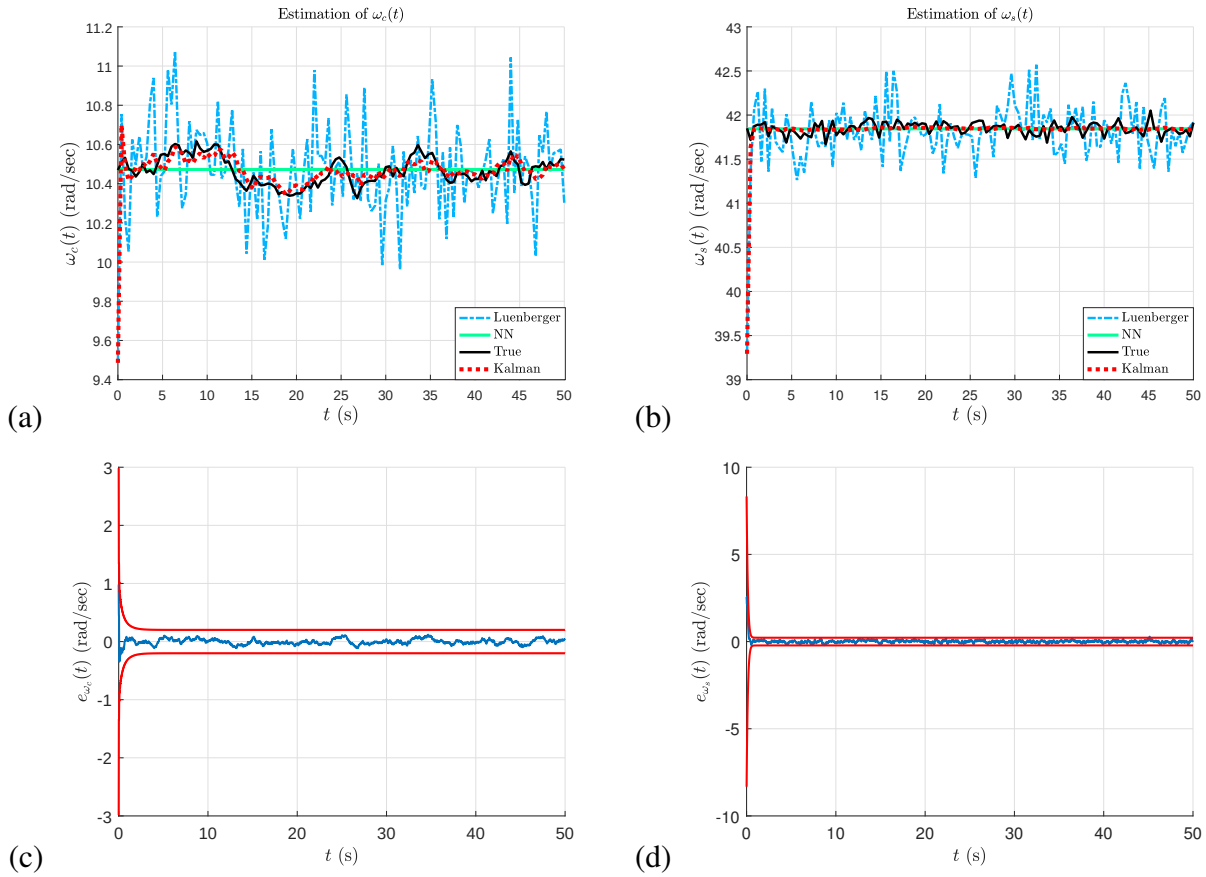

Figure 2.6: Estimation under no external load applied and $\mathbf{c}^T = [1 \quad 0]$: (a) for $\omega_c(t)$; (b) for $\omega_s(t)$; (c) error for $\omega_c(t)$ with $\pm 3\sigma_k$ bounds; and (d) error for $\omega_s(t)$ with $\pm 3\sigma_k$ bounds

to open or close the clutch, the motor should turn in different directions. To reduce the friction and achieve a smooth motion, the plastic-base fingers slide on a metal rail. In the proposed MST, the transmission is permanently connected to the EM and the final drive. Thus, there is no clutch or torque converter to disconnect the mechanical coupling during gear-shifting. Hence, in order to cancel the torque interruption and reduce fluctuations on the output, the torque of the EM should also be controlled during gear-shifting.

The transmission testbed manufactured in our lab is shown in Fig. 2.10. Each planetary gear set includes three planet gears. Note that all suns rotate at the same angular velocity, since they are attached to the same shaft. Also, all planet gears are installed on the same carrier, which is connected to another shaft. The output of the system is the angular velocity of the output shaft. Depending on the operation mode, overdrive or underdrive speed ratios, one of the friction clutches is engaged, i.e., the input and output shafts are attached either to the sun gears or to the carrier. In the former, the input and output shafts are attached to the carrier and to the sun gears, respectively; the latter operates the other way around. The inputs of the system include the torque of the EM applied to the

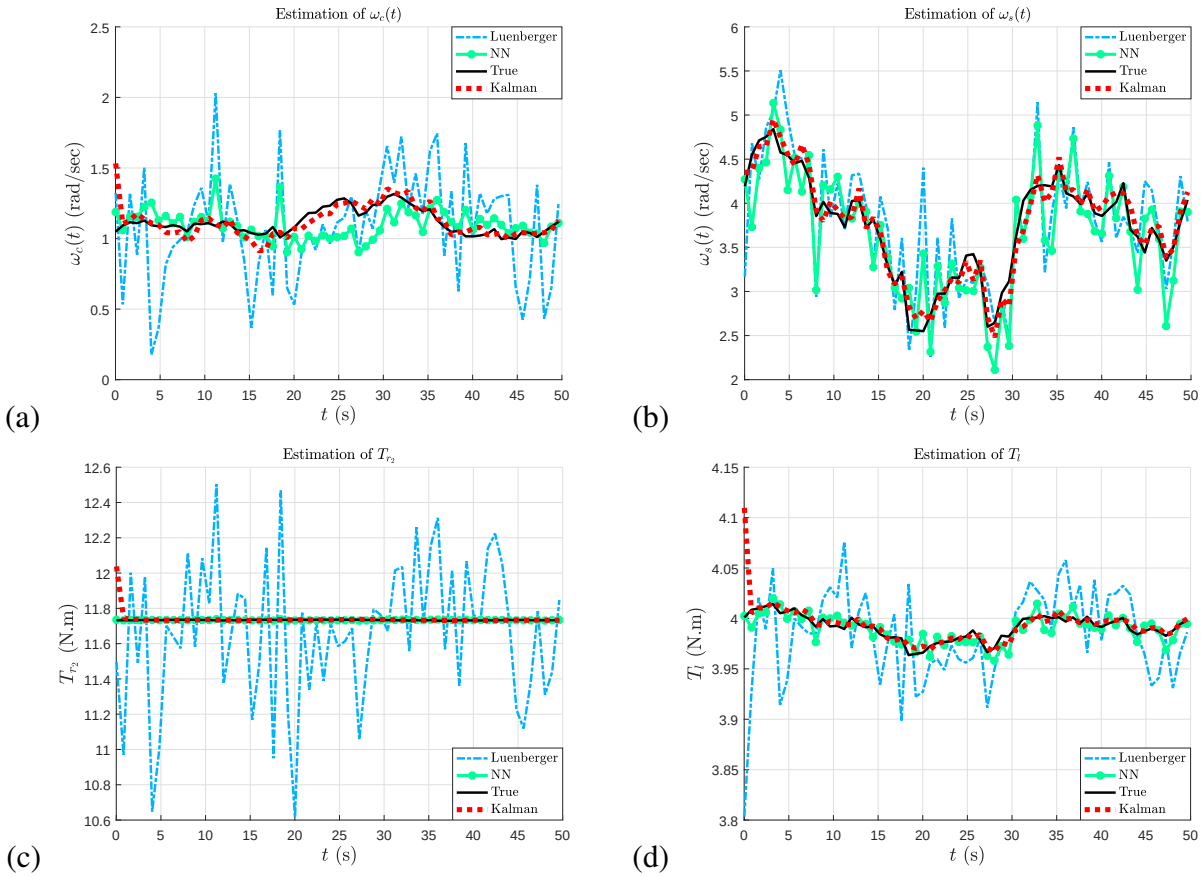

Figure 2.7: Estimation in the presence of a noisy constant disturbance for: (a) $\omega_c(t)$; (b) $\omega_s(t)$; (c) the clutch torque $\tau_{r_2}(t)$; and (d) the disturbance $\tau_l(t)$

input shaft and the torques of the clutches applied to the rings for engagement or disengagement. Different speed ratios are achieved by engaging or disengaging the rings by means of clutches. Two Glentek brushless servomotors, GMBM80550-45, are employed to apply the torque to the input shaft and simulate the external disturbance, with the specifications indicated in Table 2.2 in the Appendix. The parameters of the servomotors should be tuned using the software called Motion Maestro, provided by the same company. The encoders are also included beside the servomotors to measure the angular velocities. To drive the servomotors, Glentek omega series digital amplifiers, SMA9807-2A-2, shown in Fig. 2.11(a), are adopted. The amplifiers are used for both controlling and calibrating the servomotors and the encoders. MATLAB is applied for communication between the PC and the data-acquisition (DAQ) board and the amplifiers. The DAQ board used here is Q8 hardware-in-the-loop (HIL) control board, supplied by Quanser, depicted in Fig. 2.11(b). In fact, the DAQ board is used for commanding the motors and receiving data from encoders.

As an example, assuming that only one sensor is available to measure the angular velocity of the input, Figs. 2.12(a) and (b) represent the results obtained with the Kalman filter, the Luenberger

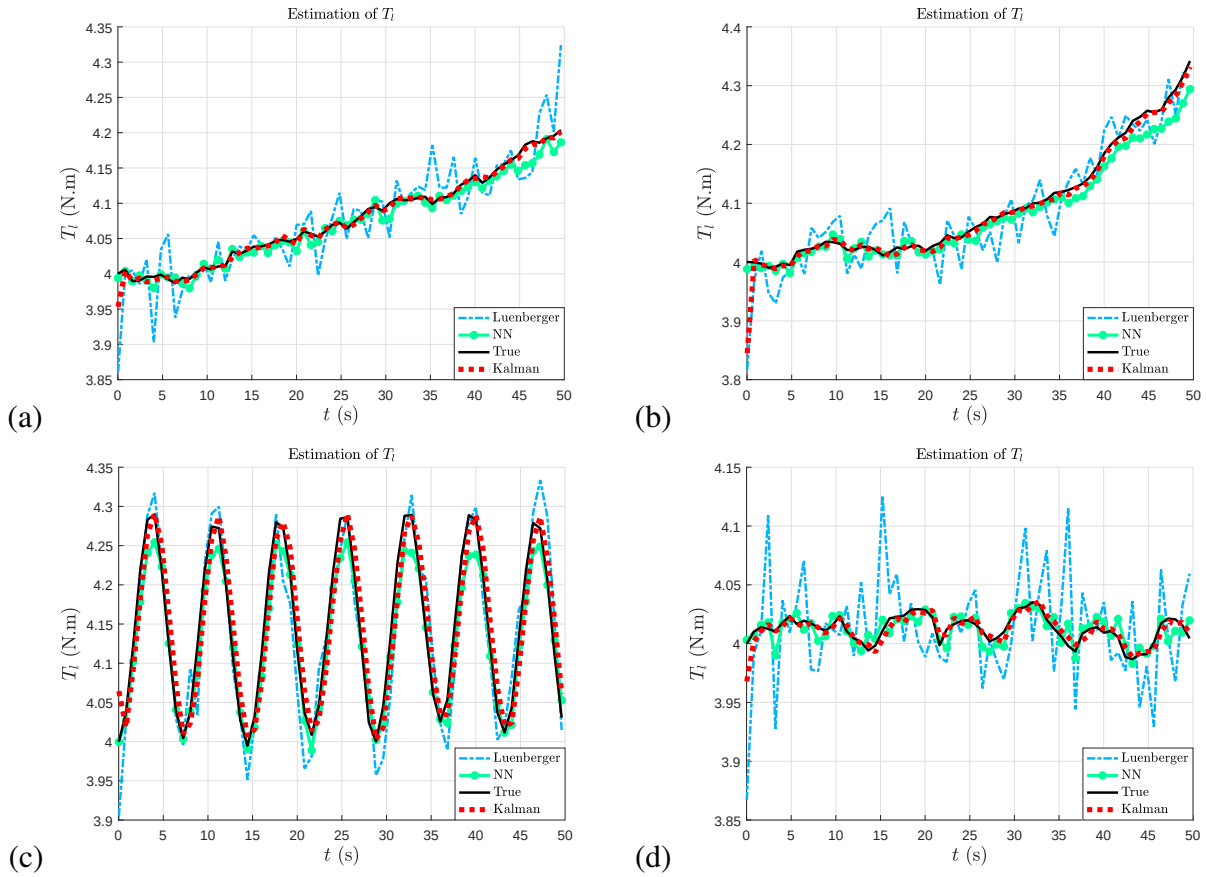

Figure 2.8: Estimation of various unknown disturbances applied: (a) a linear disturbance; (b) a parabolic disturbance; (c) a sinusoidal disturbance; and (d) an arbitrary disturbance

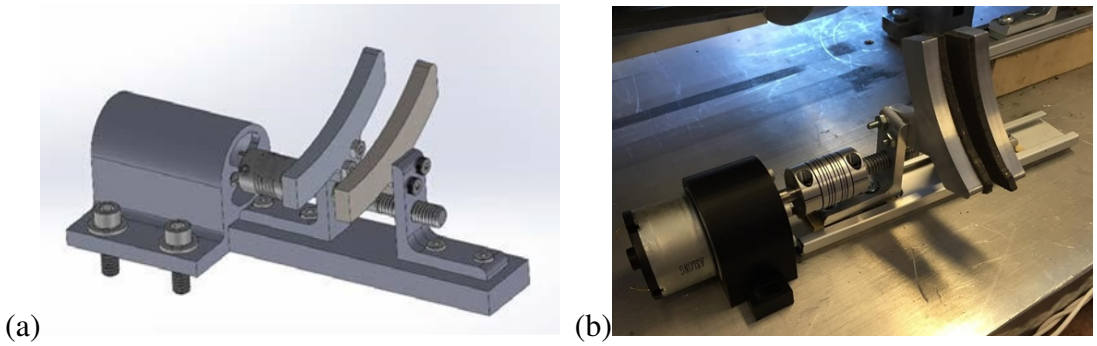

Figure 2.9: The designed ring gear clutch: (a) in SolidWorks; and (b) the manufactured one

observer and NNs to estimate the true state values coming from experiments. As expected, the Kalman filter provides more accurate results because of the reasons mentioned in Section 2.4. Additionally, the results of NNs are better than those of the Luenberger observer. Actual values of the system parameters can be found in Table 2.3 in the Appendix.

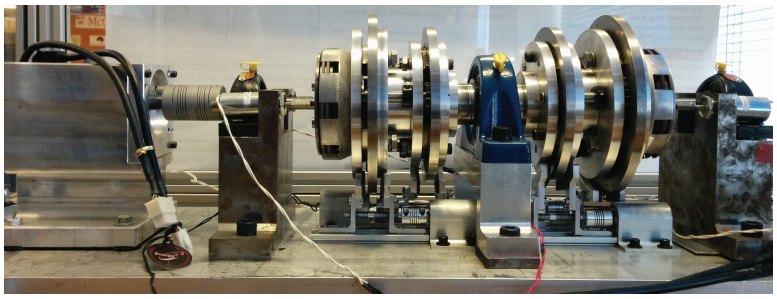

Figure 2.10: The transmission testbed

(a)  (b) 

Figure 2.11: The electronic components: (a) Glentek omega series digital amplifiers; and (b) Q8 HIL control board

(a) 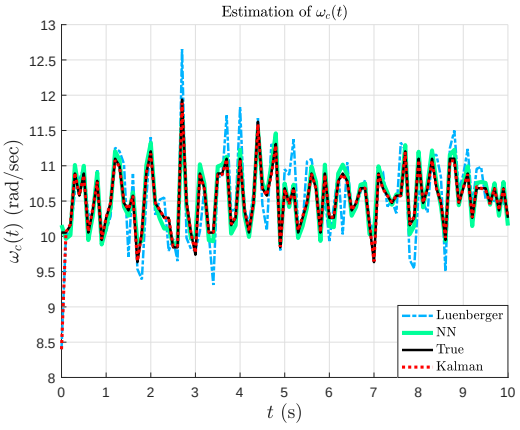

(b) 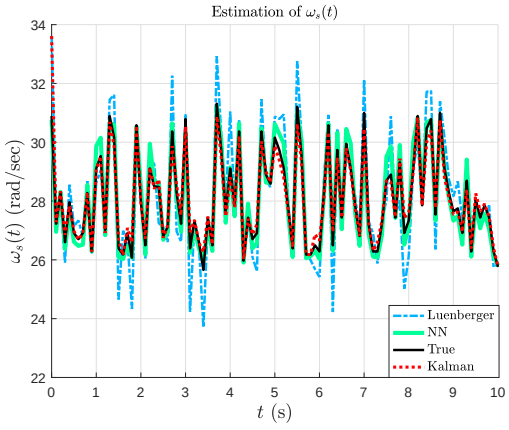

Figure 2.12: Comparison of estimated signals with experimental measurements for: (a) $\omega_c(t)$; and (b) $\omega_s(t)$

2.6 Conclusions

The mathematical modelling and estimation algorithms of a novel MST designed for EVs were investigated. First, using a Lagrangian formulation, the dynamics model of the proposed transmission system was developed. Subsequently, after finding the state-space model, the Kalman filter, the Luenberger observer and neural networks (NNs) were employed to estimate the unmeasurable states, the unknown arbitrary disturbance and the unknown clutch torque applied to the system. The

algorithms were evaluated by applying various disturbances to the system, such as linear, parabolic, sinusoidal, and arbitrary. Results showed that the Kalman filter has a better performance than the two other methods. Moreover, NNs outperform the Luenberger observer. Using the transmission testbed built in our lab, experimental results validated the simulation results [81].

Appendix

Table 2.2: Servomotor specifications

Rating	Value
rated power	550 W
rated speed	2000 rpm
max. speed	3000 rpm
cont. stall rating	2.68 N.m
peak stall torque	8.03 N.m
peak stall current	11.4 A
torque/current	0.70 N.m/A
volts/1000rpm	44.6 V

Table 2.3: Actual values for the system parameters

Parameter	Value	Unit		Parameter	Value	Unit
r_{p_1}	0.0239	m		I_{p_1}	9.6139×10^{-5}	kgm^2
r_{p_2}	0.0119	m		I_{p_2}	5.8210×10^{-6}	kgm^2
r_c	0.0478	m		I_c	0.0121	kgm^2
r_{r_1}	0.0716	m		I_{r_1}	0.0132	kgm^2
r_{r_2}	0.0597	m		I_{r_2}	0.0082	kgm^2
r_{s_1}	0.0239	m		I_{s_1}	9.6139×10^{-5}	kgm^2
r_{s_2}	0.0358	m		I_{s_2}	4.8909×10^{-4}	kgm^2
c_s	0.0200	Ns/m		m_{p_1}	0.2683	kg
c_c	0.0200	Ns/m		m_{p_2}	0.0540	kg

Chapter 3

The Optimal Gear-shifting for a Multi-speed Transmission System for Electric Vehicles

Abstract

Although electric vehicles (EVs) are more advantageous compared to their internal-combustion-engine (ICE) counterparts, they have failed to gain popularity because of the current state of battery technology. Research demonstrates that an EV equipped with a multi-speed transmission can provide the desired power in more than one way, and therefore, reduce the energy consumption of the vehicle through gear-shifting. However, gear-shifting should be as swift and seamless as possible. We investigate the gear-shifting of a multi-speed transmission for EVs with optimum performance under functional constraints. After deriving the kinematics of the transmission, calculus of variations is employed to find the schedules of the angular velocities during gear-shifting for a swift, seamless operation, which leads to the optimal trajectory in the space of transmission angular velocities. To this end, we resort to polynomial transition functions in the time-domain. After comparing the results obtained with these polynomials, while considering the limitations of the power supply, it is concluded that what we dub the 3-4-5 polynomial offers the optimal performance. The corresponding input torques are also obtained, to guarantee the continuity of the angular velocity, acceleration and jerk. Results show that the proposed approach is highly encouraging for a smooth, swift gear-shifting.

3.1 Introduction

Internal-combustion-engine (ICE) vehicles entail various problems, first and foremost pollution. Hence, the need to find an appropriate substitute has notably increased in recent years. Hybrid electric vehicles (HEVs) and electric vehicles (EVs) are suitable substitutes for their ICE counterparts, since they are capable of operating with a much lower impact on the environment. However, EVs have failed to gain popularity because of an inherent problem, as the energy-storage capacity of electric batteries is much lower than that of fossil fuels. In other words, when the source of energy changes from ICE to electricity, for longer running time on a single charge of the battery, it is required to minimize the losses of the vehicle. Most electric vehicles on the market are equipped with one single-speed gearbox that exhibits a trade-off between efficiency and dynamic performance. It is anticipated that applying a multi-speed transmission in EVs can not only reduce the size of the motor, but also provide an appropriate balance between efficiency and dynamic performance. Research demonstrates that an electric motor equipped with a multi-speed transmission can provide the desired power in more than one way, and hence, reduce the energy consumption of the vehicle through gear-shifting [1, 5, 6, 8, 9, 7].

There are different types of multi-speed transmissions for EVs, such as automated manual transmissions (AMTs) [16, 18, 21], automatic transmissions (ATs) [10, 27, 28], dual-clutch transmissions (DCTs) [30, 36, 37], and continuously variable transmissions (CVTs) [40, 50]. These transmissions were initially designed for ICE vehicles. Since the latter cannot operate below certain speeds and their speed control during gear-shifting is challenging, the presence of clutches or torque converters is indispensable for startups, idle running and gear-shifting. For EVs this is not the case, since electric motors are speed-controllable in a wide range of operating speeds. This difference provides an opportunity to design novel transmissions for EVs without any clutches or torque converters to disconnect the mechanical coupling during gear-shifting; as a result, the losses are minimized. In fact, motor and clutches are used as control inputs in the transmission to make seamless, swift gear-shifting feasible [8, 9, 10].

Gear-shifting is one of the most significant concerns in transmission systems, since it influences passenger comfort, dynamic performance and efficiency, besides drivability[1]. The main difference between transmission systems in EVs and ICE vehicles is that electric motors are speed-controllable in a wide range of operating speeds. Consequently, instead of disconnecting the mechanical coupling by means of clutches or torque converters during gear-shifting, one can design novel transmissions for EVs, in which the input motor is also an element to be controlled so as to minimize the losses. The main purpose in gear-shift control is to make it as seamless and as swift as possible. Additionally, there are other goals to be considered, such as increasing drivability, eliminating vibrations, reducing

[1]No generally acceptable definition of the term can be cited, but it usually includes the qualitative evaluation of a powertrain, such as the degree of smoothness and steadiness.

power losses and improving efficiency, while eliminating output torque interruption. Extensive research has been conducted on each of these targets [58, 65, 66, 67].

Generally, one of the main conventional strategies for gear-shifting control is based on separating the torque and inertia phases, then controlling each phase independently. This method is mostly employed for ATs and DCTs [58, 33, 8]. However, in EVs, due to the permanent connection of the power transmission paths, torques and speeds are always dependent on each other. Hence, it is not required to separate the above-mentioned phases distinctly for control purposes. Rahimi et al. [7, 9] developed a control strategy based on this idea. Employing the time-optimal hybrid minimum principle, Pakniyat and Caines [59, 60] formulated the problem of the minimum acceleration time required for reaching a speed of 100 $\mathrm{km/h}$, or 60 mph, from the stationary state, and then, found the optimal control inputs, the optimal gear ratios, and the optimal gear-changing instants. Furthermore, Rahimi et al. [61, 62, 63] designed a deterministic Luenberger observer, a fading-memory Kalman filter, and a stochastic Kalman-Bucy filter to estimate the unmeasured states and the unknown inputs for a seamless two-speed transmission for EVs. Based on the estimation, an observer-based back-stepping controller was devised to provide a seamless gear-shifting for an EV, while tracking the optimal trajectory corresponding to the minimum shifting time [64]. Although there has been intensive research on gear-shifting, there are still lacunae in gear-shifting strategies and control.

The optimal gear-shifting of a multi-speed transmission for EVs is developed in this paper. After stating the gear-shifting problem in a multi-stage planetary gear set, variational calculus is applied to determine the optimal angular-velocity schedule during gear-shifting, which leads to the optimal trajectory. Finally, what we dub the 2-3, 3-4-5 and 4-5-6-7 polynomials are suggested to be used for a swift and seamless shift. Results validate the proposed scheme. Considering motor specifications, the 3-4-5 polynomial was found to have a better performance than the other two candidates. Hence, for a smooth and swift shift, the 3-4-5 polynomial is the candidate of choice. The torques of the electric motor and the clutches during gear-shifting are also determined using the same polynomial, which guarantees the continuity of the angular velocity, acceleration and jerk.

3.2 Gear-Shifting: Problem Statement

First, consider one planetary gear set, as shown in Fig. 3.1, consisting of a sun gear, a planet carrier, a ring gear, and some planet gears (usually two to four). The system has four generalized coordinates, i.e. angular displacements of the sun, carrier, ring and planet gears, θ_s, θ_c, θ_r and θ_p, respectively. Let ω_s, ω_c, ω_r and ω_p be the corresponding angular velocities of the foregoing elements, respectively, i.e., the time derivatives of the pertinent displacements. As well, let r_s, r_r and r_p be the pitch radii of the sun, ring and planet gears, and r_c be the radius of the planet carrier. The kinematic relations below are obtained by virtue of the pure-rolling constraints at the contact points.

$$r_r\omega_r = r_c\omega_c + r_p\omega_p, \quad r_c\omega_c = r_s\omega_s + r_p\omega_p \tag{3.1}$$

with

$$r_r = r_c + r_p, \quad r_c = r_s + r_p \tag{3.2}$$

The system thus has two degrees of freedom, since it comprises four generalized coordinates subject to two constraints, Eqs. (3.1). Combining Eqs. (3.1) and (3.2), ω_p is eliminated, thereby obtaining

$$(r_s + r_r)\,\omega_c = r_s\omega_s + r_r\omega_r \tag{3.3}$$

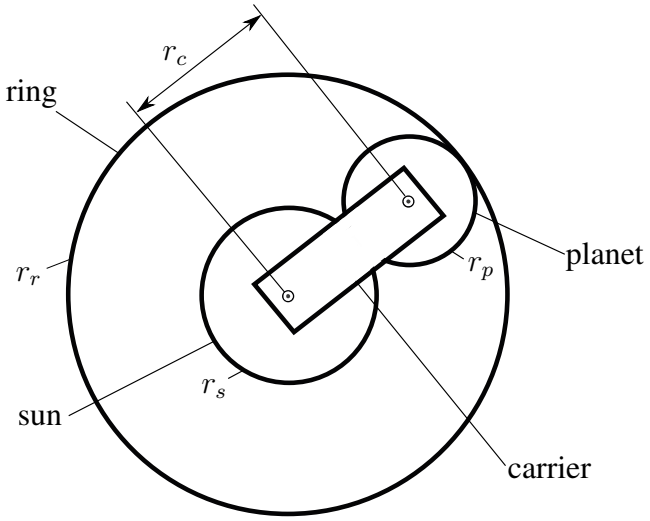

Figure 3.1: A planetary gear set

Upon assuming two planetary gear sets in the system, and letting $\nu_1 = r_{r_1}/r_{s_1}$ and $\nu_2 = r_{r_2}/r_{s_2}$, we obtain

$$\omega_{c_1} = \frac{\nu_1\omega_{r_1} + \omega_s}{\nu_1 + 1}, \quad \omega_{c_2} = \frac{\nu_2\omega_{r_2} + \omega_s}{\nu_2 + 1} \tag{3.4}$$

Note that, according to Fig. 3.2, which illustrates the overdrive and underdrive gear trains, the sun gears of all the planetary sets are attached to the same shaft. Therefore, the angular velocities of the sun gears, i.e., ω_s in the two sets, are the same. In addition, the planetary sets share the same carrier. In this light, Eqs. (3.4) lead to

$$\omega_{c_1} = \omega_{c_2} \quad \Rightarrow \quad \frac{\nu_1\omega_{r_1} + \omega_s}{\nu_1 + 1} = \frac{\nu_2\omega_{r_2} + \omega_s}{\nu_2 + 1}$$

or, equivalently,

$$(\nu_2 + 1)\,\nu_1\omega_{r_1} + (\nu_2 - \nu_1)\,\omega_s - (\nu_1 + 1)\,\nu_2\omega_{r_2} = 0 \tag{3.5}$$

which represents a plane in the space Ω of the angular velocities ω_s, ω_{r_1} and ω_{r_2}. At every instant, the system is operating at a certain point of this plane. Assuming $\nu_1 = 3$ and $\nu_2 = 5/3$, Fig. 3.3 illustrates the gear-shifting problem. The plane of motion is depicted in Fig. 3.3(a). The intersections of the planes in Figs. 3.3(b) and (c) represent the lines at which the first and the second ring gears are engaged. In fact, the gear-shifting problem reduces to devising a trajectory Γ that joins point A with point B, as depicted in Fig. 3.3(d).

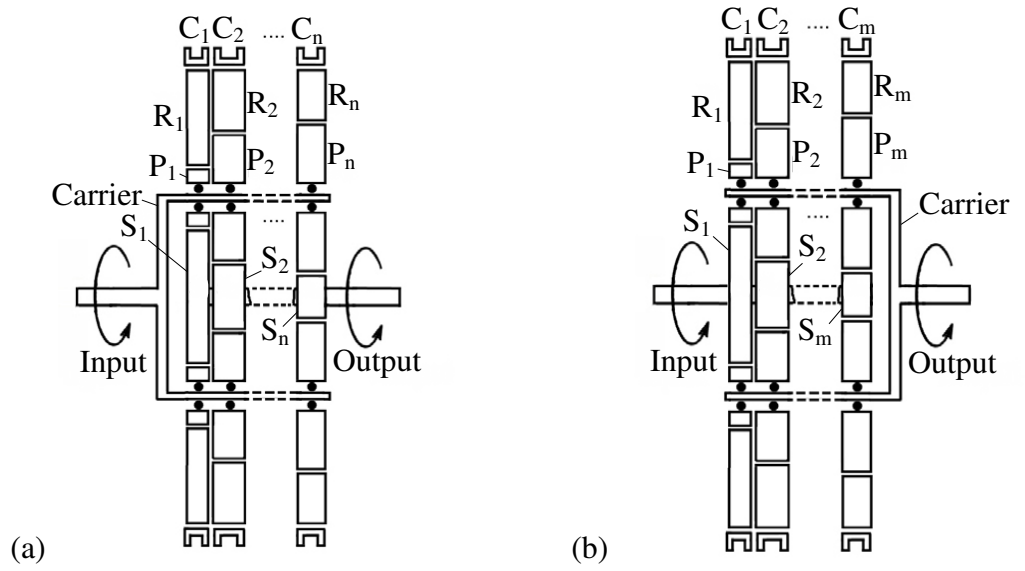

Figure 3.2: Multi-stage planetary gear sets: (a) overdrive gear train; and (b) underdrive gear train

3.3 The Optimal Gear-shifting

Trajectory-optimization problems fall in the realm of calculus of variations [70]. The Brachistochrone problem, introduced by Johann Bernoulli in 1696, is an interesting landmark within this realm. The problem consists in finding the shape of a frictionless wire, lying in a vertical plane, on which a bead slides under the gravitational field, so that the bead moves between two designated points in minimum time.

Assume that the *functional*, i.e., the performance measure to be minimized, is defined as

$$J = \int_{t_0}^{t_f} g(\mathbf{x}(t), \dot{\mathbf{x}}(t), t)dt \tag{3.6}$$

under n constraints given by

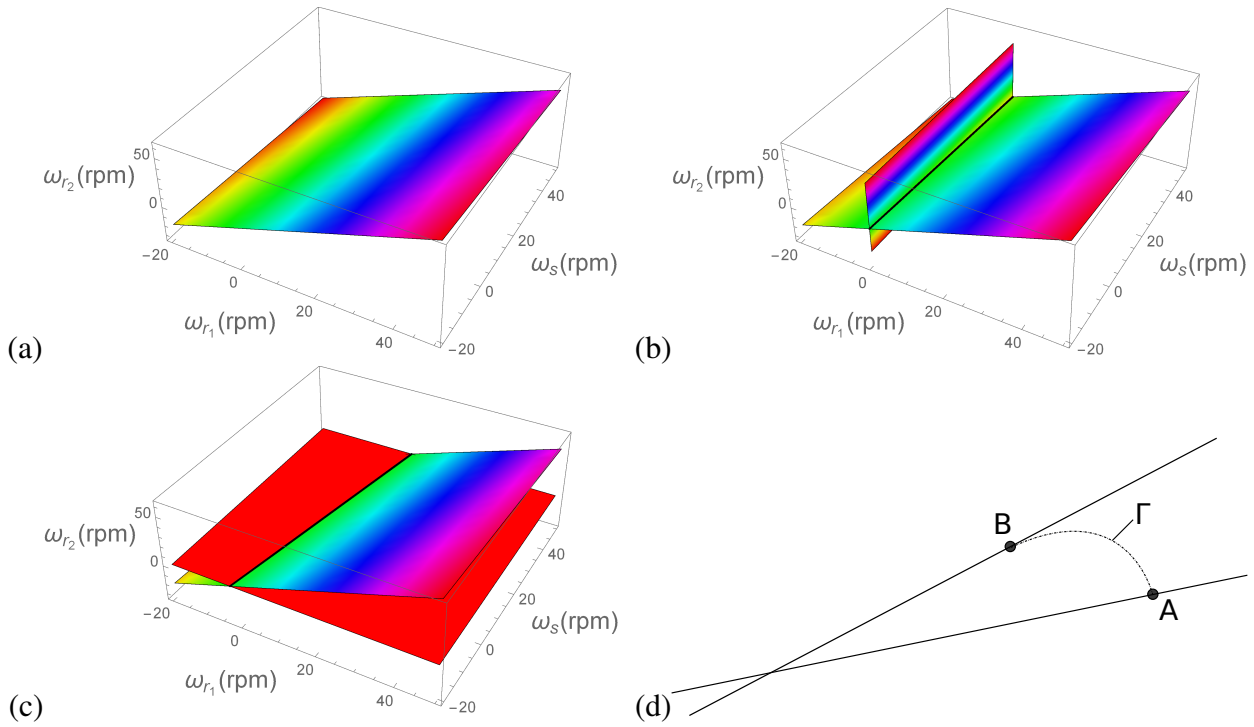

Figure 3.3: Illustration of the gear-shifting problem: (a) plane of motion; (b) first gear set engaged; (c) second gear set engaged; and (d) gear-shifting trajectory Γ

$$f_i(\mathbf{x}(t), \dot{\mathbf{x}}(t), t) = 0, \quad i = 1, 2, ..., n \tag{3.7}$$

The necessary condition for an extremal of the functional under the constraints, called the Euler equation, is

$$\frac{\partial g_a}{\partial \mathbf{x}}(\mathbf{x}(t), \dot{\mathbf{x}}(t), \mathbf{p}(t), t) - \frac{d}{dt}\left[\frac{\partial g_a}{\partial \dot{\mathbf{x}}}(\mathbf{x}(t), \dot{\mathbf{x}}(t), \mathbf{p}(t), t)\right] = \mathbf{0} \tag{3.8}$$

where

$$g_a(\mathbf{x}(t), \dot{\mathbf{x}}(t), \mathbf{p}(t), t) = g(\mathbf{x}(t), \dot{\mathbf{x}}(t), t) + \mathbf{p}^T(t)\mathbf{f}(\mathbf{x}(t), \dot{\mathbf{x}}(t), t) \tag{3.9}$$

with $\mathbf{p}(t) = [p_1(t), p_2(t), ..., p_n(t)]^T$ and $\mathbf{f}(\mathbf{x}(t), \dot{\mathbf{x}}(t), t) = [f_1, f_2, ..., f_n]^T$ denoting the vectors of Lagrange multipliers and of the constraints, respectively.

To make gear-shifting as swift and as seamless as possible, for an underdrive gear train, the performance index is defined as

$$J = \int_{t_0}^{t_f} \left\{1 + \alpha \left[\omega_c(t) - \omega_{c_0}\right]^2\right\} dt \tag{3.10}$$

where ω_{c_0} is the current angular velocity of the carrier, before gear-shifting, and α indicates a constant weight. According to the constraints (3.4), we have

$$g_a = \left\{1 + \alpha \left[\omega_c(t) - \omega_{c_0}\right]^2\right\} + p_1 \left(\omega_c - \frac{\nu_1 \omega_{r_1} + \omega_s}{\nu_1 + 1}\right) + p_2 \left(\omega_c - \frac{\nu_2 \omega_{r_2} + \omega_s}{\nu_2 + 1}\right) \tag{3.11}$$

the Euler equation for ω_c then becoming

$$\frac{\partial g_a}{\partial \omega_c} - \frac{d}{dt}\left(\frac{\partial g_a}{\partial \dot{\omega}_c}\right) = 0 \Rightarrow 2\alpha\left(\omega_c(t) - \omega_{c_0}\right) + p_1 + p_2 = 0 \tag{3.12}$$

Similarly, the Euler equations for ω_s, ω_{r_1}, and ω_{r_2} lead to

$$-\frac{p_1}{\nu_1 + 1} - \frac{p_2}{\nu_2 + 1} = 0, \quad -\frac{p_1 \nu_1}{\nu_1 + 1} = 0, \quad -\frac{p_2 \nu_2}{\nu_2 + 1} = 0 \tag{3.13}$$

Upon solving Eqs. (3.12) and (3.13) for p_1, p_2 and $\omega_c(t)$, we obtain

$$p_1 = 0, \quad p_2 = 0, \quad \omega_c(t) = \omega_{c_0} \tag{3.14}$$

As a result, we have four variables, ω_s, ω_c, ω_{r_1} and ω_{r_2}, and three constraints:

$$\omega_c = \frac{\nu_1 \omega_{r_1} + \omega_s}{\nu_1 + 1}, \quad \omega_c = \frac{\nu_2 \omega_{r_2} + \omega_s}{\nu_2 + 1}, \quad \omega_c(t) = \omega_{c_0} = \text{const.} \tag{3.15}$$

Thus, one of the variables can be freely chosen, according to our objective. Assuming $\omega_s(t)$ to be the chosen variable, the problem is to find a *blending* function $\omega_s(t)$, $t \in [t_0, t_f]$, i.e., defined over the gear-shifting interval. The function is required to be as smooth as possible, namely, it must have continuous derivatives up to some desired order in the open interval, to avoid abrupt motions and stay within the limits of the power supply. The function should also be at least of class C^1 at the ends[2], i.e., $\omega_s(t)$ and $\dot{\omega}_s(t)$ should be continuous at t_0 and t_f:

$$\omega_s(t_0) = \omega_{s_0}, \quad \dot{\omega}_s(t_0) = 0, \quad \omega_s(t_f) = \omega_{s_f}, \quad \dot{\omega}_s(t_f) = 0 \tag{3.16}$$

3.3.1 Polynomial Transition

A simple inspection of Eqs. (3.16) reveals that, since the function is required to meet four conditions, it must have at least four parameters. We thus start with a cubic polynomial.

3.3.1.1 The 2-3 polynomial

In order to represent the function $\omega_s(t)$, we use a *normal* cubic polynomial $s(\tau)$, namely,

$$s(\tau) = -2\tau^3 + 3\tau^2 \tag{3.17}$$

[2]A function $f(x)$ is said to be of class C^k if the function and its first k derivatives are continuous in a given interval.

which we call the 2-3 polynomial. The polynomial is said to be normal because it meets the conditions

$$0 \leq s(\tau) \leq 1, \quad 0 \leq \tau \leq 1, \quad \tau \equiv \frac{t - t_0}{T}, \quad T \equiv t_f - t_0 \tag{3.18}$$

Therefore, $s(\tau)$ satisfies the end-conditions

$$s(0) = 0, \quad s'(0) = 0, \quad s(1) = 1, \quad s'(1) = 0 \tag{3.19}$$

Now, $\omega_s(t)$ is represented by means of the foregoing polynomial:

$$\omega_s(t) = \Delta\omega s(\tau) + \omega_{s_0}, \quad \Delta\omega \equiv \omega_{s_f} - \omega_{s_0} \tag{3.20}$$

Hence,

$$\dot{\omega}_s(t) = \frac{\Delta\omega}{T} s'(\tau), \quad \ddot{\omega}_s(t) = \frac{\Delta\omega}{T^2} s''(\tau), \quad \dddot{\omega}_s(t) = \frac{\Delta\omega}{T^3} s'''(\tau) \tag{3.21}$$

Knowing both end-values and the time interval T, the function $\omega_s(t)$ is therefore fully defined, with T denoting the time required for gear-shifting. Thus, we have the freedom to conduct the gear-shifting in as short a time as needed. However, the time cannot be too small, for we must respect the motor specifications, such as the maximum angular velocity, jerk continuity and the maximum torque. The latter will be discussed in Subsection 3.3.3. For brevity, the maximum acceleration is considered here rather than the maximum torque. From Eq. (3.20) it is apparent that this function and its first two derivatives take on their maximum values at points corresponding to those at which the normal polynomial and its corresponding derivatives do. The latter are given below:

$$s_{\max} = s\,(1) = 1, \quad s'_{\max} = s'\left(\frac{1}{2}\right) = \frac{3}{2}, \quad s''_{\max} = s''\,(0) = 6 \tag{3.22}$$

Therefore, assuming $\Delta\omega > 0$, the maximum values of $\omega_s(t)$, $\dot{\omega}_s(t)$ and $\ddot{\omega}_s(t)$ are

$$(\omega_s)_{\max} = \omega_{s_f}, \quad (\dot{\omega}_s)_{\max} = \frac{3}{2}\frac{\Delta\omega}{T}, \quad (\ddot{\omega}_s)_{\max} = 6\frac{\Delta\omega}{T^2} \tag{3.23}$$

Hence, Eqs. (3.23) can be used to determine the minimum shifting time T according to the motor specifications.

3.3.1.2 The 3-4-5 polynomial

If, in addition to the continuity conditions of Subsection 3.3.1.1, one needs to have the second derivative of $s(\tau)$ vanish at the ends of the interval [0 , 1], we have to increase the degree of the polynomial by two, i.e.,

$$s(\tau) = 6\tau^5 - 15\tau^4 + 10\tau^3 \tag{3.24}$$

which we call the 3-4-5 polynomial [82].

According to the maximum values of the functions $s(\tau)$, $s'(\tau)$ and $s''(\tau)$, the corresponding values of $\omega_s(t)$, $\dot{\omega}_s(t)$ and $\ddot{\omega}_s(t)$ can be expressed as

$$(\omega_s)_{max} = \omega_{s_f}, \quad (\dot{\omega}_s)_{max} = \frac{15}{8}\frac{\Delta\omega}{T}, \quad (\ddot{\omega}_s)_{max} = \frac{10\sqrt{3}}{3}\frac{\Delta\omega}{T^2} \tag{3.25}$$

which can be utilized to find the minimum time T required for gear-shifting, while respecting motor specifications.

3.3.1.3 The 4-5-6-7 polynomial

If, in addition to the above conditions, the third derivative of $s(\tau)$ is required to vanish at both ends of $0 \leq \tau \leq 1$, we resort to a seventh-degree polynomial, namely,

$$s(\tau) = -20\tau^7 + 70\tau^6 - 84\tau^5 + 35\tau^4 \tag{3.26}$$

which we call the 4-5-6-7 polynomial [82].

Similarly, the extreme values of $\omega_s(t)$, $\dot{\omega}_s(t)$ and $\ddot{\omega}_s(t)$ are

$$(\omega_s)_{max} = \omega_{s_f}, \quad (\dot{\omega}_s)_{max} = \frac{35}{16}\frac{\Delta\omega}{T}, \quad (\ddot{\omega}_s)_{max} = \frac{84\sqrt{5}}{25}\frac{\Delta\omega}{T^2} \tag{3.27}$$

3.3.2 Selection of the Blending Function

A summary of the three polynomials found above follows:

$$\omega_{3s}(t) = \Delta\omega\left(-2\tau^3 + 3\tau^2\right) + \omega_{s_0} \tag{3.28a}$$

$$\omega_{5s}(t) = \Delta\omega\left(6\tau^5 - 15\tau^4 + 10\tau^3\right) + \omega_{s_0} \tag{3.28b}$$

$$\omega_{7s}(t) = \Delta\omega\left(-20\tau^7 + 70\tau^6 - 84\tau^5 + 35\tau^4\right) + \omega_{s_0} \tag{3.28c}$$

This section is devoted to the selection of the working function out of the above candidates. This can be done according to the motor specifications and our objective, to make gear-shifting as swift and as seamless as possible. Since the angular velocity of the carrier remains constant during gear-shifting, i.e. $\omega_c(t) = \omega_{c_0}$, for the three functions, the shifting is seamless. Therefore, the function with the shortest shifting time should be selected. However, the limitations of the power supply should also be considered. The angular velocity and the angular acceleration must always lie within the limits of the motor. Further, the angular jerk is desired to be continuous everywhere,

without any abrupt jumps, and as small as possible. The reason is that control engineers realized the importance of jerk for a smooth motion, to mitigate impact, suppress vibration and resonance, thereby reducing trajectory tracking errors, while providing a smoother and cooler motor operation [83]. Moreover, it is impossible for the motor to change its rotor acceleration instantly. In other words, a motor cannot change the torque instantly since the current in the armature cannot be varied instantly due to the inductance in the armature.

For all the three functions, the maximum angular velocity is the same, i.e, ω_{s_f} (or ω_{s_0}). Thus, this velocity cannot be applied as a criterion to choose the function. Assuming $\alpha_{\max}$ to be the maximum angular acceleration that the motor can supply, using Eqs. (3.23), (3.25) and (3.27), the minimum shifting times for the functions (3.28) are

$$T_{3\min} = \frac{3}{2}\frac{\Delta\omega}{\alpha_{\max}}, \quad T_{5\min} = \frac{15}{8}\frac{\Delta\omega}{\alpha_{\max}}, \quad T_{7\min} = \frac{35}{16}\frac{\Delta\omega}{\alpha_{\max}} \tag{3.29}$$

Obviously, since $\Delta\omega/\alpha_{\max}$ is the same in all three cases, we have

$$T_{3\min} < T_{5\min} < T_{7\min} \tag{3.30}$$

The 2-3 polynomial thus provides the shortest time for gear-shifting. However, the jerk corresponding to the 2-3 polynomial is not continuous at the ends; as a result, this polynomial is rejected. The 3-4-5 polynomial is the right selection, since it provides a shorter shifting time compared to the 4-5-6-7 polynomial, while its jerk vanishes at the ends of the gear-shifting interval.

3.3.3 Modelling a DC Motor

A DC motor is a common actuator in most control systems. In a DC motor, the torque τ_d supplied by the motor is related to the armature current i via the armature constant K_t, namely,

$$\tau_d = K_t i \tag{3.31}$$

the relation between the back emf e and the angular velocity ω of the rotor being

$$e = K_e \omega \tag{3.32}$$

with K_e denoting the motor constant. Moreover, the armature and motor constants are equal, i.e., $K_t = K_e = K$. Using Newton's second law and Kirchhoff's voltage law, according to Fig. 3.4, we have

$$(J_m + J_l)\dot{\omega} + b\omega = Ki \tag{3.33a}$$

$$L\frac{di}{dt} + Ri = V - K\omega \tag{3.33b}$$

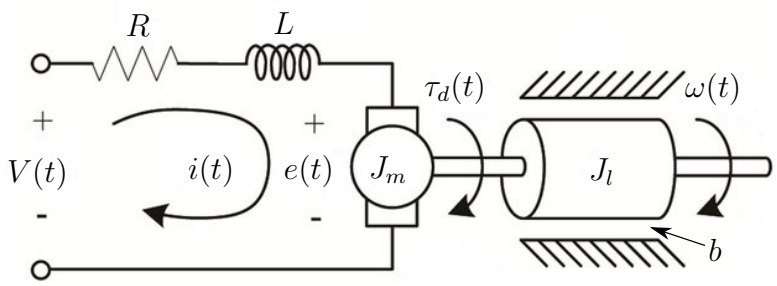

Figure 3.4: Schematic diagram of a DC motor

where J_m, J_l, b, L, R and V indicate the moment of inertia of the motor, the moment of inertia of the external load, the damping coefficient, the armature inductance, the armature resistance, and the input voltage, respectively. Combining Eqs. (3.33), after eliminating i, we obtain

$$(J_m + J_l)L\ddot{\omega} + [(J_m + J_l)R + bL]\dot{\omega} + (bR + K^2)\omega = KV \tag{3.34}$$

According to this equation, since the input voltage V is continuous, the angular jerk $\ddot{\omega}$ should also be continuous. Assuming $V(t)$ to be the input and $\omega(t)$ the output, the transfer function can be expressed as

$$\frac{\Omega(s)}{V(s)} = \frac{K}{(J_m + J_l)Ls^2 + [(J_m + J_l)R + bL]s + (bR + K^2)} \tag{3.35}$$

while the transfer function between $\Omega(s)$ and $I(s)$ is

$$\frac{\Omega(s)}{I(s)} = \frac{K}{(J_m + J_l)\,s + b} \tag{3.36}$$

Based on motor specifications and the external load, the limits for the torque, the angular velocity, the angular acceleration, the angular jerk, the current and the voltage can be determined using Eqs. (3.33–3.36).

3.4 Mathematical Model of the System

In this section, the mathematical model of the system under study is derived using a Lagrangian formulation.

The Lagrange equation of the system is given below:

$$\frac{d}{dt}\left(\frac{\partial L}{\partial \dot{\mathbf{q}}}\right) - \frac{\partial L}{\partial \mathbf{q}} = \frac{\partial}{\partial \dot{\mathbf{q}}}\left(\Pi - \Delta\right), \quad L = T - V \tag{3.37}$$

where $\mathbf{q}$, T, V, and L denote the vector of generalized coordinates, the total kinetic energy of the system, the total potential energy of the system, and the Lagrangian, respectively. As well, Π indicates the power supplied to the system by the motors delivering a controlled generalized force, and Δ is the dissipation function associated with all energy sinks in the system. For the kinetic energy, four rigid bodies intervene: carrier plus sun, ring and planet gears. In our case, the shafts are considered rigid, their moment of inertia thus being lumped with that of one of the four rigid bodies identified above. Hence, the total kinetic energy of the system becomes

$$T = T_c + T_s + T_r + nT_p \tag{3.38}$$

where T_c, T_s, T_r and T_p represent the kinetic energy of the carrier, the sun, the ring and the n planet gears, respectively. Thus,

$$T_c = \frac{1}{2} I_c \omega_c^2 \tag{3.39a}$$

$$T_s = \frac{1}{2}\left(I_{s_1} + I_{s_2}\right)\omega_s^2 \tag{3.39b}$$

$$T_r = \frac{1}{2} I_{r_1} \omega_{r_1}^2 + \frac{1}{2} I_{r_2} \omega_{r_2}^2 \tag{3.39c}$$

$$T_p = \left(\frac{1}{2} m_{p_1} v_{p_1}^2 + \frac{1}{2} I_{p_1} \omega_{p_1}^2\right) + \left(\frac{1}{2} m_{p_2} v_{p_2}^2 + \frac{1}{2} I_{p_2} \omega_{p_2}^2\right) \tag{3.39d}$$

where I_{s_1}, I_{s_2}, I_{r_1}, I_{r_2}, I_{p_1}, and I_{p_2} are the moments of inertia of the sun, ring, and planet gears of the first and the second gear sets, respectively, and I_c is the moment of inertia pertaining to the planet carrier. Moreover, m_{p_1} and m_{p_2} are the masses of each planet gear for each planetary gear set, while v_{p_1} and v_{p_2} indicate the speeds of the centers of mass of the planet gears for each planetary set, i.e.,

$$v_{p_1} = v_{p_2} = r_c \omega_c \tag{3.40}$$

Since it is assumed that the total potential energy remains constant in our model, potential energy is not considered here. This assumption is plausible under the condition that all rotating elements are statically balanced and the planet gears are symmetrically laid out. Four types of torques are applied to the system, namely,

τ_d : drive torque applied to the input shaft by an electric motor

τ_l : external load applied to the output shaft

τ_{r_1} : torque applied to the first ring by the first clutch

τ_{r_2} : torque applied to the second ring by the second clutch

Hence, assuming an underdrive gear train, the power supplied to the system is

$$\Pi = \tau_d \omega_s + \tau_l \omega_c + \tau_{r_1} \omega_{r_1} + \tau_{r_2} \omega_{r_2} \tag{3.41}$$

As well, the dissipation function can be expressed as

$$\Delta = \frac{1}{2} c_c \omega_c^2 + \frac{1}{2} c_s \omega_s^2 \tag{3.42}$$

where c_c and c_s are the damping coefficients of the bearings on which the shafts are attached to the carrier and the suns are mounted. Note that c_c and c_s are obtained either from experiments or from catalogues. In addition, c_c and c_s also include the effects of the planet-mounting bearings.

Substituting ω_{r_1}, ω_{r_2}, ω_{p_1}, and ω_{p_2} from Eqs. (3.1) and (3.3) into Eq. (3.37), the mathematical model is derived as

$$A_0 \dot{\omega}_c(t) + B_0 \dot{\omega}_s(t) = \tau_d - c_s \omega_s - \left(\frac{r_{s_1}}{r_{r_1}}\right) \tau_{r_1} - \left(\frac{r_{s_2}}{r_{r_2}}\right) \tau_{r_2} \tag{3.43a}$$

$$C_0 \dot{\omega}_c(t) + D_0 \dot{\omega}_s(t) = \tau_l - c_c \omega_c + \left(\frac{2r_c}{r_{r_1}}\right) \tau_{r_1} + \left(\frac{2r_c}{r_{r_2}}\right) \tau_{r_2} \tag{3.43b}$$

where A_0, B_0, C_0 and D_0 are four constant coefficients with units of generalized inertia.

3.4.1 Inverse Dynamics

In subsection 3.3.2, the 3-4-5 polynomial was found to be the best choice for $\omega_s(t)$. Hence, substituting $\omega_s(t)$ and $\omega_c(t)$ into Eqs. (3.43) to solve the inverse dynamics problem, we have

$$\tau_d - \left(\frac{r_{s_1}}{r_{r_1}}\right) \tau_{r_1} - \left(\frac{r_{s_2}}{r_{r_2}}\right) \tau_{r_2} = B_0 \dot{\omega}_{5s}(t) + c_s \omega_{5s}(t) \tag{3.44a}$$

$$\left(\frac{2r_c}{r_{r_1}}\right) \tau_{r_1} + \left(\frac{2r_c}{r_{r_2}}\right) \tau_{r_2} = D_0 \dot{\omega}_{5s}(t) + c_c \omega_{c_0} - \tau_l \tag{3.44b}$$

The model thus involves two equations and three unknowns, $\tau_d(t)$, $\tau_{r_1}(t)$ and $\tau_{r_2}(t)$. In other words, one torque can be freely assigned; it should be determined according to our objectives and

the constraints imposed by the motors. Assuming $\tau_d(t)$ to be the independent variable, Eq. (3.33) can be written as

$$(J_m + J_l)\dot{\omega}(t) + b\omega(t) = \tau_d(t) \Rightarrow (J_m + J_l)\ddot{\omega}(t) + b\dot{\omega}(t) = \dot{\tau}_d(t) \tag{3.45}$$

Therefore, since the angular velocity, the angular acceleration and the angular jerk are required to be continuous, $\tau_d(t)$ and $\dot{\tau}_d(t)$ must be continuous at the ends of the shifting interval. As a result, using the 2-3 *blending* polynomial, $\tau_d(t)$ can be expressed as

$$\tau_d(t) = \Delta\tau_d \left(-2\tau^3 + 3\tau^2\right) + \tau_{d_0}, \quad \Delta\tau_d = \tau_{d_f} - \tau_{d_0} \tag{3.46}$$

where τ_{d_0} and τ_{d_f} denote the initial and final values of $\tau_d(t)$ during gear-shifting. After finding $\tau_d(t)$ from Eq. (3.46), $\tau_{r_1}(t)$ and $\tau_{r_2}(t)$ can be readily determined from Eqs. (3.44). The results are reported in Section 3.5.

3.5 Results

This section provides the results when applying the 2-3, 3-4-5 and 4-5-6-7 polynomials for gear-shifting. The results are reported and compared for all polynomials.

The functions and their first three derivatives, all normalized to fall within the interval $[-1, 1]$, for the normal 2-3, 3-4-5 and 4-5-6-7 polynomials, are indicated in Figs. 3.5–3.7. As shown in Fig. 3.5, for a 2-3 polynomial, only the function and its first derivative are continuous at the ends; from Fig. 3.6, for a 3-4-5 polynomial, the second derivative is also continuous. A 4-5-6-7 polynomial leads to the continuity of the third derivative at the ends, too, as shown in Fig. 3.7.

Assuming $\nu_1 = 3$, $\nu_2 = 5/3$ and $\omega_{c_0} = 10$ rad/s, using Eqs. (3.15), for switching between the first and the second gear, we have

$$\omega_s(t_0) = 80/3 \text{ rad/s}, \quad \omega_{r_1}(t_0) = 40/9 \text{ rad/s}, \quad \omega_{r_2}(t_0) = 0 \tag{3.47a}$$

$$\omega_s(t_f) = 40 \text{ rad/s}, \quad \omega_{r_1}(t_f) = 0, \quad \omega_{r_2}(t_f) = -8 \text{ rad/s} \tag{3.47b}$$

while $\omega_c(t) = \omega_{c_0} = 10$ rad/s, i.e., ω_c remains constant during gear-shifting. Assuming $T_{7\text{min}}$ to be the reference, while considering all limitations of the power supply, we obtain $T_{5\text{min}} = (6/7)\, T_{7\text{min}}$ and $T_{3\text{min}} = (24/35)\, T_{7\text{min}}$ using Eq. (3.29). The results obtained using 2-3, 3-4-5 and 4-5-6-7 polynomials for the angular velocity $\omega_s(t)$ of the sun are depicted in Fig. 3.8. As expected, the shortest shifting time corresponds to the 2-3 polynomial. The jerks of the three functions are represented in Fig. 3.9. As shown in the figure, there is a jump in the jerk of the 2-3 polynomial, as it is not continuous at the end of gear-shifting. Also note that the difference between the extreme jerk

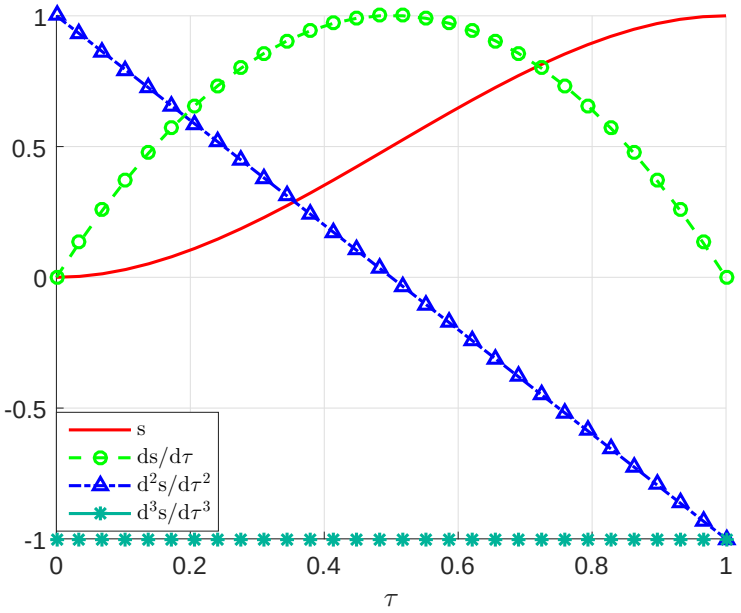

Figure 3.5: A 2-3 polynomial and its first three derivatives

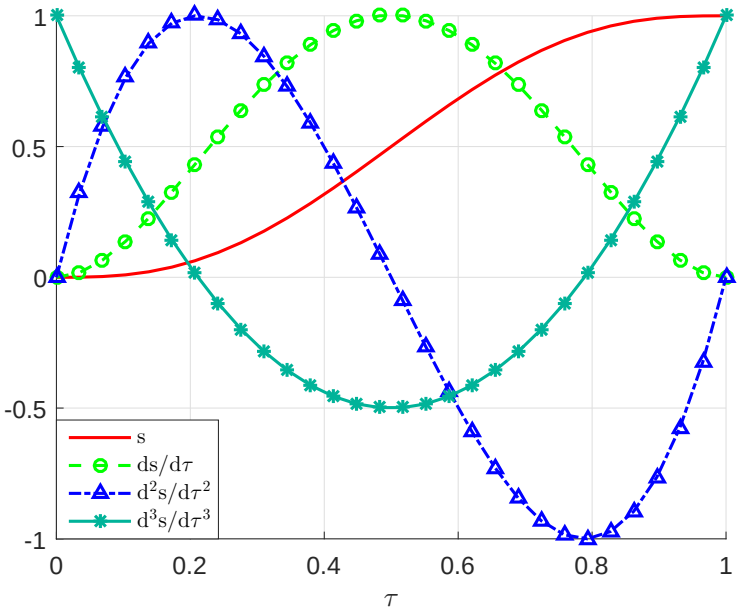

Figure 3.6: A 3-4-5 polynomial and its first three derivatives

values of the 3-4-5 and 4-5-6-7 polynomials is negligible. Thus, the 3-4-5 polynomial is the best choice, since its shifting time is $6/7$ that of its 4-5-6-7 counterpart, and hence, the shifting is swifter.

Using Eqs. (3.15), the angular velocities of the ring gears and the carrier for a 3-4-5 polynomial are indicated in Fig. 3.10. In this figure, the vertical line shows the time when the gear-shifting is

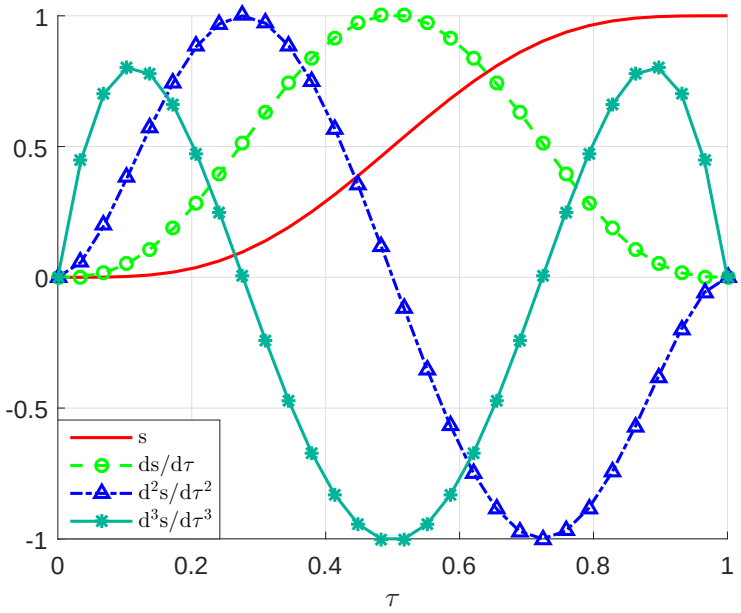

Figure 3.7: A 4-5-6-7 polynomial and its first three derivatives

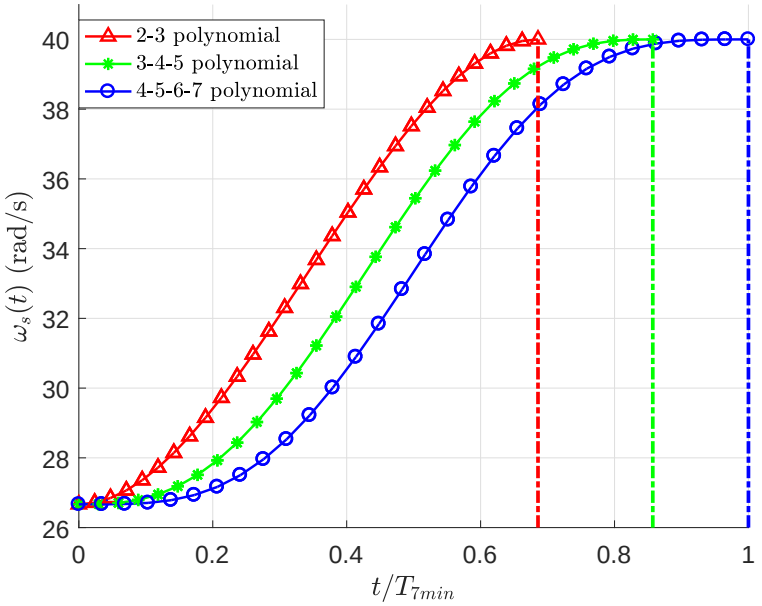

Figure 3.8: Comparison among 2-3, 3-4-5 and 4-5-6-7 polynomials for $\omega_s(t)$

finished. Note that the angular velocity of the output, i.e., $\omega_c(t)$, does not change during gear-shifting, which guarantees a seamless shift without any fluctuations on the output. As well, the torques of the electric motor, the first and the second clutch during gear-shifting are depicted in Fig. 3.11. The torques and their first time derivatives are also continuous, which guarantee the continuity of the

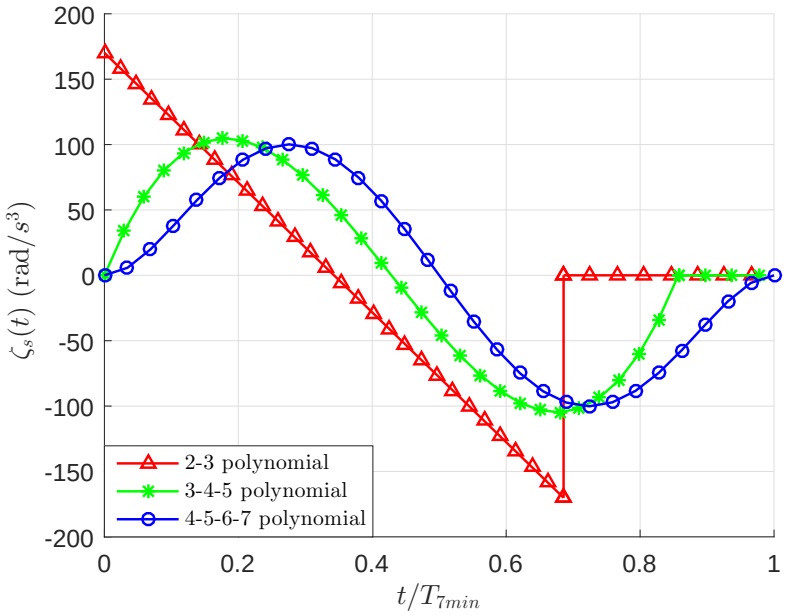

Figure 3.9: Comparison among the jerks of the three polynomials for $\omega_s(t)$

angular velocity, acceleration and jerk. As a result, motor “kicking" is eliminated in the electric vehicle.

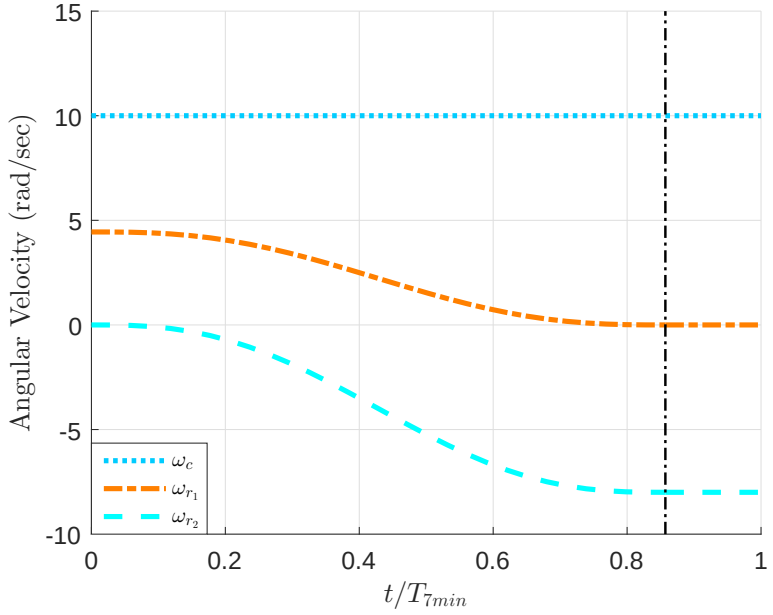

Figure 3.10: The angular velocities of the ring gears and planet carrier during gear-shifting

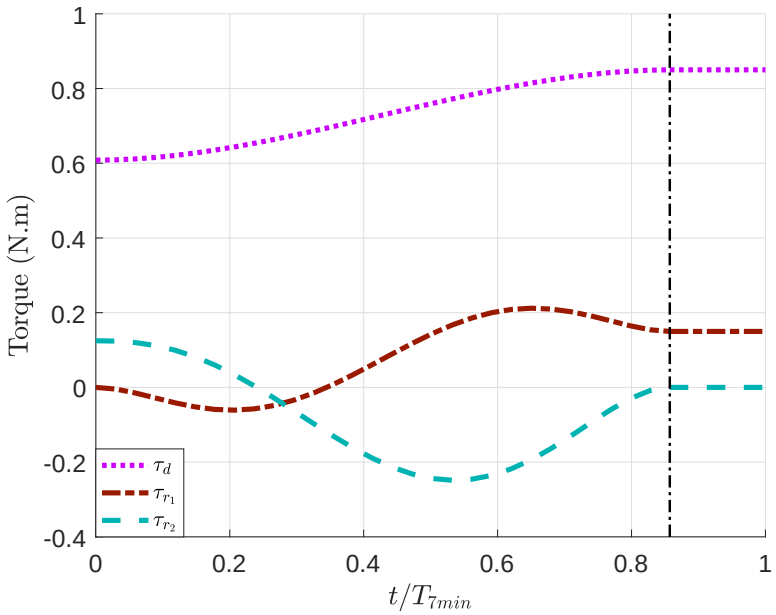

Figure 3.11: The torques of the electric motor and clutches during gear-shifting

3.6 The Path to Implementation

This section is devoted to the details of the implementation of the proposed scheme for gear-shifting in an actual MST designed for EVs. As demonstrated in Section 3.5, to guarantee the continuity of the angular velocity, acceleration and jerk of all rotating components during gear-shifting, thus avoiding jumps and discontinuities, their angular velocity should change following a 3-4-5 polynomial, except for the output, which should remain constant. As well, the torques applied by the actuators are required to follow the 2-3 polynomial, which warrants the continuity of the torques and their first time derivative. To this end, a cascade controller is recommended to be employed, including some inner and outer loops. The latter are used to control the angular velocities of all parts for tracking the 3-4-5 polynomial or remaining constant for the output. The angular velocities are measured using sensors, such as encoders. The inner loops are utilized to control the applied torques to follow the 2-3 polynomial. Since various mechanisms can be adopted for applying the required torques, such as disk brakes, band-type brakes and wet clutches for engaging the ring gears, torque or force sensors should be used for measuring the applied torques at different points. The model of the mechanism is also required for control purposes. The torque of the electric motor can be found by measuring its current and using the armature constant K_t of the motor. The external load applied to the output mostly originates from the road, aerodynamics and gravity, which can be measured directly or estimated using estimation algorithms, such as Kalman filter or neural networks (NNs). To implement the approach appropriately, all the nonlinearities, flexibility, small inertias,

and dry friction that have been neglected in the derivation of the model should be included in the unknown disturbance applied to the transmission. Considering the above-mentioned points, one can implement the proposed algorithm for gear-shifting in the real world. Note that the proposed scheme is based on the smooth blending curves that were developed in the RMSLab [84]. As an example, one of the smooth curves in question, the cycloidal curve, was implemented on a PUMA 260 robot to find the near-minimum-time trajectory, which guarantees eliminating jerky motions[3]. In this case, although only the first two derivatives of the cycloidal curve vanish at the ends of the interval of interest, the motions produced in a physical system are smooth throughout the whole interval. A 3-4-5 polynomial should do even better.

3.7 Conclusions

One of the means to improve the efficiency of EVs is to apply multi-speed transmissions. However, gear-shifting should be as swift and as seamless as possible for the shifting to be acceptable. The optimal gear-shifting of a multi-speed transmission for EVs was studied. First, the kinematic relations were invoked. Next, the optimal trajectory for gear-shifting was found using variational calculus. Three polynomials were proposed as transition functions of the angular velocities, 2-3, 3-4-5 and 4-5-6-7 polynomials, to reach a swift and seamless gear-shifting. Comparing shifting times and jerks, it was concluded that the 3-4-5 polynomial is the best candidate. Results demonstrate that the proposed approach is promising for a smooth and swift gear-shifting in EVs. Future research will be devoted to the investigation of the NVH[4] performance in the proposed MST designed for EVs [74].

[3]The related video is available at: ∼angeles/rmsl/Index/Index.htm > Courses > MECH573 Mechanics of Robotic Systems > Videos > Puma260_Near-minimun-time-trajectories.avi

[4]Noise, vibration, and harshness

Part II

Gear-shifting Control Algorithms in Electric Vehicles with Multi-speed Transmissions

Chapter 4

A Two-phase Control Algorithm for Gear-shifting in a Novel Multi-speed Transmission for Electric Vehicles

Abstract

In light of the current low energy-storage capacity of electric batteries, multi-speed transmissions (MSTs) are being considered for applications in electric vehicles (EVs), since MSTs decrease the energy consumption of the EV via gear-shifting. Nonetheless, swiftness and seamlessness are the major concerns in gear-shifting. This study focuses on developing a gear-shifting control scheme for a novel MST designed for EVs. The main advantages of the proposed MST are simplicity and modularity. Firstly, the dynamics model of the transmission is formulated. Then, a two-phase algorithm is proposed for shifting between each two gear ratios, which guarantees a smooth and swift shift. In other words, a separate control set is applied for shifting between each gear pair, which includes two independent PID controllers, tuned using trial-and-error and a genetic algorithm (GA), for the two steps of the algorithm and a switch. A supervisory controller is also employed to choose the proper PID gains, called PID gain-scheduling. Simulation results for various controllers and conditions are reported and compared, indicating that the proposed scheme is highly promising for a desired gear-shifting even in the presence of an unknown external disturbance.

4.1 Introduction

Due to a much lower impact on the environment, hybrid electric vehicles (HEVs) and electric vehicles (EVs) appear as proper substitutes for internal-combustion-engine vehicles (ICEVs). Nevertheless, since the energy-storage capacity of electric batteries is much lower than that of their ICE counterparts, EVs are not yet established as viable substitutes. Therefore, to achieve longer running time on a single charge of the electric battery, the efficiency of EVs should be improved. Research has shown that by applying a multi-speed transmission (MST) in EVs, thus providing the desired power in more than one way, one can attain a higher efficiency through gear-shifting [1, 5, 6, 7].

There are various types of MSTs for EVs, initially designed for ICEVs, such as automated manual transmissions (AMTs) [16, 21, 22], automatic transmissions (ATs) [10, 27, 28], dual-clutch transmissions (DCTs) [30, 37, 85] , and continuously variable transmissions (CVTs) [40, 50]. The presence of clutches or torque converters are vital for gear-shifting in ICEVs, since ICEs cannot operate below certain speeds and their speed control is quite challenging. On the other hand, electric motors (EMs) are speed-controllable in a wide range of operating speeds. Hence, novel MSTs can be designed for EVs, without any clutches or torque converters to disconnect the EM from the transmission during gear-shifting. In fact, EM and clutches can be adopted as control inputs in the EV transmissions to make gear-shifting seamless and swift. Since gear-shifting affects the dynamic performance, passenger comfort, and drivability[1] of the vehicle, the main objectives during gear-shifting are seamlessness, swiftness, increased drivability, vibration-elimination, cancellation of output-torque interruption, and improved efficiency. Extensive research has been conducted on each of the above-mentioned goals [58, 65, 66, 67].

Different strategies have been employed for gear-shifting control and estimation in ATs and DCTs [33]. For instance, applying the time-optimal hybrid minimum principle, Pakniyat and Caines [59, 60] found the minimum acceleration time required for reaching a speed of 100 $\mathrm{km/h}$ from rest. Next, the authors obtained the optimal gear ratios, the optimal gear-shifting instants and the optimal control inputs. Based on the dynamics model and gear-shifting objectives, an optimal shifting control strategy, including a PID controller and a robust two degree-of-freedom (dof) controller, was developed by Meng et al. [86] for an AT for automotive applications. Further, Rahimi et al. [63, 76] estimated the unmeasurable states and the unknown inputs for a seamless two-speed transmission for EVs. Then, based on the estimation results, an observer-based back-stepping controller was developed to achieve seamless gear-shifting, while tracking the optimal trajectory corresponding to the minimum shifting time [64]. Walker et al. [36] proposed a new scheme, namely, the integrated powertrain control of both the engine and the clutches, for reducing shift transient responses in DCTs. Design, modelling and estimation of the unmeasurable loads and states of a novel MST designed

[1] No generally acceptable definition of the term can be cited, but it usually includes the qualitative evaluation of a powertrain, such as the degree of smoothness and steadiness.

for EVs were studied by our team based on the Kalman filter, the Luenberger observer and neural networks (NNs) [81, 87]. Moreover, to assure acceleration and jerk continuity, the optimal trajectory for a swift and seamless gear-shifting was found employing polynomial transition functions [74]. Although intensive research has been conducted on MSTs for EVs, there are still lacunae in design, modelling, and gear-shifting strategies and control.

This paper reports on the development of a two-phase gear-shifting control algorithm for a novel modular MST designed for EVs. The main advantages of the proposed MST are simplicity and modularity. Firstly, the dynamics model of our proposed MST is devised. Then, the proposed control algorithm for gear-shifting is described, for achieving a swift, seamless shift. Using trial-and-error and a genetic algorithm (GA), different PID controllers are tuned and compared to find the appropriate control inputs for each phase of the proposed gear-shifting algorithm. In fact, for shifting between each two gear ratios in the transmission, i^{th} to j^{th}, a separate two-step control set is developed. Such controllers are called PID gain-scheduling, which means different gains have been tuned for the PID controllers. The proper gains will be selected by a supervisory controller. Simulation results indicate that the approach is highly encouraging for a smooth and swift gear-shifting.

An outline of the paper follows. Section 4.2 is devoted to the mathematical model of the proposed MST designed for EVs. The proposed gear-shifting algorithm and tuning of the corresponding controllers are discussed in Sections 4.3 and 4.4. Simulation results are reported and compared in Section 4.5.

4.2 Mathematical Model of the Proposed MST for EVs

As shown in Fig. 4.1, in the proposed MST designed for EVs, all sun gears are connected to the same shaft. Also, there is only one carrier for all planetary gear sets. In the underdrive gear train, as represented in Fig. 4.1(a), the sun gears are installed on the input shaft, while the shaft connected to the carrier is the output. The overdrive gear train, as indicated in Fig. 4.1(b), operates the other way around. Different speed ratios are achieved by engaging the corresponding clutch. In fact, the gear-shifting process includes releasing the engaged clutch and engaging another one.

One can combine both overdrive and underdrive gear trains into a single transmission, as illustrated in Fig. 4.1(c). In the combined transmission, two friction clutches should be employed between carrier and planet gears in both gear trains, $\mathrm{C_f^i}$ and $\mathrm{C_f^o}$, in order to lock the free overdrive or underdrive gear train when the associated clutch is engaged. In fact, only one of the friction clutches is closed, depending on the overdrive or underdrive mode. The combined transmission has $m + n$ main gear ratios, when only one of the gear trains is operating, as well as $m \times n$ median gear ratios when both gear trains are engaged at the same time. Note that, in median gear ratios, one ring clutch

is engaged from each side of the transmission; both friction clutches are released. Thus, the total number of speed ratios in the proposed combined transmission, including the direct drive mode, is

$$j = m + n + m \times n + 1 \tag{4.1}$$

The main advantage of the proposed transmission is modularity. In other words, the designer can determine the numbers of the underdrive and overdrive modules, including a planetary gear set and a clutch, separately, according to the application and the number of gear ratios required. We are prototyping the proposed MST designed for EVs. As depicted in Fig. 4.2, our transmission testbed includes a four-stage planetary gear set, consisting of two overdrive and two underdrive gear ratios. The dynamics model of a two-speed transmission, represented in Fig. 4.1(d), is investigated below.

Let $\mathbf{q}$, T, V, L, Π and Δ denote the vector of generalized coordinates, the kinetic energy, the potential energy, and the Lagrangian of the system, the power supplied to the system and the system dissipation function, respectively, the Lagrange equation is then given by

$$\frac{d}{dt}\left(\frac{\partial L}{\partial \dot{\mathbf{q}}}\right) - \frac{\partial L}{\partial \mathbf{q}} = \frac{\partial}{\partial \dot{\mathbf{q}}}\left(\Pi - \Delta\right), \quad L = T - V \tag{4.2}$$

Let T_c, T_s, T_r and T_p be the kinetic energies of the carrier, the sun, the ring and the planet gears, respectively, and n the number of planet gears. The total kinetic energy of the system can thus be expressed as

$$T = T_c + T_s + T_r + nT_p \tag{4.3}$$

where

$$T_c = \frac{1}{2} I_c \omega_c^2, \quad T_s = \frac{1}{2}\left(I_{s_1} + I_{s_2}\right)\omega_s^2, \quad T_r = \frac{1}{2} I_{r_1}\omega_{r_1}^2 + \frac{1}{2} I_{r_2}\omega_{r_2}^2 \tag{4.4a}$$

$$T_p = \frac{1}{2} m_{p_1} v_{p_1}^2 + \frac{1}{2} I_{p_1}\omega_{p_1}^2 + \frac{1}{2} m_{p_2} v_{p_2}^2 + \frac{1}{2} I_{p_2}\omega_{p_2}^2, \quad v_{p_1} = v_{p_2} = r_c\omega_c \tag{4.4b}$$

with I_{s_1}, I_{s_2}, I_{r_1}, I_{r_2}, I_{p_1}, and I_{p_2} denoting the moments of inertia of the sun, the ring, and the planet gears of the first and the second gear sets, respectively, and I_c the moment of inertia pertaining to the carrier. Moreover, m_{p_1}, m_{p_2}, v_{p_1} and v_{p_2} denote the masses and the speeds of the centers of mass of each planet gear for each gear set. Note that, as illustrated in Fig. 4.1(d), the planetary sets share the same carrier rotating at ω_c. As well, the sun gears are installed on the same shaft rotating at ω_s. The angular velocities of the ring gears are indicated by ω_{r_1} and ω_{r_2}.

Since all elements are considered as rigid bodies in our model, the total potential energy of the system remains constant[2]. Let τ_d, τ_l, τ_{r_1} and τ_{r_2} indicate the drive torque of an EM applied to the

[2]Note that all the nonlinearities, flexibility and dry friction that have been neglected in the model are included in the unknown disturbance applied to the transmission.

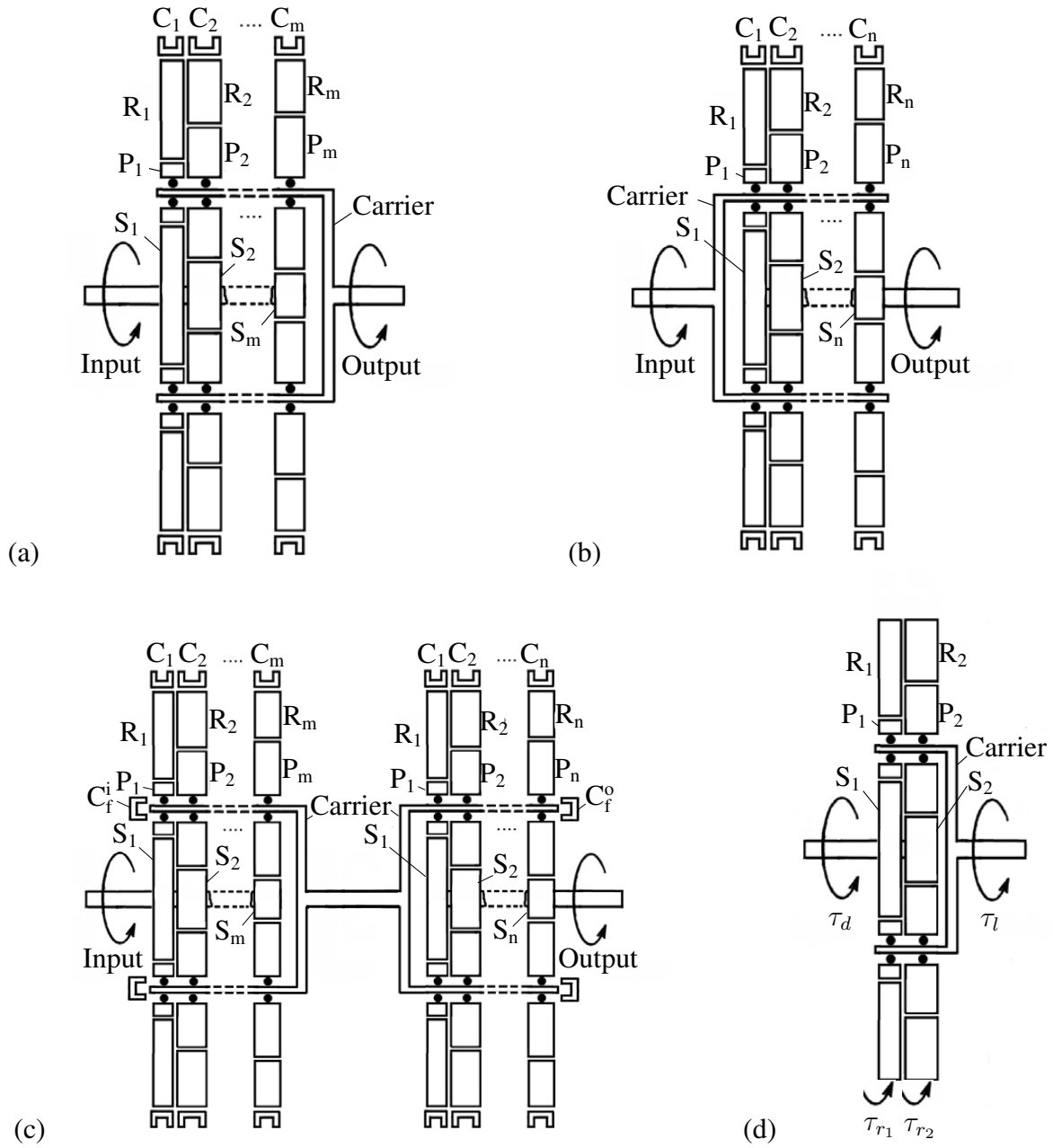

Figure 4.1: Multi-stage planetary gear sets: (a) underdrive gear train; (b) overdrive gear train; (c) combined MST; and (d) a two-stage planetary gear set

input shaft, the external load applied to the output shaft, the torque of the first clutch applied to the first ring and the torque of the second clutch applied to the second ring, respectively, as shown in Fig. 4.1(d). Under the assumption of an underdrive gear train, the power supplied to the system and the dissipation function can be expressed as

$$\Pi = \tau_d\omega_s + \tau_l\omega_c + \tau_{r_1}\omega_{r_1} + \tau_{r_2}\omega_{r_2}, \quad \Delta = \frac{1}{2}c_c\omega_c^2 + \frac{1}{2}c_s\omega_s^2 \tag{4.5}$$

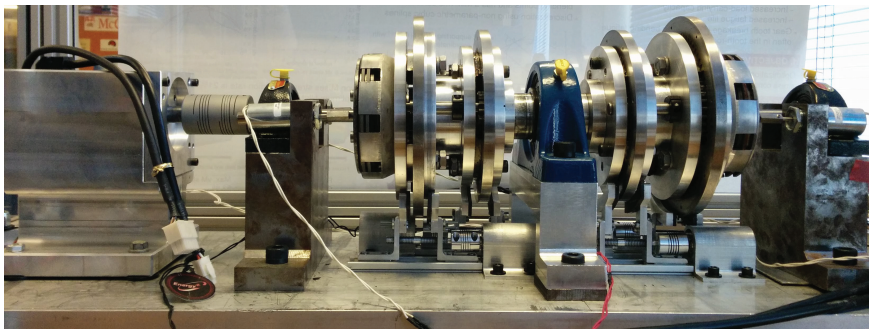

Figure 4.2: The transmission testbed built in our laboratory

with c_c and c_s denoting the resultant damping coefficients obtained from experiments, including the effects of all bearings and friction. Finally, after substitution of Eqs. (4.3)–(4.5) into Eq. (4.2), and using the kinematic relations obtained by assuming pure-rolling constraints between gears in contact, the mathematical model of the transmission system is set up as

$$\mathbf{I}\dot{\boldsymbol{\omega}} + \mathbf{C}\boldsymbol{\omega} = \boldsymbol{\tau} \tag{4.6}$$

with $\mathbf{I}$ indicating the generalized inertia matrix, $\boldsymbol{\omega}$ the generalized-velocity vector, $\boldsymbol{\tau}$ the generalized-force vector, and $\mathbf{C}$ the damping matrix, as displayed below.

$$\boldsymbol{\omega} = \begin{bmatrix} \omega_s \\ \omega_c \end{bmatrix}, \quad \mathbf{C} = \begin{bmatrix} c_s & 0 \\ 0 & c_c \end{bmatrix}, \quad \boldsymbol{\tau} = \begin{bmatrix} \tau_d - r_{s_1}\tau_{r_1}/r_{r_1} - r_{s_2}\tau_{r_2}/r_{r_2} \\ \tau_l + 2r_c\tau_{r_1}/r_{r_1} + 2r_c\tau_{r_2}/r_{r_2} \end{bmatrix} \tag{4.7}$$

4.3 The Control Algorithm Description

This section includes the description of the proposed control algorithm for gear-shifting in the MST designed for EVs. Assuming an underdrive gear train, the problem is how to switch between two gear sets, from the first gear ratio to the second one, for instance, such that, to achieve a seamless gear-shifting and cancel the torque interruptions, the angular velocity $\omega_c(t)$ of the carrier, i.e. the output, remains constant during gear-shifting. Therefore, at the beginning of the gear-shifting process, for $t = t_0$, the first clutch is completely engaged and the second one released, namely,

$$\omega_{r_1}(t_0) = 0, \quad \tau_{r_2}(t_0) = 0 \tag{4.8}$$

At the end of gear-shifting, for $t = t_f$, we should have the second clutch completely engaged and the first one released, i.e.,

$$\omega_{r_2}(t_f) = 0, \quad \tau_{r_1}(t_f) = 0 \tag{4.9}$$

The control inputs during gear-shifting are the drive torque $\tau_d(t)$ applied to the input shaft by an electric motor, the clutch torque $\tau_{r_1}(t)$ applied to the first ring by the first clutch, and the clutch torque $\tau_{r_2}(t)$ applied to the second ring by the second clutch, while an external load $\tau_l(t)$ is applied to the output shaft, as shown in Fig. 4.1(d). The control algorithm proposed here is divided into two phases:

Phase I. Approaching: $t \in [t_0, t_1]$, $t_0 < t_1 < t_f$; t_1 is achieved when $\omega_{r_2}(t_1) = 0$.

During this phase the second clutch remains released, i.e. $\tau_{r_2}(t) = 0$, $t \in [t_0, t_1]$. In other words, the control input in this step is $\mathbf{u}_1(t) = \begin{bmatrix} \tau_d(t) & \tau_{r_1}(t) \end{bmatrix}^T$ and the output is $\mathbf{y}_1(t) = \begin{bmatrix} \omega_s(t) & \omega_c(t) \end{bmatrix}^T$. The objective here is to change the gears artificially, namely, by changing the gear ratio without engaging the second clutch. To this end, we start disengaging the first clutch while controlling the drive torque $\tau_d(t)$ such that the angular velocity of the second ring becomes zero, i.e. $\omega_{r_2}(t_1) = 0$, with the angular velocity of the output remaining constant. Note that at the end of this phase, the first clutch is partially engaged, while the angular velocity of the second ring is zero, with the second clutch still released completely. During this phase, the input angular velocity follows a 3-4-5 *blending polynomial*, which guarantees the continuity of the angular acceleration and jerk at both ends [74]. In other words, assuming $\omega_s(t_0) = \omega_{s_0}$ and $\omega_s(t_1) = \omega_{s_1}$,

$$\omega_s(t) = \Delta\omega \left(6\theta^5 - 15\theta^4 + 10\theta^3\right) + \omega_{s_0}, \quad \theta \equiv \frac{t - t_0}{t_1 - t_0}, \quad \Delta\omega \equiv \omega_{s_1} - \omega_{s_0} \tag{4.10}$$

Phase II. Coasting: $t \in [t_1, t_f]$

Now since the angular velocity of the second ring is zero at t_1, we can readily engage the second clutch. Afterwards, we should start disengaging the first clutch completely, while controlling the drive torque $\tau_d(t)$ to keep the input and output angular velocities constant. Hence, the control input is $\mathbf{u}_2(t) = \begin{bmatrix} \tau_d(t) & \tau_{r_1}(t) & \tau_{r_2}(t) \end{bmatrix}^T$ and the output is $\mathbf{y}_2(t) = \begin{bmatrix} \omega_s(t) & \omega_c(t) & \tau_{r_1}(t) \end{bmatrix}^T$. At the end of this phase, the first clutch is released, $\tau_{r_1}(t_f) = 0$, and the second one is engaged completely, $\omega_{r_2}(t_f) = 0$.

For each of the above-mentioned phases, a separate discrete-time PID controller is designed, as briefly explained in Section 4.4. In fact, we just need to switch between the two controllers at t_1. For shifting between each two gear ratios in the transmission, i^{th} to j^{th}, a separate control set can be developed, each consisting of two PID controllers as well as a switch, as depicted in Fig. 4.3. Such controllers are called PID gain-scheduling, which means different gains have been tuned for the PID controllers. The proper gains will be selected by a supervisory controller, based on the two gear ratios between which we want to shift, such as one to two, two to three, etc., as well as the step, one or two, in the control algorithm explained above. Note that, because of the motor limitations, there is a saturation after each control input, in order to make implementation on a real prototype feasible.

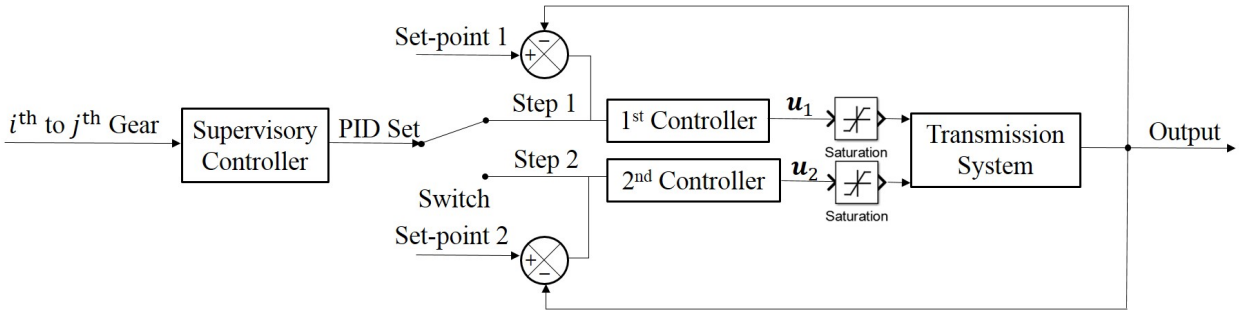

Figure 4.3: The proposed control loop for gear-shifting

4.4 Discrete-time PID Controller

One of the best control schemes, readily implementable, is the proportional-integral-derivative (PID) controller. The continuous-time representation of a PID controller for a multi-input-multi-output (MIMO) system is given by

$$\mathbf{u}(t) = \mathbf{K}_p\mathbf{e}(t) + \mathbf{K}_i \int_0^t \mathbf{e}(\tau)d\tau + \mathbf{K}_d\dot{\mathbf{e}}(t), \quad \mathbf{e}(t) = \mathbf{r}(t) - \mathbf{y}(t) \tag{4.11}$$

where $\mathbf{u}(t)$ is the control input and $\mathbf{e}(t)$ is the error between the reference signal $\mathbf{r}(t)$ and the output of the system $\mathbf{y}(t)$. Upon Laplace-transforming Eq. (4.11), we obtain

$$\mathbf{u}(s) = \left(\mathbf{K}_p + \frac{1}{s}\mathbf{K}_i + s\mathbf{K}_d\right)\mathbf{e}(s), \quad \mathbf{e}(s) = \mathbf{r}(s) - \mathbf{y}(s) \tag{4.12}$$

Further, using the $\mathcal{Z}$-transform, the Laplace operators of the derivative and the integral can be approximated by

$$s \approx \frac{1 - z^{-1}}{T_s}, \quad \frac{1}{s} \approx \frac{T_s}{2}\frac{1 + z^{-1}}{1 - z^{-1}} \tag{4.13}$$

with T_s denoting the constant sampling time. Hence, the discrete-time version of the feedback control input takes the form

$$\mathbf{u}(z) = \left(\mathbf{K}_p + \frac{T_s}{2}\frac{1 + z^{-1}}{1 - z^{-1}}\mathbf{K}_i + \frac{1 - z^{-1}}{T_s}\mathbf{K}_d\right)\mathbf{e}(z) \tag{4.14}$$

or, equivalently,

$$\mathbf{u}(z) = \left[\left(\mathbf{K}_p + \frac{T_s}{2}\mathbf{K}_i + \frac{1}{T_s}\mathbf{K}_d\right) + z^{-1}\left(-\mathbf{K}_p + \frac{T_s}{2}\mathbf{K}_i - \frac{2}{T_s}\mathbf{K}_d\right) + \frac{z^{-2}}{T_s}\mathbf{K}_d\right]\frac{1}{1 - z^{-1}}\mathbf{e}(z) \tag{4.15}$$

Finally, for implementation of the discrete-time PID controller, we have

$$\mathbf{u}_k = \mathbf{u}_{k-1} + \mathbf{A}_c\mathbf{e}_k + \mathbf{B}_c\mathbf{e}_{k-1} + \mathbf{C}_c\mathbf{e}_{k-2} \tag{4.16}$$

with

$$\mathbf{A}_c = \mathbf{K}_p + \frac{T_s}{2}\mathbf{K}_i + \frac{1}{T_s}\mathbf{K}_d, \quad \mathbf{B}_c = -\mathbf{K}_p + \frac{T_s}{2}\mathbf{K}_i - \frac{2}{T_s}\mathbf{K}_d, \quad \mathbf{C}_c = \frac{1}{T_s}\mathbf{K}_d \tag{4.17}$$

The dimensions of $\mathbf{A}_c$, $\mathbf{B}_c$ and $\mathbf{C}_c$ (or $\mathbf{K}_p$, $\mathbf{K}_i$ and $\mathbf{K}_p$) depend on the system. In a MIMO system, these matrices consist of many entries. Therefore, it is very complicated to find these matrices by trial-and-error. There are two ways to accomplish this task: one is reducing the number of unknowns by applying some constraints, the other is employing a genetic algorithm (GA) to find the optimum matrices, while minimizing the tracking error. In the GA, the control inputs can be treated as optimal, numerically-investigated, not symbolically-derived [88]. Both methods are discussed below.

4.4.1 Tuning the PID Gains Using the Monic Form of the Model

The mathematical model of our system is given in Eq. (4.6). At this step, the system is massaged to take it into *monic form*, i.e., with the leading-term coefficient equal to the identity matrix. To this end, since $\mathbf{I}$ is positive-definite, it can be expressed in the form

$$\mathbf{I} = \mathbf{J}^2, \quad \mathbf{J} = \sqrt{\mathbf{I}} \tag{4.18}$$

where $\mathbf{J}$ is the positive-definite square root of $\mathbf{I}$, and hence, can be assumed to be symmetric. Now Eq. (4.6) becomes

$$\mathbf{J}^2\dot{\boldsymbol{\omega}} + \mathbf{C}\boldsymbol{\omega} = \boldsymbol{\tau} \quad \text{or} \quad \mathbf{J}\dot{\boldsymbol{\omega}} + \mathbf{J}^{-1}\mathbf{C}\boldsymbol{\omega} = \mathbf{J}^{-1}\boldsymbol{\tau} \tag{4.19}$$

Now, upon the change of variable $\boldsymbol{\psi} = \mathbf{J}\boldsymbol{\omega}$, we have the monic form of Eq. (4.6):

$$\dot{\boldsymbol{\psi}} + \boldsymbol{\Delta}\boldsymbol{\psi} = \mathbf{t}, \quad \boldsymbol{\Delta} = \mathbf{J}^{-1}\mathbf{C}\mathbf{J}^{-1}, \quad \mathbf{t} = \mathbf{J}^{-1}\boldsymbol{\tau} \tag{4.20}$$

with $\boldsymbol{\Delta}$ and $\mathbf{t}$ denoting the positive-definite dissipation matrix and the new input vector, respectively. Therefore, using Eq. (4.12) and the Laplace transform, the relation between the output $\boldsymbol{\psi}(s)$ and the reference signal $\mathbf{r}(s)$ can be expressed as

$$\left[s^2\left(\mathbf{1} + \mathbf{K}_d\right) + s\left(\boldsymbol{\Delta} + \mathbf{K}_p\right) + \mathbf{K}_i\right]\boldsymbol{\psi}(s) = \left(s^2\mathbf{K}_d + s\mathbf{K}_p + \mathbf{K}_i\right)\mathbf{r}(s) \tag{4.21}$$

For the system to be strictly proper and also reducing the left-hand-side of Eq. (4.21) to a monic form, a PI controller should be applied, i.e., $\mathbf{K}_d = \mathbf{0}$. Further, for stability, the matrices $\boldsymbol{\Delta} + \mathbf{K}_p$ and $\mathbf{K}_i$ are required to be positive-definite and, preferably, symmetric. The coefficient of $\boldsymbol{\psi}(s)$ in

Eq. (4.21) can be diagonalized if and only if $\mathbf{\Delta} + \mathbf{K}_p$ and $\mathbf{K}_i$ share the same set of eigenvectors. A simple way of achieving this is by rendering these two matrices proportional to each other, i.e.,

$$\mathbf{K}_i = \alpha \left(\mathbf{\Delta} + \mathbf{K}_p \right), \quad \alpha \, \epsilon \, \mathbb{R}^+ \tag{4.22}$$

This way, we can reduce the number of unknowns for tuning the PID gains in n-dimensional first-order systems from $3n^2$ to $n(n+1)/2$ distinct entries plus a suitable value for α. Thus, tuning the gains by trial-and-error becomes feasible.

4.4.2 The Genetic Algorithm (GA)

A GA can be applied to find the optimum PID gains in the controller design, i.e., the matrices in Eq. (4.16), while minimizing the tracking error. To this end, the objective function can be written as

$$J = \sum_k \|\mathbf{e}_k\|^2, \quad \mathbf{e}_k = \mathbf{r}_k - \mathbf{y}_k \tag{4.23}$$

GAs are part of the larger class of evolutionary algorithms (EAs). Since GAs are self-tuning, they are employed to find the fittest solution, with the minimum value for the objective function (4.23), without any complex numerical procedures, by relying on bio-inspired operators, such as mutation, crossover and selection. Each individual in the population, including a set of chromosomes, indicates a value for the PID gains in the search space, i.e., a possible solution to the optimization problem. After each iteration, the tracking error is evaluated and the best fit individuals are selected for reproducing to yield the next generation [89, 90]. Hence, the GA-based optimization can be summarized in three steps: initialization, selection and reproduction. These steps repeat until finding the optimum PID gains with a reasonable tracking error or reaching the threshold in the number of generations, both preassigned by the user.

4.4.3 Stability Analysis

The stability of the closed-loop control system, i.e., a multi-input multi-output (MIMO) system, is studied in this subsection. Assume that in the closed-loop control system including the PID controller, the reference signal $\mathbf{r}(s)$ and the output of the system $\mathbf{y}(s)$ are related by the transfer matrix function $\mathbf{G}_c(s)$, namely,

$$\mathbf{y}(s) = \mathbf{G}_c(s)\mathbf{r}(s) \tag{4.24}$$

The continuous-time system (4.24) is stable if and only if all the poles of $\mathbf{G}_c(s)$ lie in the left-half of the complex plane, i.e., if the poles of all entries of the transfer matrix $\mathbf{G}_c(s)$ have negative real parts. Similarly, the discrete-time version of the above system

$$\mathbf{y}(z) = \mathbf{G}_c(z)\mathbf{r}(z) \tag{4.25}$$

is stable if and only if the poles of all entries of the transfer matrix $\mathbf{G}_c(z)$ lie inside the unit circle on the $\mathcal{Z}$-plane, i.e., each pole of $\mathbf{G}_c(z)$ has a magnitude less than unity [91].

Hence, the gains of the PID controller, included in $\mathbf{G}_c(s)$ or $\mathbf{G}_c(z)$, should be chosen to ensure that the closed-loop control system is always stable.

4.5 Simulation Results

The simulation results obtained with the proposed gear-shifting algorithm for switching between two planetary gear sets in the proposed MST, designed for EVs, are reported here. Different PID controllers are tuned and compared, to find the appropriate control inputs for the gear-shifting algorithm.

As discussed in Section 4.3, the algorithm consists of two phases, i.e., the approaching phase and the coasting phase. Therefore, two different PID controllers are required to be designed for each step. However, we need to switch between the controllers at the right time, i.e., at the end of the first phase when $t = t_1$. First, using trial-and-error to find the appropriate entries of the matrices $\mathbf{A}_c$, $\mathbf{B}_c$ and $\mathbf{C}_c$ in Eq. (4.16), the simulation results for switching from the second to the first gear ratio are depicted in Figs. 4.4. In this case,

$$\omega_{r_2}(t_0) = 0, \quad \tau_{r_1}(t_0) = 0, \quad \omega_{r_1}(t_f) = 0, \quad \tau_{r_2}(t_f) = 0 \tag{4.26}$$

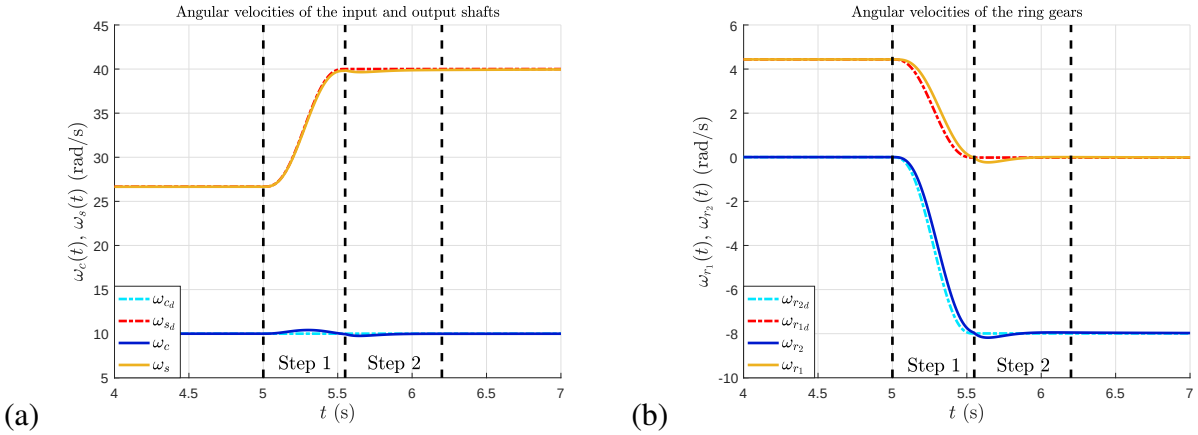

(a) (b)

Figure 4.4: The angular velocities during gear-shifting: (a) the input and output shafts; and (b) the ring gears

where $t_0 = 5$ s, while t_1 and t_f are achieved when $\omega_{r_1}(t_1) = 0$ and $\tau_{r_2}(t_f) = 0$, respectively. Note that in this case, the first clutch remains completely released during the approaching phase, i.e.,

$\tau_{r_1}(t) = 0$, $t \in [t_0, t_1]$. The desired and output values for the angular velocities of the input shaft $\omega_s(t)$ and the output shaft $\omega_c(t)$ are compared in Fig. 4.4(a). As shown in the figure, the angular velocity of the input shaft follows the 3-4-5 polynomial, while the angular velocity of the output shaft remains constant during gear-shifting. The angular velocities of the first and the second ring gears are shown in Fig. 4.4(b). As observed, at the beginning of gear-shifting, the angular velocity of the second ring gear is zero, i.e. the second gear set is engaged, while at the end of gear-shifting, the first gear set is engaged.

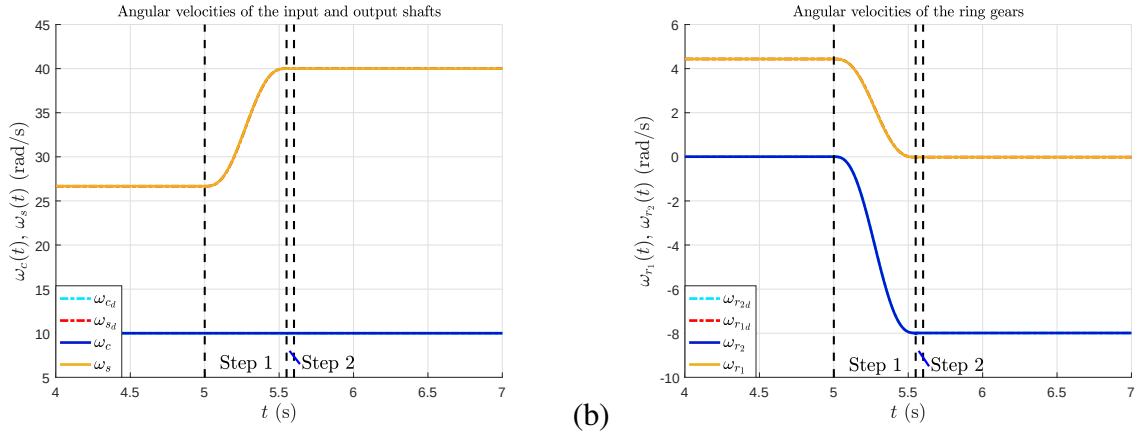

(a) (b)

Figure 4.5: The angular velocities during gear-shifting using GA: (a) the input and output shafts; and (b) the ring gears

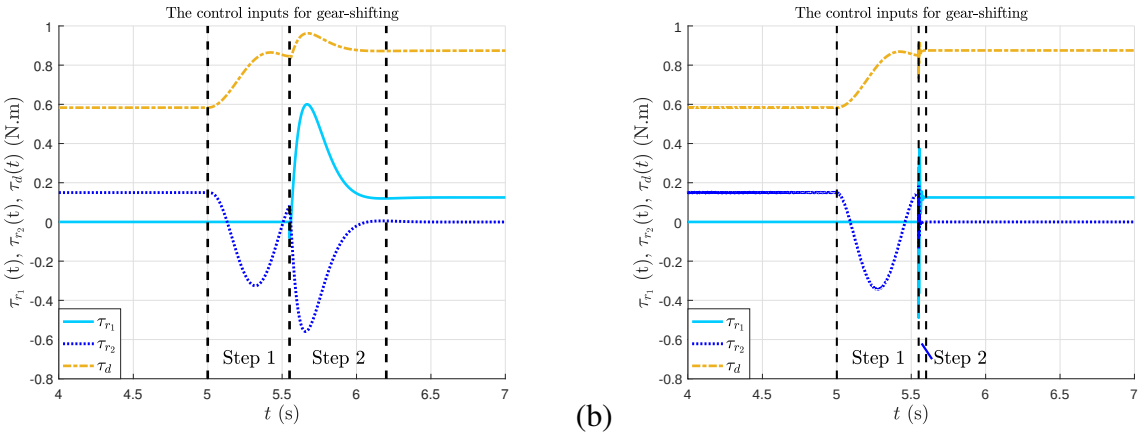

(a) (b)

Figure 4.6: The control inputs during gear-shifting: (a) using trial-and-error; and (b) using GA

In a general case, applying the GA-based optimization method to find the appropriate entries for the PID matrices, the simulation results are indicated in Figs. 4.5. The tracking errors are much smaller when using the GA. Therefore, it is highly recommended to use the GA-based optimization technique to find the proper matrices for each PID controller, then switch between them when necessary using a supervisory controller. The corresponding control inputs for both controllers are

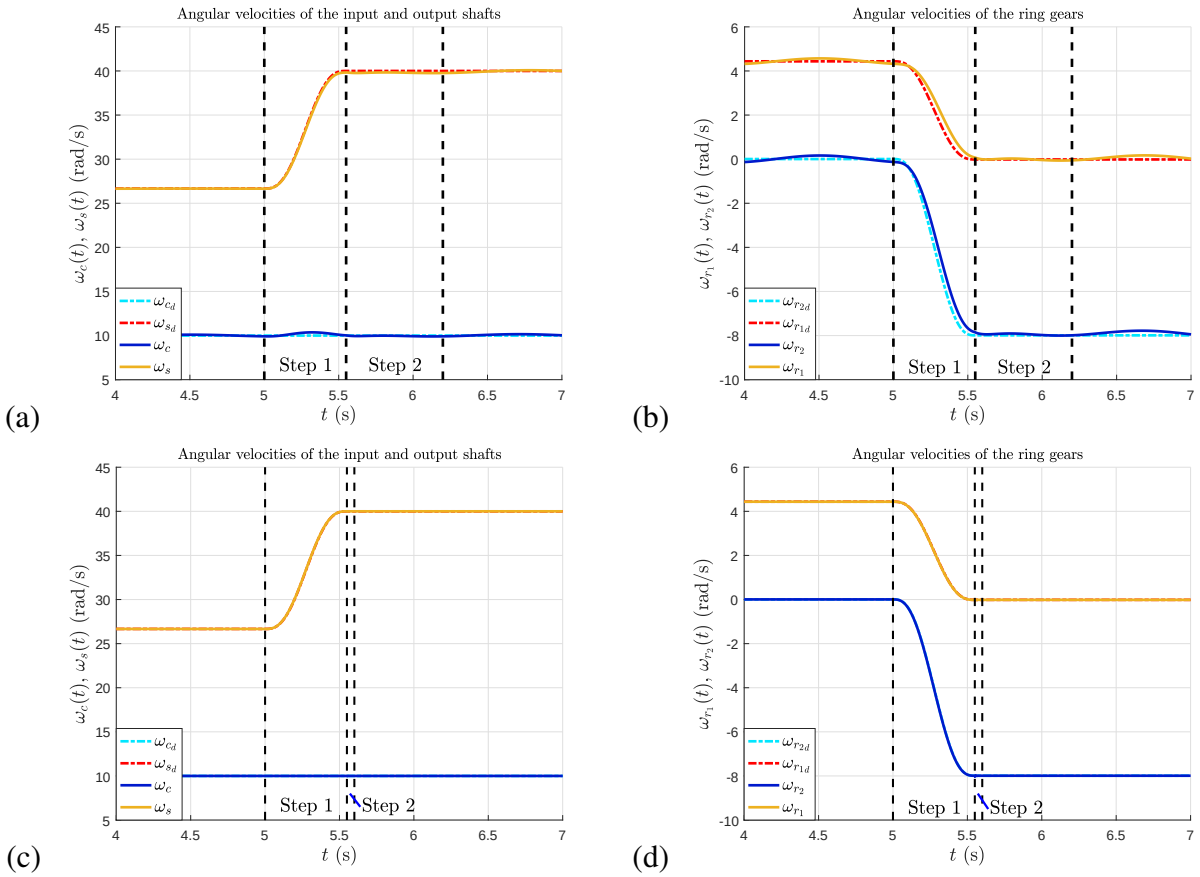

Figure 4.7: The angular velocities in the presence of an external disturbance: the input and output shafts using trial-and-error; (b) the ring gears using trial-and-error; (c) the input and output shafts using GA; and (d) the ring gears using GA

represented in Figs. 4.6. According to the figure, the torque τ_{r_1} applied to the first ring gear is zero until $t = t_1$. At the end of gear-shifting, the torque τ_{r_2} applied to the second ring gear is zero, i.e., the second gear set is completely released. Note that the values of the control inputs remain bounded all the time. As shown in the same figure, the shifting time is about 50% shorter when the GA is applied.

Assuming an unknown external disturbance applied to the transmission, to evaluate the performance of the tuned controllers, Figs. 4.7(a)–(d) provide a comparison of the results of both controllers. According to these figures, not only does the GA-based controller reduce the shifting time considerably, but also provides a better performance. Simulation results demonstrate that the proposed gear-shifting algorithm is very promising for a swift and seamless shift in the proposed MST designed for EVs, since the angular velocity of the output shaft remains constant during gear-shifting and the angular velocities of the input shaft and both ring gears follow the 3-4-5 polynomial, which guarantees the continuity of the angular acceleration and jerk.

4.6 Conclusions

Applying MSTs is a way to improve the efficiency of EVs. Nevertheless, swiftness and seamlessness are significant concerns in gear-shifting. A two-phase control algorithm was proposed for gear-shifting in a novel modular MST designed for EVs. First, the mathematical model of the proposed transmission was derived. Next, after a brief description of the shifting algorithm, different PID controllers were designed for each step using trial-and-error and a GA. Simulation results demonstrate that the GA-based controller provides both a much shorter shifting time and a better performance when an unknown external disturbance is applied. The proposed gear-shifting algorithm appears promising for a swift, seamless shift, since the output angular velocity remains constant during gear-shifting and the input angular velocity follows the 3-4-5 polynomial, which guarantees the continuity of the angular acceleration and jerk. Future research will be devoted to the implementation of the proposed gear-shifting control algorithm on a physical MST [92].

Chapter 5

Gear-shifting in a Novel Modular Multi-speed Transmission for Electric Vehicles Using Linear Quadratic Integral Control

Abstract

The efficiency of electric vehicles (EVs) can be improved by applying multi-speed transmissions (MSTs), while ensuring that gear-shifting is swift and smooth. This paper establishes a gear-shifting control algorithm for a novel MST, with the advantages of simplicity and modularity, designed for EVs. Firstly, the mathematical model of the proposed MST is derived. Next, the control algorithm developed for gear-shifting is clarified, which guarantees seamlessness and swiftness. The system under study is over-actuated, with end constraints on some control inputs. Therefore, for acceleration and jerk continuity, while satisfying the input terminal constraints, one input is suggested to be changed independently, based on a 2-3 blending polynomial. Then, the new fully-actuated system is controlled using a linear quadratic integral (LQI) controller, which is an extension of the linear quadratic regulator (LQR) for tracking problems. Simulation results indicate the effectiveness of the proposed control algorithm in the presence of unknown external disturbances.

5.1 Introduction

Electric vehicles (EVs) suffer from the current low energy-storage capacity of electric batteries. Hence, to improve the efficiency of EVs, multi-speed transmissions (MSTs) are being considered for applications in EVs [1, 5, 6, 7]. This way, since the power provided by the electric motor (EM) is transmitted to the wheels by different gear ratios, the maximum operating efficiency can be achieved for various conditions via proper gear-shifting.

Automated manual transmissions (AMTs) [16, 21, 22], automatic transmissions (ATs) [10, 27, 28], dual-clutch transmissions (DCTs) [30, 37, 85], and continuously variable transmissions (CVTs) [40, 50] are different kinds of MSTs for EVs. The above-mentioned transmissions were initially designed for internal-combustion-engine vehicles (ICEVs). However, in ICEVs, since the engine cannot operate below certain speeds, and their speed control is quite challenging, clutches or torque converters are essential to disconnect the engine from the transmission system during gear-shifting. On the contrary, one can remove such clutches or torque converters in designing MSTs for EVs, since the speed of EMs can be controlled in an extensive range. In fact, in EVs, to make gear-shifting seamless and swift, the torque provided by the motor can be employed as an independent control input [9]. Gear-shifting affects drivability of the vehicle, dynamic performance, and passenger comfort. Hence, the key goals during gear-shifting are seamlessness, swiftness, vibration-elimination, cancellation of output-torque interruption, and increased drivability. There has been intensive research on the above-mentioned targets [58, 65, 66, 67].

Many approaches have been applied for design, modelling, and gear-shifting control and estimation in MSTs [33]. For instance, Pakniyat and Caines [59, 60] employed the time-optimal hybrid minimum principle to reach a certain speed from rest in minimum time. The same authors also found the optimal gear-shifting instants, the optimal gear ratios, and the optimal control inputs. Considering gear-shifting goals, Meng et al. [86] established an optimal shifting control algorithm, i.e., the combination of a PID and a robust controller, based on their dynamics model. Moreover, Rahimi et al. [76, 63] estimated the unmeasurable states and the unknown inputs of a transmission for EVs. Next, using the estimation results, these authors built an observer-based back-stepping controller to attain a seamless shift [64]. Based on the integrated powertrain control of both the engine and the clutches, a new strategy was introduced by Walker et al. [36] to improve the gear-shifting transient response in DCTs. Design, mathematical modelling and estimation of the unmeasurable loads and states of a novel MST designed for EVs was investigated employing the Kalman filter, the Luenberger observer and neural networks (NNs) [81, 87]. Further, applying polynomial transition functions, the optimal trajectory for gear-shifting was found, which guarantees velocity, acceleration and jerk continuity [74]. Although there has been extensive research on MSTs for EVs, there are still lacunae in gear-shifting algorithms and control.

In this paper, a gear-shifting control algorithm is developed for a novel modular MST designed for EVs. The designed MST has the advantages of simplicity and modularity. Firstly, after a brief description of the proposed MST, its dynamics model is established. Then, after stating the gear-shifting problem, the proposed control algorithm for a swift, seamless shift is explained. From a control point of view, the system under study is over-actuated, i.e., the number of control inputs is greater than the number of outputs. Besides, there are terminal constrains on some of the control inputs. Hence, it is suggested to change one of the inputs independently based on a 2-3 blending polynomial, which, besides meeting the end constraints, guarantees the continuity of the acceleration and jerk at the ends of the gear-shifting interval. Next, for controlling the new fully-actuated system, a linear quadratic integral (LQI) controller is employed, which is an extension of the linear quadratic regulator (LQR) for tracking problems. Simulation results demonstrate that the proposed control algorithm is very promising for a seamless, swift shift in the designed MST, even in the presence of unknown disturbances.

An outline of the paper follows. In Section 5.2, the proposed MST designed for EVs is briefly described. The mathematical model of the transmissions is derived in Subsection 5.2.1, while the gear-shifting problem is explained in Subsection 5.2.2. The proposed gear-shifting control algorithm is discussed in Section 5.3. Simulation results are reported in Section 5.4.

5.2 The Proposed MST Designed for EVs

First, the mathematical model of the proposed MST designed for EVs is derived using a Lagrangian formulation. Next, the gear-shifting problem is discussed.

5.2.1 Mathematical Modelling

All planetary gear sets in the proposed MST designed for EVs share the same carrier, as represented in Fig. 5.1. As well, all sun gears on each side of the transmission are installed on the same shaft. In the underdrive gear train, the sun gears and the carrier are connected to the input and output shafts, respectively, as depicted in Fig. 5.1(a), while the overdrive gear train operates the other way around, as shown in Fig. 5.1(b). To achieve the desired speed ratio, the corresponding clutch should be engaged. For shifting between speed ratios, the engaged clutch should be released and another one should be engaged. The underdrive and overdrive gear trains can be combined into one single transmission, as indicated in Fig. 5.1(c). In the new MST, two friction clutches, C_f^i and C_f^o, are applied between carrier and planet gears to lock the free overdrive or underdrive gear train. The main advantages of the proposed MST designed for EVs are modularity and simplicity. The

mathematical model of a two-speed underdrive gear train, illustrated in Fig. 5.1(d), is now derived using a Lagrangian formulation.

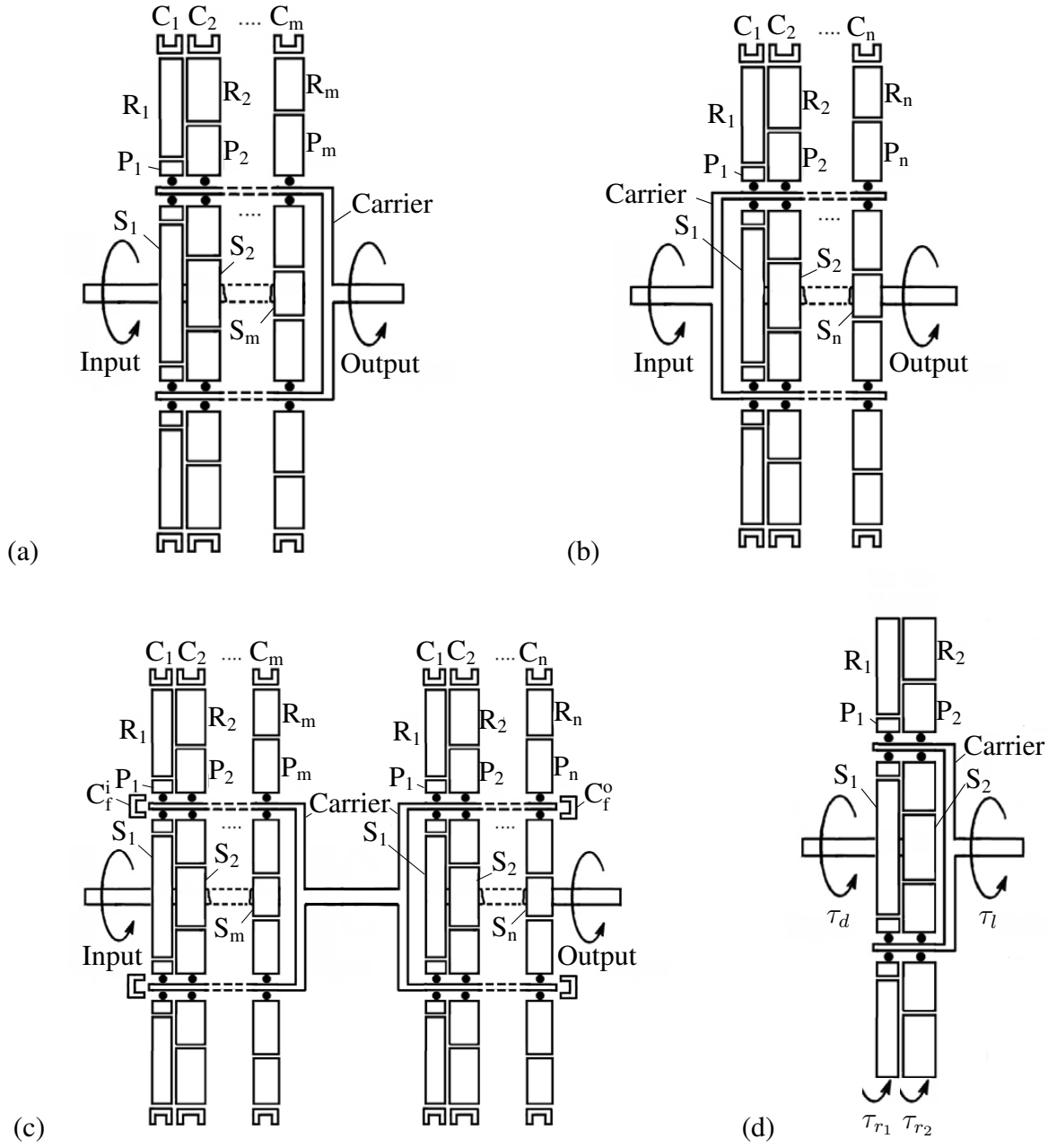

Figure 5.1: Multi-stage planetary gear sets: (a) underdrive gear train; (b) overdrive gear train; (c) combined MST; and (d) a two-stage planetary gear set

The Lagrange equation is given below.

$$\frac{d}{dt}\left(\frac{\partial L}{\partial \dot{\mathbf{q}}}\right) - \frac{\partial L}{\partial \mathbf{q}} = \frac{\partial}{\partial \dot{\mathbf{q}}}\left(\Pi - \Delta\right), \quad L = T - V \tag{5.1}$$

with $\mathbf{q}$, T, V, L, Π and Δ denoting the vector of generalized coordinates, the kinetic energy, the potential energy, the Lagrangian, the power supplied and the dissipation function, respectively. The total kinetic energy of the system is

$$T = T_c + T_s + T_r + nT_p \tag{5.2}$$

where T_c, T_s, T_r and T_p indicate the kinetic energies of the carrier, the sun, the ring and the planet gears, respectively, while n is the number of planet gears in each set. These items are given by

$$T_c = \frac{1}{2} I_c \omega_c^2, \quad T_s = \frac{1}{2} \left(I_{s_1} + I_{s_2} \right) \omega_s^2, \quad T_r = \frac{1}{2} I_{r_1} \omega_{r_1}^2 + \frac{1}{2} I_{r_2} \omega_{r_2}^2 \tag{5.3a}$$

$$T_p = \frac{1}{2} m_{p_1} v_{p_1}^2 + \frac{1}{2} I_{p_1} \omega_{p_1}^2 + \frac{1}{2} m_{p_2} v_{p_2}^2 + \frac{1}{2} I_{p_2} \omega_{p_2}^2, \quad v_{p_1} = v_{p_2} = r_c \omega_c \tag{5.3b}$$

with I_{s_1}, I_{s_2}, I_{r_1}, I_{r_2}, I_{p_1}, and I_{p_2} denoting the moments of inertia of the sun, the ring, and the planet gears of the first and the second gear sets, respectively, and I_c that of the carrier. Besides, m_{p_1}, m_{p_2}, v_{p_1} and v_{p_2} denote the masses and the speeds of the centers of mass of each planet gear for each gear set. Also, ω_s, ω_c, ω_{r_1} and ω_{r_2} represent the angular velocities of the sun, carrier, and the first and the second ring gears, respectively, while r_c the radius of the carrier. Note that, since all elements are modeled as statically and dynamically balanced rigid bodies in this paper, the total potential energy of the system is assumed to remain constant.[1] The power supplied to the system and the dissipation function can be expressed as

$$\Pi = \tau_d \omega_s + \tau_l \omega_c + \tau_{r_1} \omega_{r_1} + \tau_{r_2} \omega_{r_2}, \quad \Delta = \frac{1}{2} c_c \omega_c^2 + \frac{1}{2} c_s \omega_s^2 \tag{5.4}$$

with τ_d, τ_l, τ_{r_1} and τ_{r_2} indicating the drive torque of an EM applied to the input shaft, the external load applied to the output shaft, and the torques of the first and the second clutch applied to the first and the second ring, respectively, as shown in Fig. 5.1(d). Moreover, c_c and c_s denote the resultant damping coefficients obtained from experiments, including the effects of all bearings and friction. Substituting Eqs. (5.2)–(5.4) into Eq. (5.1) and using the kinematic relations obtained by the pure-rolling assumption between gears in contact, the dynamics model of the system is derived as

$$A_0 \dot{\omega}_s + B_0 \dot{\omega}_c = \tau_d - c_s \omega_s - \frac{r_{s_1}}{r_{r_1}} \tau_{r_1} - \frac{r_{s_2}}{r_{r_2}} \tau_{r_2} \tag{5.5a}$$

$$B_0 \dot{\omega}_s + C_0 \dot{\omega}_c = \tau_l - c_c \omega_c + \frac{2 r_c}{r_{r_1}} \tau_{r_1} + \frac{2 r_c}{r_{r_2}} \tau_{r_2} \tag{5.5b}$$

[1] Everything neglected in the model derivation, such as nonlinearities, flexibility and dry friction, can be included in the unknown disturbance and external load applied to the transmission system. For a more detailed model of the transmission, the reader is referred to a previous work [87].

with A_0, B_0 and C_0 defined as the entries of the 2×2 generalized inertia matrix:

$$A_0 = I_{s_1} + I_{s_2} + \left(\frac{r_{s_1}}{r_{r_1}}\right)^2 I_{r_1} + \left(\frac{r_{s_2}}{r_{r_2}}\right)^2 I_{r_2} + n\left(\left(\frac{r_{s_1}}{r_{p_1}}\right)^2 I_{p_1} + \left(\frac{r_{s_2}}{r_{p_2}}\right)^2 I_{p_2}\right) \tag{5.6a}$$

$$B_0 = -4r_c\left(\frac{r_{s_1}}{r_{r_1}^2} I_{r_1} + \frac{r_{s_2}}{r_{r_2}^2} I_{r_2}\right) - 2nr_c\left(\frac{r_{s_1}}{r_{p_1}^2} I_{p_1} + \frac{r_{s_2}}{r_{p_2}^2} I_{p_2}\right) \tag{5.6b}$$

$$C_0 = I_c + 4r_c^2\left(\frac{I_{r_1}}{r_{r_1}^2} + \frac{I_{r_2}}{r_{r_2}^2}\right) + nr_c^2\left(m_{p_1} + m_{p_2} + \frac{I_{p_1}}{r_{p_1}^2} + \frac{I_{p_2}}{r_{p_2}^2}\right) \tag{5.6c}$$

Note that r_{s_1}, r_{s_2}, r_{r_1}, r_{r_2}, r_{p_1} and r_{p_2} denote the pitch radius of the sun, the ring, and the planet gears of the first and the second planetary gear sets, respectively.

5.2.2 Gear-shifting Problem

With $x_1(t) = \omega_c(t)$ and $x_2(t) = \omega_s(t)$ denoting the state variables, using Eqs. (5.5) under no external load, the state-space equations can be expressed as

$$\dot{\mathbf{x}}(t) = \mathbf{A}\mathbf{x}(t) + \mathbf{B}\mathbf{u}(t) \tag{5.7}$$

with $\mathbf{u}(t) = \begin{bmatrix}\tau_{r_1}(t) & \tau_{r_2}(t) & \tau_d(t)\end{bmatrix}^T$ indicating the control input. As well, $\mathbf{A}$ and $\mathbf{B}$ are constant 2×2 and 2×3 matrices, with the entries depending on the parameters in Eqs. (5.5), such as radii of the elements, the generalized inertias, and the damping coefficients. Further, we assume that, for instance, we want to switch from the first to the second gear ratio, i.e., upshifting. In this case, at the beginning of the gear-shifting process, at $t = t_0$, the first ring gear is engaged and the second one released, i.e.,

$$\omega_{r_1}(t_0) = 0, \quad \tau_{r_2}(t_0) = 0 \tag{5.8}$$

At $t = t_f$, the end of gear-shifting, we should have the second ring gear engaged and the first one released, namely,

$$\omega_{r_2}(t_f) = 0, \quad \tau_{r_1}(t_f) = 0 \tag{5.9}$$

Note that Eqs. (5.8) and (5.9) represent initial and final constraints on some control inputs.

5.3 Gear-shifting Control

For a swift, seamless shift, the angular velocity $\omega_c(t)$ of the output shaft should remain constant during gear-shifting, i.e., $\omega_c(t) = \omega_{c_0}$, $t \in [t_0, t_f]$, where ω_{c_0} is the angular velocity of the output before shifting. As well, assuming $\omega_s(t_0) = \omega_{s_0}$ and $\omega_s(t_f) = \omega_{s_f}$, the angular velocity $\omega_s(t)$ of the input shaft should follow the 3-4-5 *blending polynomial* introduced in an earlier paper [74], namely,

$$\omega_{5s}(t) = \Delta\omega \left(6\theta^5 - 15\theta^4 + 10\theta^3\right) + \omega_{s_0}, \quad \theta \equiv \frac{t - t_0}{t_f - t_0}, \quad \Delta\omega \equiv \omega_{s_f} - \omega_{s_0} \tag{5.10}$$

which guarantees the continuity of the angular velocity, acceleration and jerk at both ends. In other words, the desired value of the state vector is $\mathbf{r}(t) = [\omega_{c_0} \quad \omega_{5s}(t)]^T$. However, the system is over-actuated; there are only two states to be controlled but three control inputs. Also, according to Eqs. (5.8) and (5.9), there are initial and final constraints on some of the control inputs. One way to cope with the above-mentioned issues is to assign one of the inputs independently, such that the terminal constraints are satisfied, and find the other control inputs using an appropriate controller. Since it is assumed that at the beginning of gear-shifting the first ring gear is engaged and the second released, conditions (5.8) are satisfied automatically. Accordingly, the first input is assigned here to satisfy the second condition in Eq. (5.9), i.e., the first planetary gear set should be released at the end. In other words, since $\tau_{r_1}(t_0) = \tau_{r_{10}}$ is assumed to be known and $\tau_{r_1}(t_f) = \tau_{r_{1f}}$, to guarantee the continuity of the angular velocity, acceleration and jerk at both ends, we can use a 2-3 blending polynomial for the first input, namely,

$$\tau_{r_1}(t) = \Delta\tau_{r_1} \left(-2\theta^3 + 3\theta^2\right) + \tau_{r_{10}}, \quad \theta \equiv \frac{t - t_0}{t_f - t_0}, \quad \Delta\tau_{r_1} \equiv \tau_{r_{1f}} - \tau_{r_{10}} \tag{5.11}$$

For details of different blending polynomials and their properties, we refer to a previous work [74].

Since $\tau_{r_{1f}} = 0$, Eq. (5.11) reduces to

$$\tau_{r_1}(t) = \tau_{r_{10}} \left(2\theta^3 - 3\theta^2 + 1\right) \tag{5.12}$$

If the first input changes independently, based on Eq. (5.12), the new control input will be $\mathbf{u}(t) = \begin{bmatrix}\tau_{r_2}(t) & \tau_d(t)\end{bmatrix}^T$. The new tracking problem can be controlled using a linear quadratic integral (LQI) controller, which is briefly explained below.

5.3.1 Linear Quadratic Integral (LQI) Control

LQI is an extension of the linear quadratic regulator (LQR) for tracking problems. In LQI, an integral compensator, i.e., the integral of the tracking error, is introduced to guarantee robust tracking [93, 94], as represented in Fig. 5.2. The LQI is briefly described below.

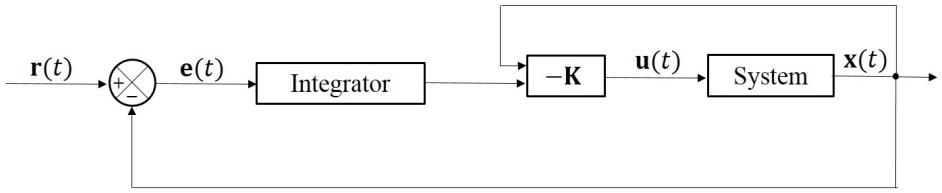

Figure 5.2: The LQI control loop

Consider an n-dimensional fully-actuated linear time-varying (LTV) system given by

$$\dot{\mathbf{x}}(t) = \mathbf{A}(t)\mathbf{x}(t) + \mathbf{B}(t)\mathbf{u}(t) \tag{5.13}$$

The objective of LQI control is to find the optimal feedback law of the form

$$\mathbf{u}(t) = -\mathbf{K}(t)\mathbf{z}(t), \quad \mathbf{z}(t) = \begin{bmatrix} \mathbf{x}(t) \\ \mathbf{e}_I(t) \end{bmatrix}, \quad \mathbf{e}(t) = \mathbf{r}(t) - \mathbf{x}(t) \tag{5.14}$$

which minimizes the performance index

$$J = \int_{t_0}^{t_f} \left[\mathbf{z}^T(t)\mathbf{Q}(t)\mathbf{z}(t) + \mathbf{u}^T(t)\mathbf{R}(t)\mathbf{u}(t)\right] dt \tag{5.15}$$

with $\mathbf{r}(t)$ and $\mathbf{e}_I(t)$ indicating the desired state vector and the integral of the error $\mathbf{e}(t)$, respectively. Also, $\mathbf{Q}(t)$ and $\mathbf{R}(t)$ denote the weighting matrices; $\mathbf{Q}(t)$ is positive semi-definite, while $\mathbf{R}(t)$ is positive definite. In fact, $\mathbf{e}_I(t)$ is

$$\mathbf{e}_I(t) = \int_{t_0}^{t} \left[\mathbf{r}(\tau) - \mathbf{x}(\tau)\right] d\tau \tag{5.16}$$

Hence,

$$\dot{\mathbf{e}}_I(t) = \mathbf{r}(t) - \mathbf{x}(t) \tag{5.17}$$

which can be considered as a new state equation. Combining Eqs. (5.13) and (5.17) yields the new state-space equation

$$\begin{bmatrix} \dot{\mathbf{x}}(t) \\ \dot{\mathbf{e}}_I(t) \end{bmatrix} = \begin{bmatrix} \mathbf{A}(t) & \mathbf{O} \\ -\mathbf{1} & \mathbf{O} \end{bmatrix} \begin{bmatrix} \mathbf{x}(t) \\ \mathbf{e}_I(t) \end{bmatrix} + \begin{bmatrix} \mathbf{B}(t) \\ \mathbf{O} \end{bmatrix} \mathbf{u}(t) + \begin{bmatrix} \mathbf{O} \\ \mathbf{1} \end{bmatrix} \mathbf{r}(t) \tag{5.18}$$

with $\mathbf{O}$ and $\mathbf{1}$ indicating the $n \times n$ zero and identity matrices, respectively. Applying a change of variables, the new state-space equation (5.18) and the performance index (5.15) can be proven to define the LQR problem with the new state matrices [95]

$$\mathbf{A}_n(t) = \begin{bmatrix} \mathbf{A}(t) & \mathbf{O} \\ -\mathbf{1} & \mathbf{O} \end{bmatrix}, \quad \mathbf{B}_n(t) = \begin{bmatrix} \mathbf{B}(t) \\ \mathbf{O} \end{bmatrix} \tag{5.19}$$

The above-mentioned optimization problem leads to a differential *Riccati* equation (DRE). After finding the solution to the Riccati equation, the optimal gain $\mathbf{K}(t)$, and hence the optimal control input $\mathbf{u}(t)$, can be determined using Eq. (5.14).

5.4 Simulation Results

This section provides the simulation results obtained with the proposed approach, i.e., the 2-3 blending polynomial and the LQI controller, for gear-shifting control in MSTs for EVs.

The desired state vector is $\mathbf{r}(t) = [\omega_{c_0} \quad \omega_{5s}(t)]^T$, as mentioned in Section 5.3. Assuming that the gear-shifting process begins at $t_0 = 5$ s and ends at[2] $t_f = 6$ s, while the gear ratios are 4 and $8/3$, and $\omega_{c_0} = 10$ rad/s, for upshifting we have

$$\omega_s(t_0) = 40 \text{ rad/s}, \quad \omega_s(t_f) = \frac{80}{3} \text{ rad/s} \tag{5.20}$$

As well,

$$\omega_{r_1}(t_0) = 0, \quad \tau_{r_2}(t_0) = 0, \quad \omega_{r_2}(t_f) = 0, \quad \tau_{r_1}(t_f) = 0 \tag{5.21}$$

The desired and output values of the states, i.e., $\omega_c(t)$ and $\omega_s(t)$, are compared in Fig. 5.3(a). As observed, the states track the reference signals acceptably; $\omega_s(t)$ tracks the 3-4-5 blending polynomial, while $\omega_c(t)$ remains constant during gear-shifting, as expected. Also, for the ring gears, the reference and output values of the angular velocities are compared in Fig. 5.3(b). As shown in the figure, at the beginning of the gear-shifting, the first planetary gear set is engaged, i.e., ω_{r_1} is zero, while at the end of gear-shifting, ω_{r_2} is zero, namely, the second planetary gear set is engaged. Note that, according to the kinematic constraints, the angular velocities of the ring gears also track the 3-4-5 blending polynomial, which assures the angular velocity, acceleration and jerk continuity.

The control inputs during gear-shifting are also indicated in Fig. 5.4. As illustrated in the figure, the torques change smoothly. The torque τ_{r_1} applied to the first ring gear changes independently, based on the 2-3 blending polynomial (5.12), starting from its initial value $\tau_{r_{1_0}}$ to zero. The other torques, τ_{r_2} and τ_d, are determined by the LQI controller, as discussed in Subsection 5.3.1. As expected, at the beginning, the torque τ_{r_2} applied to the second ring gear is zero, while at the end, the torque τ_{r_1} applied to the first ring gear is zero, i.e., the first gear set is disengaged completely.

To assess the performance of the proposed approach and the LQI controller, a sudden unknown external disturbance is assumed to be applied to the transmission system during gear-shifting, which includes the effect of the terms neglected in the model derivation. The results are depicted in

[2]This is just an example to show that the algorithm works. In fact, depending on the limitations of the power supply, the gear-shifting time can be reduced considerably.

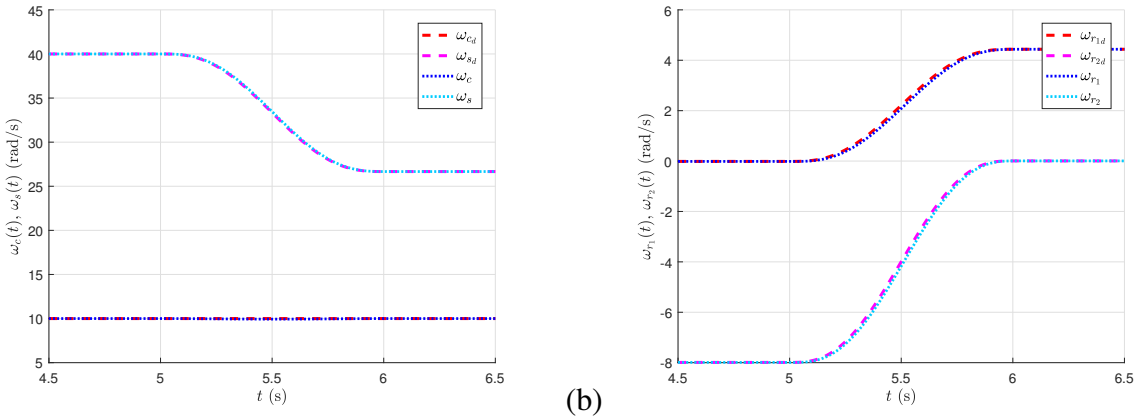

Figure 5.3: The angular velocities during upshifting: (a) the input and output shafts; and (b) the ring gears

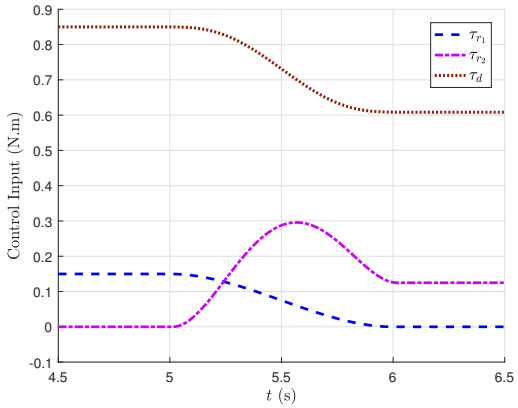

Figure 5.4: The control inputs during upshifting

Figs. 5.5 and 5.6; the states and the ring gear angular velocities are represented in Figs. 5.5(a) and (b), while the inputs are shown in Fig. 5.6. In this case, the disturbance does not affect the first input $\tau_{r_1}(t)$, since it is not included in the new control input, i.e., $\mathbf{u}(t) = \begin{bmatrix} \tau_{r_2}(t) & \tau_d(t) \end{bmatrix}^T$. In fact, $\tau_{r_1}(t)$ changes independently, based on the 2-3 blending polynomial.

In a real EV, some parameters, such as the mass of the vehicle, the vehicle speed, the forces between road and tires, the road slope and the aerodynamic drag force, influence the size of the EMs used and the ranges of power and the torques applied significantly. For instance, assuming an external load applied to the output shaft, which includes the effects of all parameters mentioned above, Figs. 5.7 and 5.8 illustrate the results for downshifting in higher angular velocities, where $\omega_{c_0} = 100$ rad/s, $\omega_s(t_0) = 800/3$ rad/s and $\omega_s(t_f) = 400$ rad/s. As shown in these figures, the results of the proposed scheme are plausible in this case too; the states and the ring gears follow the command signals adequately, while all terminal state and control conditions are satisfied. Note that, in this case, because of the presence of the external load, the torques applied by the EMs increase

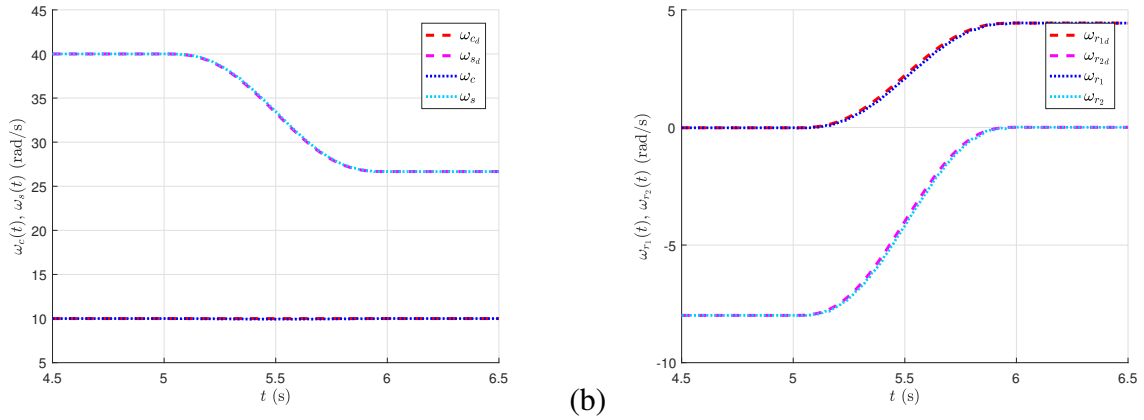

Figure 5.5: The angular velocities for upshifting in the presence of an unknown disturbance applied at $t_0 = 5$ s: (a) the input and output shafts; and (b) the ring gears

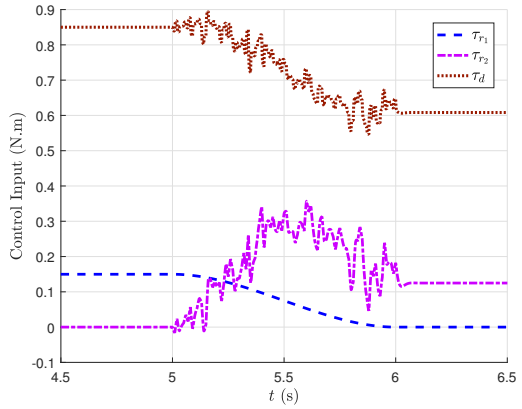

Figure 5.6: The control inputs for upshifting in the presence of an unknown disturbance

considerably.

Simulation results show that the proposed approach is highly encouraging for gear-shifting control in MSTs for EVs, which is an over-actuated system with terminal constraints on the control input. In other words, a smooth shift can be achieved, while the end constrains are met, even in the presence of various unknown disturbances and external loads. In fact, in comparison to an earlier two-phase control algorithm for gear-shifting in EVs, with approaching and coasting phases, developed recently by our team [92], the strategy proposed here is much simpler and readily implementable in the real world. Furthermore, the control inputs vary more smoothly than in the prior study.

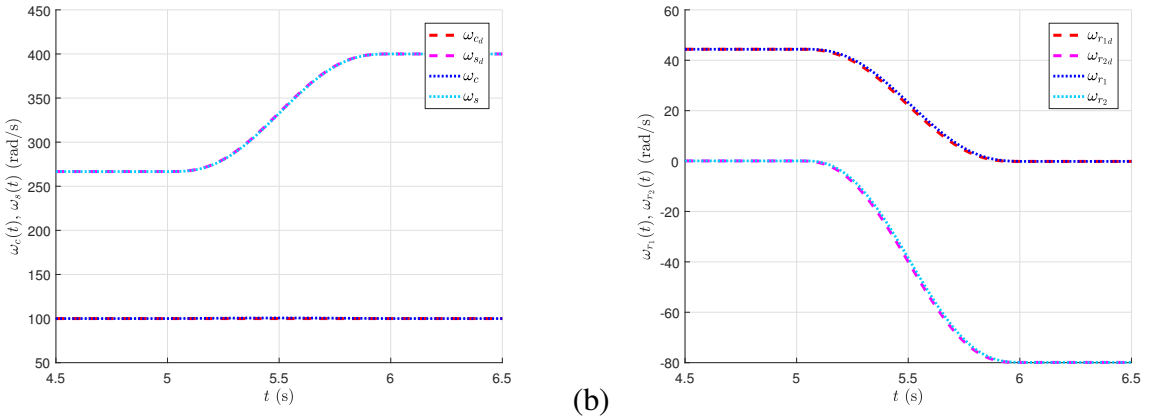

Figure 5.7: The angular velocities for downshifting in the presence of an external load on the output: (a) the input and output shafts; and (b) the ring gears

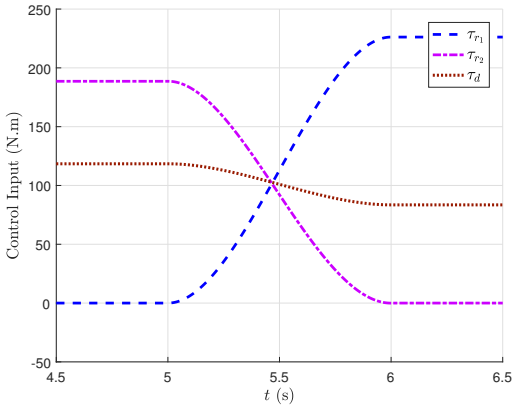

Figure 5.8: The control inputs for downshifting in the presence of an external load on the output

5.5 Conclusions

By adopting MSTs, with a seamless and swift gear-shifting, one can enhance the performance of EVs. Based on the mathematical model derived here, a gear-shifting control scheme was built for a novel modular MST designed for EVs, to assure smoothness and swiftness. Since there were terminal constraints on some of the control inputs and also the transmission system was over-actuated, it was suggested to change one input separately, based on a 2-3 blending polynomial. This way, the continuity of the acceleration and jerk are guaranteed [74]. Also, the input end constraints are met. An LQI controller, i.e., an extension of the LQR for tracking problems, was then used to control the new fully-actuated system. Simulation results show that the proposed control approach is promising for a swift, seamless shift, even in the presence of unknown external disturbances. This is made apparent by the desired smooth trajectories followed by the angular velocities and the inputs [96].

Part III

Developing Optimal Control Schemes for Gear-shifting in Electric Vehicles with Multi-speed Transmissions

Chapter 6

Optimal Control with Terminal Control Constraints and Over-actuation

Abstract

Necessary optimality conditions for several types of optimal control problems with terminal constraints on both the system state and its control are derived using a direct variational approach under strong regularity conditions. Imposing additional constraints restricts the set of admissible controls that might endanger the existence of solutions. The properties of attainable sets for selected, restricted classes of admissible controls are thus discussed for the case of linear systems to explain the advantages of over-actuation. The results are used to achieve control allocation in an over-actuated linear quadratic tracking problem that accomplishes gear-shifting in a multi-speed transmission system of an electric vehicle. The application of the results extends to optimal control problems in which imposing terminal constraints on the state, its time derivative, and/or its controls is necessary to guarantee smooth system operation over extended periods, i.e., seamless blending of operation modes.

6.1 Introduction

Rapid progress in the development of high-end engineering technologies poses new challenges in the design and operation of machinery. In machine design, increasing importance is assigned to

reliability, precision, and functionality of mechanisms. At the same time, only low cost and energy saving designs are acceptable. Such strenuous quality specifications almost always require the use of optimization tools.

Specifically, the class of problems that provided motivation for the work reported here concerns the optimal design of a new generation of multi-speed transmissions (MSTs) that will significantly improve the functioning of electrical vehicles (EVs) [92, 68, 86]. The EV technology is developing rapidly, as it is becoming increasingly important in modern transportation systems.

EV gear-shifting mechanisms must have the capacity to perform rapid changes of motor speed while securing smooth roll of the car chassis before and after every speed change. The industry standards are very high, calling for up to 98% efficiency, safety, high running stability, minimum maintenance, and minimum operating noise. For these reasons, the gear-shifting patterns are best sought as solutions to a minimum-time, minimum-effort finite-horizon optimal control problem. For the speed of the vehicle to vary smoothly, hard constraints on both the system state and the control effort must be imposed at the terminal instant of the gear shifting horizon. The resulting optimal control problem formulation is not typical due to the presence of the explicit, hard terminal constraints on the control effort that cannot be circumvented while maintaining equivalent operational quality of the resulting design. Interestingly, the necessary conditions for optimality in the presence of such terminal control-effort constraints, and specifically the explicit statement of the boundary conditions that they require, have been omitted from the existing literature, which is exceptionally rich.

With variational analysis as a precursor subject—see the exhaustive work [97, 98]—classical texts on optimal control [99, 100, 101, 102] cover both the minimum principle and dynamic programming, while restricting the class of admissible controls to continuous or piecewise continuous functions. More recent texts favor significant relaxation of optimality conditions for a much larger class of only measurable admissible controls [103, 104, 105]. The latter employs generalized gradients and discusses the properties of viscosity solutions to the Hamilton-Jacobi-Bellman (HJB) equation. The hybrid minimum principle and hybrid dynamic programming are further extensions of the theory [104, 106, 107, 108].

From a pure optimality viewpoint, the wider the class of admissible controls, the lower the cost value achieved and the higher the chances of existence of solutions. Although switched or hybrid approaches in the control of gear-shifting in hybrid electric vehicles have been considered [109, 110, 111, 112], such results are valued as a proof of concept (of rapid control being achievable) rather than a practical solution to the actual problem. In switching or hybrid optimal control, the continuity of the control effort is no issue, while optimality is strictly limited to the interior of a given time interval with little interest on how the optimal trajectories may affect the future evolution of the system.

Many industrial applications hence still require restricted sets of smooth admissible controls; examples abound in robotics, vehicle control, or machine design, where smooth operation is a valued attribute and the pieces of optimum trajectories must connect seamlessly [113, 114]; other recent developments requiring smooth control effort can be cited [115, 116, 117, 118].

Optimization problems that call for high regularity of trajectories can achieve the above goal by imposing point constraints on both ends of the optimization interval. Such problem statements then lend themselves directly to solution methods in classical variational analysis. While the necessary conditions for strong optimality always involve the Euler-Lagrange equations that hold under well-established regularity assumptions, the major difficulty resides in the derivation of adequate boundary conditions that secure the satisfaction of the constraints imposed on the system. As already mentioned above, the boundary conditions corresponding to the presence of hard terminal constraints on the control effort (rather than on the state) are absent from the current literature. The reason may lie in that enforcing such constraints can be achieved indirectly by imposing an adequately high end-point penalty, while smoothness of trajectories can be achieved by extending the state of the system (adding integrators). Since neither of these alternatives can deliver fully equivalent designs, the desired boundary conditions are developed here explicitly.

When many, or higher-order constraints are imposed on the system, the existence of admissible controls that satisfy the required boundary conditions is an obvious concern. In such instances, the existence of extremals can be secured by introducing additional, seemingly redundant, actuation. This leads to the notion of over-actuated systems, i.e. systems with fewer states than control variables, which then need to be adequately "allocated" to carry out the required optimal control task [119, 120, 121, 122].

Based on the above problem statement, the contributions of this paper are described below.

Assuming suitable regularity, necessary conditions for optimality are derived for optimal control problems with soft (penalty-type) and hard terminal constraints on controls and state variables for both fixed or free terminal time. The conditions are shown to follow naturally from the solution of the general Lagrange variational problem with nonholonomic constraints. A comprehensive treatment of optimality conditions pertaining to a broad spectrum of optimal control problem formulations in the presence of end-point constraints is absent from the literature. The necessary conditions are then interpreted to apply to regulator and trajectory-tracking control problems with soft or hard constraints on terminal values of the state and the controls in a possibly over-actuated setting.

The discussion of the properties of the attainable sets for problems with terminal control and state constraints and the role of over-actuation is limited (for simplicity) to linear time-invariant (LTI) systems. It is shown that, for completely controllable LTI systems, the attainable set is insensitive to terminal constraints on the controls. On the other hand, satisfaction of additional higher-order constraints on the terminal states, such as terminal constraints on the state derivative, generally

requires additional control power (over-actuation) and adequate control allocation. In both cases, imposition of end-point control constraints can be viewed as adding isoperimetric constraints to the underlying variational problem.

The necessary conditions and associated results are applied to achieve closed-loop control allocation in the problem of gear-shifting [92, 68, 86] in a novel design of an MST for EVs [81, 87]. The study aims to track a pre-planned "blending trajectory" that achieves the gear-shift, as previously reported [74]. Although the strict optimality of the blending trajectory cannot be claimed (it is just one of infinitely many possible solutions of an Euler-Lagrange equation for a singular variational problem), the latter is shown to satisfy the imposed terminal conditions as necessary for seamless gear-shifting. It is shown that the blending trajectory can be tracked exactly, as the problem is over-actuated. The two-stage feedback control approach to gear-shifting proposed here constitutes a significant improvement over the previous non-robust, open-loop trajectory following approach based on the inverse dynamics of the system [74].

The paper organization follows. Section 6.2 establishes the necessary conditions for optimality in general smooth optimal control problems with terminal constraints on both the state and the control, but in the absence of any hard functional constraints (except for the constraint involving the dynamical system equation). Without loss of generality, the class of problems considered includes systems that are over-actuated. In Section 6.3, the potential benefits of over-actuation are briefly discussed. Since the necessary results of Section 6.2 pertain to systems that may be time-varying, the latter are further specified as linear quadratic trajectory tracking problems in Section 6.4. Finally, the necessary conditions developed here are employed to deliver an optimal control for gear-shifting in multi-speed EVs.

6.2 Necessary Conditions for Optimality in Problems with Terminal Control and State Constraints

The derivation below extends the standard optimality conditions for general time-varying nonlinear problems of class $C^2[t_0, t_f]$ on an interval $[t_0, t_f]$ to the case when the set of admissible controls may be restricted to contain functions satisfying point constraints at the final time t_f. Admissible control efforts might further be required to steer the system to a given terminal state $\mathbf{x}(t_f)$, if such a constraint is present. For simplicity, it is assumed that magnitude constraints on the controls and state over the entire horizon $[t_0, t_f]$ can be enforced implicitly by shaping the cost functional. Such formulation lends itself naturally to the methods of variational analysis used here in similarity with the classical approaches of Kirk [70] and Naidu [71]. A similar notation used by Kirk [70] is also adopted so that the reader can easily trace the differences.

As expected, the necessary conditions for the special case described above coincide with those of Kirk [70], inasmuch as they both require the solution of the Euler-Lagrange equations, the state and co-state equations, and lead to the same Hamiltonian function. The difference appears in the variational statement of the boundary conditions, as per Eq. (6.5), which now contains an additional term associated with the variation $\delta\mathbf{u}_f$ that is absent from the optimality conditions considered elsewhere. The development of this term may be traced through Eqs. (6.13)–(6.21) in the proof of the theorem. The difference in boundary conditions also appears in the discussion of the possible cases of constrained problems (6.22)–(6.24) and in the compact Hamiltonian re-statement of the results of Theorem 1, for which the untypical "transversality conditions" of Eq. (6.27) are missing in the optimal-control literature.

Theorem 1 *Consider a, potentially over-actuated, optimal control problem with the cost functional*

$$J(\mathbf{u}) = h(t_f, \mathbf{x}(t_f), \mathbf{u}(t_f)) + \int_{t_0}^{t_f} g(t, \mathbf{x}(t), \mathbf{u}(t))dt \tag{6.1}$$

subject to differential constraints

$$\dot{\mathbf{x}}(t) = \mathbf{f}(t, \mathbf{x}(t), \mathbf{u}(t)), \;\; \mathbf{x}(t) \in \mathbb{R}^n, \;\; \mathbf{u}(t) \in \mathbb{R}^m, \;\; t \in [t_0, t_f] \tag{6.2}$$

where all the functions, including the admissible controls, are assumed to be of class $C^2[t_0, t_f]$, while the initial conditions of the system and the initial control values are considered fixed: $\mathbf{x}(t_0) = \mathbf{x}_0$; $\mathbf{u}(t_0) = \mathbf{u}_0$. The general necessary conditions for optimality (comprising a variety of terminal constraints) take the form described below:
The Euler-Lagrange equation comes first

$$\frac{\partial g}{\partial \mathbf{u}}(t, \mathbf{x}(t), \mathbf{u}(t)) + \left[\frac{\partial \mathbf{f}}{\partial \mathbf{u}}(t, \mathbf{x}(t), \mathbf{u}(t))\right]^T \mathbf{p}(t) = \mathbf{0} \tag{6.3}$$

followed by the co-state (Lagrange multiplier) equation

$$\dot{\mathbf{p}}(t) = -\left[\frac{\partial \mathbf{f}}{\partial \mathbf{x}}(t, \mathbf{x}(t), \mathbf{u}(t))\right]^T \mathbf{p}(t) - \left[\frac{\partial g}{\partial \mathbf{x}}(t, \mathbf{x}(t), \mathbf{u}(t))\right] \tag{6.4}$$

subject to the system constraints (6.2) *and end-point boundary conditions written in variational form:*

$$\begin{aligned} &\left[\frac{\partial h}{\partial \mathbf{x}}(t_f, \mathbf{x}(t_f), \mathbf{u}(t_f)) - \mathbf{p}(t_f)\right]^T \delta\mathbf{x}_f + \left[\frac{\partial h}{\partial \mathbf{u}}(t_f, \mathbf{x}(t_f), \mathbf{u}(t_f))\right]^T \delta\mathbf{u}_f \\ &+ \left[g(t_f, \mathbf{x}(t_f), \mathbf{u}(t_f)) + \mathbf{p}^T(t_f)\mathbf{f}(t_f, \mathbf{x}(t_f), \mathbf{u}(t_f)) + \frac{\partial h}{\partial t}(t_f, \mathbf{x}(t_f), \mathbf{u}(t_f))\right] \delta t_f = 0 \end{aligned} \tag{6.5}$$

■

Proof (Employing a variational approach):

Under the assumed regularity of the functions involved

$$h(\mathbf{x}(t_f), \mathbf{u}(t_f), t_f) = h(\mathbf{x}(t_0), \mathbf{u}(t_0), t_0) + \int_{t_0}^{t_f} \frac{d}{dt} \left[h(\mathbf{x}(t), \mathbf{u}(t), t) \right] dt \tag{6.6}$$

the cost functional takes a simpler form

$$J(\mathbf{u}) = h(\mathbf{x}(t_0), \mathbf{u}(t_0), t_0) + \int_{t_0}^{t_f} \left\{ g(\mathbf{x}(t), \mathbf{u}(t), t) + \frac{d}{dt} \left[h(\mathbf{x}(t), \mathbf{u}(t), t) \right] \right\} dt \tag{6.7}$$

As t_0, $\mathbf{x}(t_0)$ and $\mathbf{u}(t_0)$ are considered fixed, the first term of the RHS of Eq. (6.7) does not involve any optimization variables; it is therefore omitted, $J(\mathbf{u})$ then becoming

$$J(\mathbf{u}) = \int_{t_0}^{t_f} \left\{ g(\mathbf{x}(t), \mathbf{u}(t), t) + \frac{d}{dt} \left[h(\mathbf{x}(t), \mathbf{u}(t), t) \right] \right\} dt \tag{6.8}$$

$$= \int_{t_0}^{t_f} \left\{ g(\mathbf{x}(t), \mathbf{u}(t), t) + \left[\frac{\partial h}{\partial \mathbf{x}}(\mathbf{x}(t), \mathbf{u}(t), t) \right]^T \dot{\mathbf{x}}(t) + \left[\frac{\partial h}{\partial \mathbf{u}}(\mathbf{x}(t), \mathbf{u}(t), t) \right]^T \dot{\mathbf{u}}(t) + \frac{\partial h}{\partial t}(\mathbf{x}(t), \mathbf{u}(t), t) \right\} dt \tag{6.9}$$

Using Lagrange multipliers $\mathbf{p}(t) \in \mathbb{R}^n$ to include the constraints (6.2) in the cost index (6.1) delivers the augmented index

$$J_a(\mathbf{u}) = \int_{t_0}^{t_f} \left\{ g(\mathbf{x}(t), \mathbf{u}(t), t) + \left[\frac{\partial h}{\partial \mathbf{x}}(\mathbf{x}(t), \mathbf{u}(t), t) \right]^T \dot{\mathbf{x}}(t) + \left[\frac{\partial h}{\partial \mathbf{u}}(\mathbf{x}(t), \mathbf{u}(t), t) \right]^T \dot{\mathbf{u}}(t) + \frac{\partial h}{\partial t}(\mathbf{x}(t), \mathbf{u}(t), t) + \mathbf{p}^T(t) \left[\mathbf{f}(\mathbf{x}(t), \mathbf{u}(t), t) - \dot{\mathbf{x}}(t) \right] \right\} dt \tag{6.10}$$

or, equivalently,

$$J_a(\mathbf{u}) = \int_{t_0}^{t_f} g_a(\mathbf{x}(t), \dot{\mathbf{x}}(t), \mathbf{u}(t), \dot{\mathbf{u}}(t), \mathbf{p}(t), t) dt \tag{6.11}$$

with

$$g_a(\mathbf{x}(t), \dot{\mathbf{x}}(t), \mathbf{u}(t), \dot{\mathbf{u}}(t), \mathbf{p}(t), t) = g(\mathbf{x}(t), \mathbf{u}(t), t) + \left[\frac{\partial h}{\partial \mathbf{x}}(\mathbf{x}(t), \mathbf{u}(t), t) \right]^T \dot{\mathbf{x}}(t) + \left[\frac{\partial h}{\partial \mathbf{u}}(\mathbf{x}(t), \mathbf{u}(t), t) \right]^T \dot{\mathbf{u}}(t) + \frac{\partial h}{\partial t}(\mathbf{x}(t), \mathbf{u}(t), t) + \mathbf{p}^T(t) \left[\mathbf{f}(\mathbf{x}(t), \mathbf{u}(t), t) - \dot{\mathbf{x}}(t) \right] \tag{6.12}$$

Introducing variations $\delta\mathbf{x}$, $\delta\dot{\mathbf{x}}$, $\delta\mathbf{u}$, $\delta\dot{\mathbf{u}}$, $\delta\mathbf{p}$ and δt_f, the first variation of the augmented cost index is

$$\begin{aligned}\delta J_a(\mathbf{u}) = \int_{t_0}^{t_f} \Bigg\{ & \left[\frac{\partial g_a}{\partial \mathbf{x}}(\mathbf{x}(t),\dot{\mathbf{x}}(t),\mathbf{u}(t),\dot{\mathbf{u}}(t),\mathbf{p}(t),t)\right]^T \delta\mathbf{x}(t) \\ & + \left[\frac{\partial g_a}{\partial \dot{\mathbf{x}}}(\mathbf{x}(t),\dot{\mathbf{x}}(t),\mathbf{u}(t),\dot{\mathbf{u}}(t),\mathbf{p}(t),t)\right]^T \delta\dot{\mathbf{x}}(t) \\ & + \left[\frac{\partial g_a}{\partial \mathbf{u}}(\mathbf{x}(t),\dot{\mathbf{x}}(t),\mathbf{u}(t),\dot{\mathbf{u}}(t),\mathbf{p}(t),t)\right]^T \delta\mathbf{u}(t) \\ & + \left[\frac{\partial g_a}{\partial \dot{\mathbf{u}}}(\mathbf{x}(t),\dot{\mathbf{x}}(t),\mathbf{u}(t),\dot{\mathbf{u}}(t),\mathbf{p}(t),t)\right]^T \delta\dot{\mathbf{u}}(t) \\ & + \left[\frac{\partial g_a}{\partial \mathbf{p}}(\mathbf{x}(t),\dot{\mathbf{x}}(t),\mathbf{u}(t),\dot{\mathbf{u}}(t),\mathbf{p}(t),t)\right]^T \delta\mathbf{p}(t) \Bigg\} dt \\ & + \int_{t_f}^{t_f+\delta t_f} g_a(\mathbf{x}(t),\dot{\mathbf{x}}(t),\mathbf{u}(t),\dot{\mathbf{u}}(t),\mathbf{p}(t),t)dt + \text{HOT} = 0 \end{aligned} \tag{6.13}$$

where HOT denotes “higher-order terms". To a first-order approximation,

$$\int_{t_f}^{t_f+\delta t_f} g_a(\mathbf{x}(t),\dot{\mathbf{x}}(t),\mathbf{u}(t),\dot{\mathbf{u}}(t),\mathbf{p}(t),t)dt \approx \left[g_a(\mathbf{x}(t_f),\dot{\mathbf{x}}(t_f),\mathbf{u}(t_f),\dot{\mathbf{u}}(t_f),\mathbf{p}(t_f),t_f)\right]\delta t_f \tag{6.14}$$

Since $\delta\dot{\mathbf{x}}(t) = d(\delta\mathbf{x}(t))/dt$ and $\delta\dot{\mathbf{u}}(t) = d(\delta\mathbf{u}(t))/dt$, integration by parts yields

$$\begin{aligned} & \int_{t_0}^{t_f} \left\{ \left[\frac{\partial g_a}{\partial \dot{\mathbf{x}}}(\mathbf{x}(t),\dot{\mathbf{x}}(t),\mathbf{u}(t),\dot{\mathbf{u}}(t),\mathbf{p}(t),t)\right]^T \delta\dot{\mathbf{x}}(t) + \left[\frac{\partial g_a}{\partial \dot{\mathbf{u}}}(\mathbf{x}(t),\dot{\mathbf{x}}(t),\mathbf{u}(t),\dot{\mathbf{u}}(t),\mathbf{p}(t),t)\right]^T \delta\dot{\mathbf{u}}(t) \right\} dt \\ & = \left[\frac{\partial g_a}{\partial \dot{\mathbf{x}}}(\mathbf{x}(t_f),\dot{\mathbf{x}}(t_f),\mathbf{u}(t_f),\dot{\mathbf{u}}(t_f),\mathbf{p}(t_f),t_f)\right]^T \delta\mathbf{x}(t_f) \\ & \quad + \left[\frac{\partial g_a}{\partial \dot{\mathbf{u}}}(\mathbf{x}(t_f),\dot{\mathbf{x}}(t_f),\mathbf{u}(t_f),\dot{\mathbf{u}}(t_f),\mathbf{p}(t_f),t_f)\right]^T \delta\mathbf{u}(t_f) \\ & \quad - \int_{t_0}^{t_f} \Bigg\{ \frac{d}{dt}\left[\frac{\partial g_a}{\partial \dot{\mathbf{x}}}(\mathbf{x}(t),\dot{\mathbf{x}}(t),\mathbf{u}(t),\dot{\mathbf{u}}(t),\mathbf{p}(t),t)\right]^T \delta\mathbf{x}(t) \\ & \quad + \frac{d}{dt}\left[\frac{\partial g_a}{\partial \dot{\mathbf{u}}}(\mathbf{x}(t),\dot{\mathbf{x}}(t),\mathbf{u}(t),\dot{\mathbf{u}}(t),\mathbf{p}(t),t)\right]^T \delta\mathbf{u}(t) \Bigg\} dt \end{aligned} \tag{6.15}$$

Furthermore, since t_0, $\mathbf{x}(t_0)$ and $\mathbf{u}(t_0)$ are fixed, with $\delta\mathbf{x}(t_0) = \mathbf{0}$ and $\delta\mathbf{u}(t_0) = \mathbf{0}$, substitution of Eqs. (6.14) and (6.15) into Eq. (6.13), while noting that

$$\delta\mathbf{x}(t_f) = \delta\mathbf{x}_f - \dot{\mathbf{x}}(t_f)\delta t_f, \quad \delta\mathbf{u}(t_f) = \delta\mathbf{u}_f - \dot{\mathbf{u}}(t_f)\delta t_f \tag{6.16}$$

yields an expression for the first variation of the cost, namely,

$$
\begin{aligned}
&\delta J_a(\mathbf{u}) = \\
&\left[\frac{\partial g_a}{\partial \dot{\mathbf{x}}}(\mathbf{x}(t_f), \dot{\mathbf{x}}(t_f), \mathbf{u}(t_f), \dot{\mathbf{u}}(t_f), \mathbf{p}(t_f), t_f)\right]^T \delta \mathbf{x}_f + \left[\frac{\partial g_a}{\partial \dot{\mathbf{u}}}(\mathbf{x}(t_f), \dot{\mathbf{x}}(t_f), \mathbf{u}(t_f), \dot{\mathbf{u}}(t_f), \mathbf{p}(t_f), t_f)\right]^T \delta \mathbf{u}_f \\
&+ \Bigg\{ g_a(\mathbf{x}(t_f), \dot{\mathbf{x}}(t_f), \mathbf{u}(t_f), \dot{\mathbf{u}}(t_f), \mathbf{p}(t_f), t_f) - \left[\frac{\partial g_a}{\partial \dot{\mathbf{x}}}(\mathbf{x}(t_f), \dot{\mathbf{x}}(t_f), \mathbf{u}(t_f), \dot{\mathbf{u}}(t_f), \mathbf{p}(t_f), t_f)\right]^T \dot{\mathbf{x}}(t_f) \\
&- \left[\frac{\partial g_a}{\partial \dot{\mathbf{u}}}(\mathbf{x}(t_f), \dot{\mathbf{x}}(t_f), \mathbf{u}(t_f), \dot{\mathbf{u}}(t_f), \mathbf{p}(t_f), t_f)\right]^T \dot{\mathbf{u}}(t_f) \Bigg\} \delta t_f \\
&+ \int_{t_0}^{t_f} \Bigg\{ \left[\left[\frac{\partial g_a}{\partial \mathbf{x}}(\mathbf{x}(t), \dot{\mathbf{x}}(t), \mathbf{u}(t), \dot{\mathbf{u}}(t), \mathbf{p}(t), t)\right]^T - \frac{d}{dt}\left[\frac{\partial g_a}{\partial \dot{\mathbf{x}}}(\mathbf{x}(t), \dot{\mathbf{x}}(t), \mathbf{u}(t), \dot{\mathbf{u}}(t), \mathbf{p}(t), t)\right]^T \right] \delta \mathbf{x}(t) \\
&+ \left[\left[\frac{\partial g_a}{\partial \mathbf{u}}(\mathbf{x}(t), \dot{\mathbf{x}}(t), \mathbf{u}(t), \dot{\mathbf{u}}(t), \mathbf{p}(t), t)\right]^T - \frac{d}{dt}\left[\frac{\partial g_a}{\partial \dot{\mathbf{u}}}(\mathbf{x}(t), \dot{\mathbf{x}}(t), \mathbf{u}(t), \dot{\mathbf{u}}(t), \mathbf{p}(t), t)\right]^T \right] \delta \mathbf{u}(t) \\
&+ \left[\frac{\partial g_a}{\partial \mathbf{p}}(\mathbf{x}(t), \dot{\mathbf{x}}(t), \mathbf{u}(t), \dot{\mathbf{u}}(t), \mathbf{p}(t), t)\right]^T \delta \mathbf{p}(t) \Bigg\} dt
\end{aligned} \tag{6.17}
$$

It is noteworthy that $\dot{\mathbf{p}}(t)$ does not appear in the above expression. As the second partial derivatives of the function $h(\mathbf{x}(t), \mathbf{u}(t), t)$ are assumed continuous, it can be readily verified (by direct calculation) that the terms including $h(\mathbf{x}(t), \mathbf{u}(t), t)$ in the augmented cost integrand g_a cancel each other. Based on this observation, the integral term in Eq. (6.17) changes to

$$
\begin{aligned}
&\int_{t_0}^{t_f} \Bigg\{ \left[\left[\frac{\partial g}{\partial \mathbf{x}}(\mathbf{x}(t), \mathbf{u}(t), t)\right]^T + \mathbf{p}^T(t) \left[\frac{\partial \mathbf{f}}{\partial \mathbf{x}}(\mathbf{x}(t), \mathbf{u}(t), t)\right] + \frac{d}{dt}(\mathbf{p}^T(t)) \right] \delta \mathbf{x}(t) \\
&+ \left[\left[\frac{\partial g}{\partial \mathbf{u}}(\mathbf{x}(t), \mathbf{u}(t), t)\right]^T + \mathbf{p}^T(t) \left[\frac{\partial \mathbf{f}}{\partial \mathbf{u}}(\mathbf{x}(t), \mathbf{u}(t), t)\right] \right] \delta \mathbf{u}(t) + \left[(\mathbf{f}(\mathbf{x}(t), \mathbf{u}(t), t) - \dot{\mathbf{x}}(t)\right]^T \delta \mathbf{p}(t) \Bigg\} dt
\end{aligned} \tag{6.18}
$$

Regardless of the boundary conditions, the above integral must vanish on an extremal. This implies that the coefficients of the independent variations $\delta\mathbf{x}$, $\delta\mathbf{u}$ and $\delta\mathbf{p}$ must be zero, which delivers the state and co-state equations below:

$$
\dot{\mathbf{x}}(t) = \mathbf{f}(\mathbf{x}(t), \mathbf{u}(t), t), \quad \dot{\mathbf{p}}(t) = -\left[\frac{\partial \mathbf{f}}{\partial \mathbf{x}}(\mathbf{x}(t), \mathbf{u}(t), t)\right]^T \mathbf{p}(t) - \left[\frac{\partial g}{\partial \mathbf{x}}(\mathbf{x}(t), \mathbf{u}(t), t)\right] \tag{6.19}
$$

together with the Euler-Lagrange equation

$$
\frac{\partial g}{\partial \mathbf{u}}(\mathbf{x}(t), \mathbf{u}(t), t) + \left[\frac{\partial \mathbf{f}}{\partial \mathbf{u}}(\mathbf{x}(t), \mathbf{u}(t), t)\right]^T \mathbf{p}(t) = \mathbf{0}. \tag{6.20}
$$

The terms outside of the integral in Eq. (6.17) must then also satisfy

$$\left[\frac{\partial h}{\partial \mathbf{x}}(\mathbf{x}(t_f),\mathbf{u}(t_f),t_f)-\mathbf{p}(t_f)\right]^T\delta\mathbf{x}_f+\left[\frac{\partial h}{\partial \mathbf{u}}(\mathbf{x}(t_f),\mathbf{u}(t_f),t_f)\right]^T\delta\mathbf{u}_f$$
$$+\left[g(\mathbf{x}(t_f),\mathbf{u}(t_f),t_f)+\mathbf{p}^T(t_f)\mathbf{f}(\mathbf{x}(t_f),\mathbf{u}(t_f),t_f)+\frac{\partial h}{\partial t}(\mathbf{x}(t_f),\mathbf{u}(t_f),t_f)\right]\delta t_f=0 \tag{6.21}$$

which completes the proof. □

The variational statement of the boundary conditions (6.21) captures the six different situations for which the corresponding explicit boundary conditions are listed below:

- Fixed terminal time t_f yields $\delta t_f = 0$, while free terminal time t_f requires:

$$g(t_f,\mathbf{x}(t_f),\mathbf{u}(t_f))+\mathbf{p}^T(t_f)\mathbf{f}(t_f,\mathbf{x}(t_f),\mathbf{u}(t_f))+\frac{\partial h}{\partial t}(t_f,\mathbf{x}(t_f),\mathbf{u}(t_f))=0 \tag{6.22}$$

- Fixed terminal state $\mathbf{x}(t_f)$ yields $\delta\mathbf{x}_f = \mathbf{0}$, while free terminal state $\mathbf{x}_f$ requires:

$$\frac{\partial h}{\partial \mathbf{x}}(t_f,\mathbf{x}(t_f),\mathbf{u}(t_f))-\mathbf{p}(t_f)=\mathbf{0} \tag{6.23}$$

- Fixed terminal control $\mathbf{u}(t_f)$ yields $\delta\mathbf{u}_f = \mathbf{0}$, while free terminal control $\mathbf{u}_f$ requires:

$$\frac{\partial h}{\partial \mathbf{u}}(t_f,\mathbf{x}(t_f),\mathbf{u}(t_f))=\mathbf{0} \tag{6.24}$$

The boundary conditions can be applied component-wise. Note that, in the absence of the soft penalty; i.e. when $h \equiv 0$, while the time horizon and the final state are considered fixed, the variational boundary condition Eq. (6.21) vanish identically. This is not equivalent to the absence of an actual control constraint, however. The control effort is still constrained by the definition of the class U_a of admissible controls, which requires that its members satisfy $\mathbf{u} \in C^2[t_0,t_f]$, with $\mathbf{u}(t_0)=\mathbf{u}_0$ and $\mathbf{u}(t_f)=\mathbf{u}_f$.

6.2.1 Hamiltonian Formulation

The Legendre transformation, whose validity is due to the assumed regularity conditions, conveniently leads to the definition of the Hamiltonian function:

$$\mathcal{H}(\mathbf{x}(t),\mathbf{u}(t),\mathbf{p}(t),t)=g(\mathbf{x}(t),\mathbf{u}(t),t)+\mathbf{p}^T(t)\mathbf{f}(t,\mathbf{x}(t),\mathbf{u}(t)) \tag{6.25}$$

which permits to re-state the necessary conditions for optimality in the familiar compact form of Eqs. (6.19)–(6.21):

$$\begin{aligned}\dot{\mathbf{x}}(t)&=\frac{\partial \mathcal{H}}{\partial \mathbf{p}}(\mathbf{x}(t),\mathbf{u}(t),\mathbf{p}(t),t)\\ \dot{\mathbf{p}}(t)&=-\frac{\partial \mathcal{H}}{\partial \mathbf{x}}(\mathbf{x}(t),\mathbf{u}(t),\mathbf{p}(t),t)\\ \frac{\partial \mathcal{H}}{\partial \mathbf{u}}(\mathbf{x}(t),\mathbf{u}(t),\mathbf{p}(t),t)&=\mathbf{0}\end{aligned} \tag{6.26}$$

$$\left[\frac{\partial h}{\partial \mathbf{x}}(\mathbf{x}(t_f),\mathbf{u}(t_f),t_f)-\mathbf{p}(t_f)\right]^T\delta\mathbf{x}_f+\left[\frac{\partial h}{\partial \mathbf{u}}(\mathbf{x}(t_f),\mathbf{u}(t_f),t_f)\right]^T\delta\mathbf{u}_f$$
$$+\left[\mathcal{H}(\mathbf{x}(t_f),\mathbf{u}(t_f),\mathbf{p}(t_f),t_f)+\frac{\partial h}{\partial t}(\mathbf{x}(t_f),\mathbf{u}(t_f),t_f)\right]\delta t_f=0 \qquad (6.27)$$

6.3 Benefits of Over-Actuation

Sufficiency conditions for optimality are omitted here due to the complexity of the problem and the need of the second variation of the cost. Agreeably, existence of extremals does not warrant existence of optimal solutions in general. Similarly, existence analysis, which usually involves continuity and compactness arguments [97, 98], is substituted here by a few considerations pertaining to attainable sets under control restrictions and the potential benefits of over-actuation. The precise question to ask is whether the set of admissible controls is non-empty, given that both states and controls must satisfy given boundary conditions. Questions of this kind lead to the notion of attainable sets under restricted classes of controls. The definition below is relevant to the discussion:

Definition: (Attainable set)

Given a dynamical system with an initial condition $\mathbf{x}(t_0)=\mathbf{x}_0$, and a class of admissible controls U_a defined on a control horizon $[t_0,t_f]$, the set of attainable states is

$$\mathcal{A}(\mathbf{x}_0,t_0,t_f,U_a):=\{\mathbf{x}_f\in\mathbb{R}^n \mid \text{s.t. } \exists\ \mathbf{u}\in U_a \text{ that transfers } \mathbf{x}(t_0)=\mathbf{x}_0 \text{ to } \mathbf{x}(t_f)=\mathbf{x}_f\} \qquad (6.28)$$

With reference to controllable LTI systems, it can be readily shown that constraining terminal values of the controls does not shrink the set of attainable terminal states of the system.

Theorem 2 *Given a completely controllable LTI system:*

$$\dot{\mathbf{x}}(t)=\mathbf{A}\mathbf{x}(t)+\mathbf{B}\mathbf{u}(t);\ \ \mathbf{x}(t)\in\mathbb{R}^n;\ \mathbf{u}(t)\in\mathbb{R}^m \qquad (6.29)$$

and two different sets of admissible controls:

$$U_a^1=\{\ \mathbf{u}\in C^1[t_0,t_f]\mid \mathbf{u}(t_0)=\mathbf{u}_0,\mathbf{u}(t_f)=\mathbf{u}_f\ \}$$
$$U_a^2=\{\ \mathbf{u}\in C^1[t_0,t_f]\mid \mathbf{u}(t_0)=\mathbf{u}_0\ \} \qquad (6.30)$$

the corresponding attainable sets are equal, i.e. for every $(\mathbf{x}_0,t_0,t_f)$*:*

$$\mathcal{A}(\mathbf{x}_0,t_0,t_f,U_a^1)=\mathcal{A}(\mathbf{x}_0,t_0,t_f,U_a^2) \qquad (6.31)$$

■

Proof:

Complete controllability of the system (6.29) (by controls from the admissible set U_a^2) implies that the controllability matrix

$$\boldsymbol{\mathcal{C}} = \left[\begin{array}{ccccc} \mathbf{B} & \mathbf{AB} & \mathbf{A}^2\mathbf{B} & \ddots & \mathbf{A}^{n-1}\mathbf{B} \end{array} \right] \tag{6.32}$$

has full rank. The proof will be completed by showing that any state $\mathbf{x}_f \in \mathbb{R}^n$ can also be reached from $\mathbf{x}_0$ at time t_0 by a control from U_a^1, which is a more restrictive class of controls than U_a^2. Apparently, it suffices to show the existence of a dynamical system extension to Eq. (6.29) that is completely controllable and such that its state vector contains both $\mathbf{x}$ and $\mathbf{u}$. To this end, consider a cascaded system

$$\begin{aligned} &\dot{\mathbf{x}}(t) = \mathbf{A}\mathbf{x}(t) + \mathbf{B}\mathbf{w}(t); \;\; \mathbf{x}(t) \in \mathbb{R}^n; \; \mathbf{w}(t) \in \mathbb{R}^m \\ &\dot{\mathbf{w}}(t) = \mathbf{v}(t); \quad \mathbf{v}(t) \in \mathbb{R}^m \end{aligned} \tag{6.33}$$

where $\mathbf{v}$ is considered as a new unrestrained input. The controllability matrix for the cascade is

$$\boldsymbol{\mathcal{C}}_c = \left[\begin{array}{cccccc} \mathbf{O}_{nm} & \mathbf{B} & \mathbf{AB} & \mathbf{A}^2\mathbf{B} & \ddots & \mathbf{A}^{n-1}\mathbf{B} \\ \mathbf{1}_m & \mathbf{O}_m & \mathbf{O}_m & \mathbf{O}_m & \cdots & \mathbf{O}_m \end{array} \right] \tag{6.34}$$

with $\mathbf{O}_{nm}$ as the $n \times m$ zero matrix, and $\mathbf{1}_m$ and $\mathbf{O}_m$ as the $m \times m$ identity and zero matrices, respectively. As the controllability matrix $\boldsymbol{\mathcal{C}}_c$ inherits the full rank property from $\boldsymbol{\mathcal{C}}$, there exists a surrogate control $\mathbf{v}^*$ that steers the cascade to any desired state $(\mathbf{x}, \mathbf{w}) \in \mathbb{R}^n \times \mathbb{R}^m$. Imposing that $\mathbf{x}(t_f) = \mathbf{x}_f$ and $\mathbf{w}(t_f) = \mathbf{u}_f$, makes the function $\mathbf{w}$, which corresponds to an exogenous control $\mathbf{v}^*$, play the role of the desired control $\mathbf{u} \equiv \mathbf{w} \in U_a^1$ that accomplishes the transfer of the system state from $\mathbf{x}_0$ to $\mathbf{x}_f$, thereby completing the proof. □

Apparently, from the system equations (6.29), imposing terminal conditions on $\mathbf{u}$ automatically constrains the system time derivative to $\dot{\mathbf{x}}(t_f) = \mathbf{A}\mathbf{x}(t_f) + \mathbf{B}\mathbf{u}(t_f)$; hence, the terminally constrained control $\mathbf{u}$ cannot generally steer the system to an arbitrarily selected terminal state along with its time derivative. It is possible to circumvent this problem if the system can be equipped with a redundant control, the system thereby becoming over-actuated. For brevity, such a development is explained by way of a simple example.

Example: Consider a system in the form of a chain of two integrators and its dynamic extension, as introduced in Theorem 2:

$$\begin{aligned} \dot{x}_1 &= x_2 \\ \dot{x}_2 &= u \end{aligned} \qquad \begin{aligned} \dot{x}_1 &= x_2 \\ \dot{x}_2 &= w \\ \dot{w} &= v \end{aligned} \tag{6.35}$$

Both systems are clearly controllable; hence, there exists a control v that steers both (x_1, x_2) and w to any desired terminal points $(x_1(t_f), x_2(t_f))$ and $w(t_f)$. Then, $u = \int_{t_0}^{t} v(\tau)d\tau$ steers the first system to $(x_1(t_f), x_2(t_f))$ and also satisfies $u(t_f) = w(t_f)$, as required. The problem of steering with terminal constraints on both the state and the control is hence seen as equivalent to steering the extended system to a terminal state under an isoperimetric constraint

$$w(t_f) = \int_{t_0}^{t_f} v(\tau)d\tau. \tag{6.36}$$

Now let us assume that the terminal derivative $\dot{x}_2(t_f)$ is also subject to a terminal constraint with $\dot{x}_2(t_f) \neq u(t_f)$. Clearly, this is not achievable, as the system model requires that $\dot{x}_2 = u$, unless additional control power can be introduced. The simplest over-actuated system (and its extension) by which to attain the desired values of $(x_1, x_2, \dot{x}_2)$ at time t_f by a control that takes any prescribed terminal value $u(t_f)$ is proposed in the form

$$\begin{aligned} \dot{x}_1 &= x_2 \\ \dot{x}_2 &= u + r \end{aligned} \qquad \begin{aligned} \dot{z}_1 &= z_2 \\ \dot{z}_2 &= z_3 \\ \dot{z}_3 &= s_1 + s_2 \\ \dot{s}_1 &= s_2 \\ \dot{s}_2 &= v \end{aligned} \quad := \mathbf{A}\mathbf{w} + \mathbf{b}v \tag{6.37}$$

The state and control variables of the extended system have been assigned as:

$$\begin{aligned} &z_1 := x_1;\ z_2 := \dot{x}_1 = x_2;\ z_3 := \ddot{x}_1 = \dot{x}_2 \\ &s_1 := \int_{t_0}^{t}\int_{t_0}^{\sigma} v(\tau)d\tau d\sigma;\ s_2 := \int_{t_0}^{t} v(\tau)d\tau \end{aligned} \tag{6.38}$$

with $u = s_1$; $\dot{r} = s_1$; $\mathbf{w} := [z_1, z_2, z_3, s_1, s_2]^T$, yielding $\ddot{x}_2 = \dot{z}_3 = \dot{u} + \dot{r} = s_2 + s_1$, as required.

The extended system matrices are

$$\mathbf{A} = \begin{bmatrix} 0 & 1 & 0 & 0 & 0 \\ 0 & 0 & 1 & 0 & 0 \\ 0 & 0 & 0 & 1 & 1 \\ 0 & 0 & 0 & 0 & 1 \\ 0 & 0 & 0 & 0 & 0 \end{bmatrix};\ \mathbf{b} = [0, \cdots, 0, 1]^T \tag{6.39}$$

from which it is apparent that the above pair $[\mathbf{A}, \mathbf{b}]$ is controllable. It follows that v can control the entire extended state $\mathbf{w}$ to any pre-specified end-point $\mathbf{w}(t_f)$. This includes $x_1, x_2, \dot{x}_2$ and $u = s_1$, as required. Further skillful system extensions can accommodate additional constraints on the over-actuation control variable r, should the latter be necessary due to a specific desired control configuration. The redundant variable provides a feedback signal that "decouples" $\dot{x}_2$ from u so that both can be steered independently to meet their respective end-point constraints.

6.4 Linear Quadratic Tracking with Terminal Constraints

Due to their generality, the results of Theorem 1 readily deliver necessary optimality conditions for the class of linear quadratic tracking (LQT) problems with terminal constraints. As the latter will be employed in a case study in Section 6.5, it is useful to state them explicitly here.

Consider the following LQT problem

$$\dot{\mathbf{x}}(t) = \mathbf{A}(t)\mathbf{x}(t) + \mathbf{B}(t)\mathbf{u}(t) \tag{6.40}$$

with cost functional

$$\begin{aligned} J = &\frac{1}{2}\left[\mathbf{u}(t_f) - \mathbf{v}(t_f)\right]^T \mathbf{H}\left[\mathbf{u}(t_f) - \mathbf{v}(t_f)\right] \\ &+ \frac{1}{2}\int_{t_0}^{t_f} \left\{ \left[\mathbf{x}(t) - \mathbf{r}(t)\right]^T \mathbf{Q}(t)\left[\mathbf{x}(t) - \mathbf{r}(t)\right] + \mathbf{u}^T(t)\mathbf{R}(t)\mathbf{u}(t) \right\} dt \end{aligned} \tag{6.41}$$

where $\mathbf{v}(t_f)$ is the desired terminal value of the control, and $\mathbf{r}(\cdot)$ is the trajectory to be tracked. The above weighting matrices are required to satisfy: $\mathbf{H} \geq \mathbf{O}$, $\mathbf{Q}(t) \geq \mathbf{O}$, and $\mathbf{R}(t) > \mathbf{O}$. Using Eq. (6.25), the Hamiltonian is

$$\begin{aligned} \mathcal{H}(\mathbf{x}(t), \mathbf{u}(t), \mathbf{p}(t), t) = &\frac{1}{2}\left\{ \left[\mathbf{x}(t) - \mathbf{r}(t)\right]^T \mathbf{Q}(t)\left[\mathbf{x}(t) - \mathbf{r}(t)\right] + \mathbf{u}^T(t)\mathbf{R}(t)\mathbf{u}(t) \right\} \\ &+ \mathbf{p}^T(t)\mathbf{A}(t)\mathbf{x}(t) + \mathbf{p}^T(t)\mathbf{B}(t)\mathbf{u}(t) \end{aligned} \tag{6.42}$$

and

$$h(\mathbf{x}(t_f), \mathbf{u}(t_f), t_f) = \frac{1}{2}\left[\mathbf{u}(t_f) - \mathbf{v}(t_f)\right]^T \mathbf{H}\left[\mathbf{u}(t_f) - \mathbf{v}(t_f)\right] \tag{6.43}$$

The normality conditions follow from Eqs. (6.26):

$$\begin{aligned} \dot{\mathbf{x}}(t) &= \frac{\partial \mathcal{H}}{\partial \mathbf{p}} = \mathbf{A}(t)\mathbf{x}(t) + \mathbf{B}(t)\mathbf{u}(t) \\ \dot{\mathbf{p}}(t) &= -\frac{\partial \mathcal{H}}{\partial \mathbf{x}} = -\mathbf{Q}(t)\mathbf{x}(t) - \mathbf{A}^T(t)\mathbf{p}(t) + \mathbf{Q}(t)\mathbf{r}(t) \\ \frac{\partial \mathcal{H}}{\partial \mathbf{u}} &= \mathbf{R}(t)\mathbf{u}(t) + \mathbf{B}^T(t)\mathbf{p}(t) = \mathbf{0} \quad \Rightarrow \quad \mathbf{u}(t) = -\mathbf{R}^{-1}(t)\mathbf{B}^T(t)\mathbf{p}(t) \end{aligned} \tag{6.44}$$

It can be shown that the co-states $\mathbf{p}(t)$ are linear functions of the states $\mathbf{x}(t)$ [70, 71]; thus, there exist matrix and vector functions $\mathbf{S}(\cdot)$ and $\boldsymbol{\phi}(\cdot)$ such that Eqs. (6.44) can be re-written as

$$\mathbf{p}(t) = \mathbf{S}(t)\mathbf{x}(t) + \boldsymbol{\phi}(t) \tag{6.45}$$

which leads to

$$\dot{\mathbf{p}}(t) = \dot{\mathbf{S}}(t)\mathbf{x}(t) + \mathbf{S}(t)\dot{\mathbf{x}}(t) + \dot{\boldsymbol{\phi}}(t) \tag{6.46}$$

Combining Eqs. (6.44)–(6.46) yields

$$\left[-\mathbf{Q}(t) - \mathbf{A}^T(t)\mathbf{S}(t)\right]\mathbf{x}(t) - \mathbf{A}^T(t)\boldsymbol{\phi}(t) + \mathbf{Q}(t)\mathbf{r}(t) = \left[\dot{\mathbf{S}}(t) + \mathbf{S}(t)\mathbf{A}(t) - \mathbf{S}(t)\mathbf{E}(t)\mathbf{S}(t)\right]\mathbf{x}(t) - \mathbf{S}(t)\mathbf{E}(t)\boldsymbol{\phi}(t) + \dot{\boldsymbol{\phi}}(t) \tag{6.47}$$

with $\mathbf{E}(t) = \mathbf{B}(t)\mathbf{R}^{-1}(t)\mathbf{B}^T(t)$. Equation (6.47) must be satisfied for all $\mathbf{x}(t)$ and all $\mathbf{r}(t)$, which leads to the familiar differential Riccati equation (DRE), namely,

$$\dot{\mathbf{S}}(t) = -\mathbf{S}(t)\mathbf{A}(t) - \mathbf{A}^T(t)\mathbf{S}(t) - \mathbf{Q}(t) + \mathbf{S}(t)\mathbf{E}(t)\mathbf{S}(t) \tag{6.48}$$

as well as

$$\dot{\boldsymbol{\phi}}(t) = -\left[\mathbf{A}^T(t) - \mathbf{S}(t)\mathbf{E}(t)\right]\boldsymbol{\phi}(t) + \mathbf{Q}(t)\mathbf{r}(t) \tag{6.49}$$

Assuming that t_f and $\mathbf{x}(t_f) = \mathbf{x}_f$ are fixed, $\delta t_f = 0$, and $\delta\mathbf{x}_f = \mathbf{0}$. In this case, $\mathbf{u}(t_f)$ is considered to be free, Eq. (6.27) thus reducing to

$$\begin{aligned} &\frac{\partial h}{\partial \mathbf{u}}(\mathbf{x}(t_f), \mathbf{u}(t_f), t_f) = \mathbf{0} \\ &\text{i.e. } \mathbf{H}\left[\mathbf{u}(t_f) - \mathbf{v}(t_f)\right] = \mathbf{0} \end{aligned} \tag{6.50}$$

Since $\mathbf{u}(t) = -\mathbf{K}(t)\mathbf{x}(t) - \boldsymbol{\psi}(t)$, $\mathbf{K}(t) = \mathbf{R}^{-1}(t)\mathbf{B}^T(t)\mathbf{S}(t)$ and $\boldsymbol{\psi}(t) = \mathbf{R}^{-1}(t)\mathbf{B}^T(t)\boldsymbol{\phi}(t)$, Eq. (6.50) can be re-written as

$$\mathbf{H}\left[-\mathbf{R}^{-1}(t_f)\mathbf{B}^T(t_f)\mathbf{S}(t_f)\mathbf{x}(t_f) - \mathbf{R}^{-1}(t_f)\mathbf{B}^T(t_f)\boldsymbol{\phi}(t_f) - \mathbf{v}(t_f)\right] = \mathbf{0} \tag{6.51}$$

Hence, to satisfy condition (6.51), matrix $\mathbf{S}(t_f)$ and vector $\boldsymbol{\phi}(t_f)$ should be found such that the vector in brackets lies in the null space of matrix $\mathbf{H}$. As $\mathbf{u}(t_0) = \mathbf{u}_0$ is known, the relation below must hold

$$-\mathbf{R}^{-1}(t_0)\mathbf{B}^T(t_0)\mathbf{S}(t_0)\mathbf{x}(t_0) - \mathbf{R}^{-1}(t_0)\mathbf{B}^T(t_0)\boldsymbol{\phi}(t_0)) = \mathbf{u}_0 \tag{6.52}$$

6.5 Case Study: Gear-shifting in Electric Vehicles

A novel two-speed transmission system for EVs, as previously designed and discussed [81, 87], consists of two planetary gear sets, as shown in Fig. 6.1. The planetary sets share the same carrier, which is connected to the output shaft. The sun gears are mounted on the same input shaft. To achieve a desired speed ratio, the corresponding ring gear should be fixed. For shifting between speed ratios, the fixed ring gear should be released and the second one should be fixed.

Employing the Lagrangian formalism, a mathematical model of the system is derived as

$$A_0\dot{\omega}_c + B_0\dot{\omega}_s = \tau_d - c_s\omega_s - \frac{r_{s_1}}{r_{r_1}}\tau_{r_1} - \frac{r_{s_2}}{r_{r_2}}\tau_{r_2} \tag{6.53a}$$

$$C_0\dot{\omega}_c + D_0\dot{\omega}_s = \tau_l - c_c\omega_c + \frac{2r_c}{r_{r_1}}\tau_{r_1} + \frac{2r_c}{r_{r_2}}\tau_{r_2} \tag{6.53b}$$

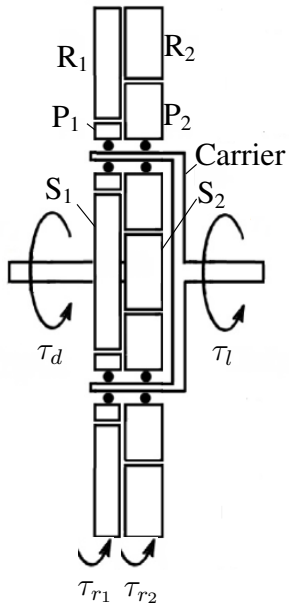

Figure 6.1: A two-speed transmission system for EVs

where A_0, B_0, C_0 and D_0 indicate generalized inertia terms, ω_c and ω_s denoting the angular velocities of the carrier and the sun gears, while c_c and c_s are generalized damping coefficients. Also, τ_d, τ_l, τ_{r_1} and τ_{r_2} denote, respectively, the driving torque of the electric motor applied to the input shaft, the external load applied to the output shaft, and the torques applied to the first and the second ring gears. The variables, r_{s_1}, r_{s_2}, r_{r_1} and r_{r_2} are the pitch radii of the sun and the ring gears of the first and the second planetary sets, respectively, and r_c is the radius of the planet carrier.

Let $x_1(t) = \omega_c(t)$ and $x_2(t) = \omega_s(t)$ denote the state variables of the system. In the absence of any external load, the state-space model is an LTI system:

$$\dot{\mathbf{x}}(t) = \mathbf{A}\mathbf{x}(t) + \mathbf{B}\mathbf{u}(t)$$

where $\mathbf{u}(t) = \begin{bmatrix} \tau_{r_1}(t) & \tau_{r_2}(t) & \tau_d(t) \end{bmatrix}^T$ is the control input. The system matrices $\mathbf{A} \in \mathbb{R}^{2\times 2}$ and $\mathbf{B} \in \mathbb{R}^{2\times 3}$ are

$$\mathbf{A} = \begin{bmatrix} a_c & a_s \\ b_c & b_s \end{bmatrix}, \quad \mathbf{B} = \begin{bmatrix} a_{r_1} & a_{r_2} & a_d \\ b_{r_1} & b_{r_2} & b_d \end{bmatrix} \tag{6.54}$$

whose entries are functions of the system parameters appearing in Eqs. (6.53), namely, the radii of the elements, the generalized inertias, and the damping coefficients.

To further explain the physical model, consider shifting from the first gear ratio to the second. In this case, at the beginning of the gear-shifting process ($t = t_0$), the first ring gear is fixed and the

second one released, i.e.,

$$\omega_{r_1}(t_0) = 0, \quad \tau_{r_2}(t_0) = 0 \tag{6.55}$$

At the end of gear-shifting, i.e. at $t = t_f$, the second ring gear is fixed and the first one is released, i.e.,

$$\omega_{r_2}(t_f) = 0, \quad \tau_{r_1}(t_f) = 0 \tag{6.56}$$

Note that Eqs. (6.55) and (6.56) represent initial and final constraints on the control input. For a swift, seamless gear-shifting, without any torque interruptions and discontinuities, the angular velocity $\omega_c(t)$ of the output shaft should remain constant during the whole operation, i.e., $\omega_c(t) = \omega_{c_0}$, $t \ \epsilon [t_0, t_f]$, where ω_{c_0} is the angular velocity of the output before shifting. Also, assuming that $\omega_s(t_0) = \omega_{s_0}$ and $\omega_s(t_f) = \omega_{s_f}$, the angular velocity $\omega_s(t)$ of the input shaft should follow the 3-4-5 *blending polynomial* [74]. The latter is defined as

$$\omega_{5s}(t) = \Delta\omega \left(6\theta^5 - 15\theta^4 + 10\theta^3\right) + \omega_{s_0}, \quad \theta \equiv \frac{t - t_0}{t_f - t_0}, \quad \Delta\omega \equiv \omega_{s_f} - \omega_{s_0} \tag{6.57}$$

which guarantees the continuity of the angular velocity, acceleration and jerk at $t = t_0$ and $t = t_f$. In other words, the desired value of the state vector is $\mathbf{r}(t) = [\omega_{c_0} \quad \omega_{5s}(t)]^T$. According to Eq. (6.56), only the final value of the first control input is required to vanish; assuming a suitable value for a constant β a soft constraint is adopted, namely,

$$h(\mathbf{x}(t_f), \mathbf{u}(t_f), t_f) = \frac{1}{2}\beta\tau_{r_1}^2(t_f) = \frac{1}{2}\left[\mathbf{x}(t_f) - \mathbf{r}(t_f)\right]^T \mathbf{H}\left[\mathbf{x}(t_f) - \mathbf{r}(t_f)\right]; \ \mathbf{H} = \begin{bmatrix} \beta & 0 & 0 \\ 0 & 0 & 0 \\ 0 & 0 & 0 \end{bmatrix} \tag{6.58}$$

6.5.1 Simulation Results

The desired state vector is $\mathbf{r}(t) = [\omega_{c_0} \quad \omega_{5s}(t)]^T$; then, assuming $t \ \epsilon [0, 0.075]$, $\omega_{c_0} = 10$ rad/s, and the first and the second gear ratios of 4 and $8/3$, respectively, imposes

$$\omega_s(t_0) = 40 \text{ rad/s}, \quad \omega_s(t_f) = \frac{80}{3} \text{ rad/s} \tag{6.59}$$

$$\omega_{r_1}(t_0) = 0, \quad \tau_{r_2}(t_0) = 0, \quad \omega_{r_2}(t_f) = 0, \quad \tau_{r_1}(t_f) = 0 \tag{6.60}$$

Note that, since the initial control input $\mathbf{u}(t_0)$ is assumed known, for a smooth shift, the condition $\mathbf{u}(t_0) = \mathbf{u}_0$ should be met in finding the control input.

A shooting method [123] was employed to solve the two-point boundary-value-problem (BVP) (6.48) and (6.49), with conditions (6.51) and (6.52), that delivers the optimal tracking control $\mathbf{u}(t)$.

In fact, the shooting method is based on reducing the two-point BVP to a sequence of initial value problems (IVPs), each being readily solvable.

The reference and output values of $\omega_c(t)$ and $\omega_s(t)$ are compared in Fig. 6.2(a). As seen in the figure, the states follow the desired trajectory exactly; $\omega_c(t)$ remains constant during gear-shifting, while $\omega_s(t)$ follows the 3-4-5 polynomial. The angular velocities of the ring gears are depicted in Fig. 6.2(b). As expected, at t_0, $\omega_{r_1} = 0$, i.e., the first gear set is engaged, while at t_f, the second gear set is engaged. Note that the angular velocities of the ring gears also follow the 3-4-5 polynomial.

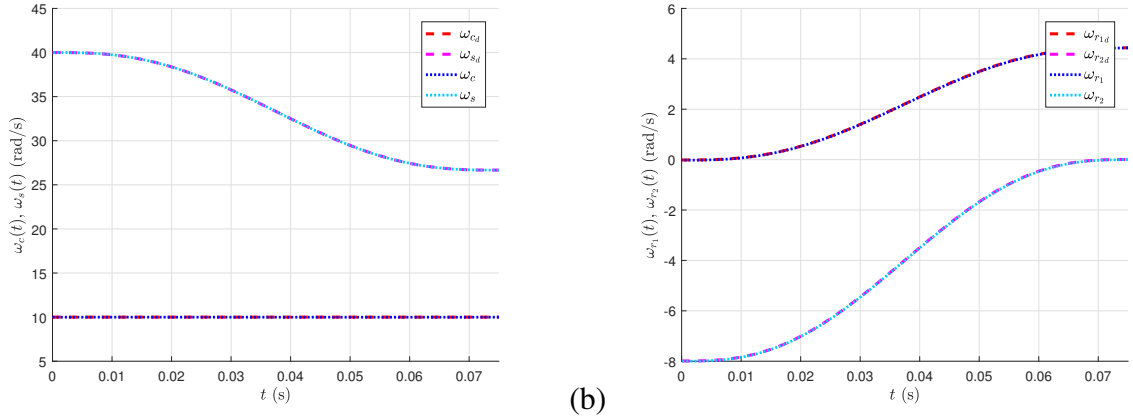

(a) (b)

Figure 6.2: The angular velocities during gear-shifting: (a) the input and output shafts; and (b) the ring gears

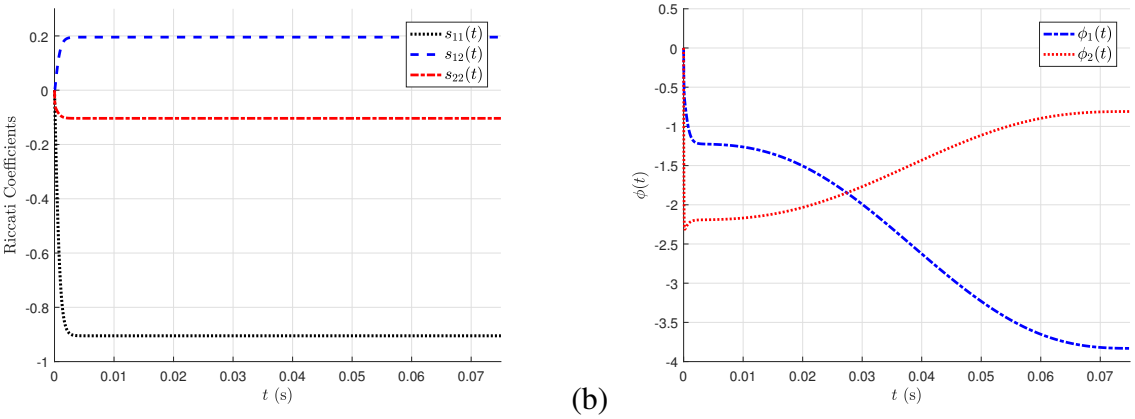

(a) (b)

Figure 6.3: The solution to: (a) Riccati equation; and (b) vector ϕ equation

The components of the matrix and vector functions, $\mathbf{S}$ and ϕ are shown in Figs. 6.3(a) and (b), respectively. The optimal control inputs during gear-shifting are shown in Fig. 6.4. Note that the torque τ_{r_2} applied to the second ring gear is near zero at t_0. At t_f, the torque τ_{r_1} applied to the first ring gear is near zero, i.e., the first gear set is released. Also, the control input before shifting

is correct, i.e., $\mathbf{u}(t_0) = \begin{bmatrix} -0.15 & 0 & 0.75 \end{bmatrix}^T$, so that the constraints are met at both ends of the gear-shifting horizon while control inputs vary considerably during gear-shifting.

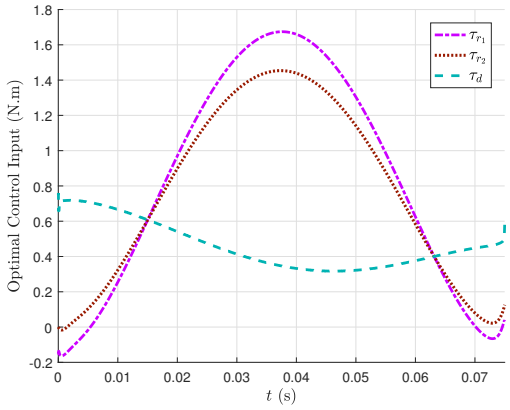

Figure 6.4: The optimal control inputs during gear-shifting

Simulation results demonstrate that the approach is highly promising for the optimal control of over-actuated systems with constraints on the initial and final values of the control input. Note that even if the system is not over-actuated, the approach can still be applied, as long as the constraints at the end points of the control interval $[t_0, t_f]$ are such that a solution exists.

6.6 Conclusions

The results reported in this paper complement the classical literature in discussing the intricacies of optimal control problems in which imposing terminal constraints on the state, its time derivative, and/or its controls is necessary to guarantee smooth system operation over extended periods, i.e., seamless blending of operation modes. The necessary conditions were first derived using a general variational approach to optimal control, then applied to a variety of optimization problems with both soft and hard end-point constraints.

The results were applied to deliver optimal seamless gear-shifting in recent novel designs of MSTs driven by electrical motors. Future contributions will aim to eliminate the need for generation of blending trajectories, including additional smoothness constraints at the boundaries of the gear-shifting interval, and further exploring the benefits of over-actuation [124].

Chapter 7

Optimal Control of Over-actuated Systems Applying Smooth Control Inputs with Terminal Constraints

Abstract

An optimal control scheme is proposed for over-actuated systems, where the control effort is required to be smooth in the given time interval while satisfying a given set of boundary conditions. Firstly, applying variational calculus, the necessary conditions of optimality are derived for a novel optimal control problem with terminal control and state constraints. Next, these conditions are employed to develop the well-known linear quadratic tracking problem for linear time-varying systems while applying end control and state constraints. The results obtained are then used to solve a specific optimal control problem, i.e., gear-shifting control in a multi-speed transmission system designed for electric vehicles. This is an over-actuated system with boundary conditions on the states and the control input. The results show that the proposed approach is applicable to the smooth optimal control of over-actuated systems with terminal-point control and state conditions.

7.1 Introduction

New optimization problems in the design and operation of modern machinery in industry require novel optimal control formulations. This paper investigates a class of such new problems, where, besides the state, there are constraints on the end values of the control input in the given time interval. Moreover, the control effort must be seamless and smooth.

In a common optimal control problem, the continuity of the control effort at the ends is not an issue, as the problem is solved within a given time interval, without considering the response outside of this interval. However, discontinuities may influence the performance of the entire system substantially, unless conditions are imposed on the end values of some of the control inputs. There are examples in machine design and operation where the smoothness before and/or after the optimum trajectories is essential [113, 114]. A classical optimization problem, solved by variational calculus, usually involves constraints on the state values at both ends of the given time interval. Nonetheless, optimal control problems with terminal control constraints have not been considered in the literature. Guaranteeing the existence of admissible smooth controls that satisfy the boundary conditions may require actuation redundancy. There has been an extensive research effort on the control of over-actuated systems [125, 119, 120, 121, 126]. Accordingly, the contributions of this paper are described below.

In this paper, we report on the optimal control of over-actuated systems where the control input is required to be smooth and terminal-point constraints on the controls arise. In other words, firstly, a variational problem is formulated to find a seamless optimal control input for over-actuated systems in a given time interval, in the presence of end constraints on the states and the control effort. In fact, the normality conditions are derived for such problems. Then, applying the results obtained, the well-known optimal trajectory-tracking problem, i.e., linear quadratic tracking (LQT), is formulated for linear time-varying (LTV) systems with end-point control conditions.

Further, the scheme developed is employed for closed-loop control of a system of current interest, i.e., the gear-shifting problem [92, 68, 73, 127] in a novel modular multi-speed-transmission system (MSTS) designed for electric vehicles (EVs) [81, 87], which is an over-actuated system with terminal control constraints. In fact, the states are required to track a pre-planned "blending trajectory" leading to a swift, seamless shift [74]. Also, besides looking for a smooth control, there are end constraints on the states and the control input in the given time-interval. It is shown that, as the system is over-actuated, the desired trajectory can be followed acceptably and the boundary conditions can be satisfied exactly.

An outline of this paper follows. Section 7.2 is devoted to finding the necessary conditions for optimality in a general smooth optimal control problem with end-point constraints on the state and the control effort. In Section 7.3, the results of Section 7.2 are used to solve the LQT problem

for LTV systems in the presence of state and control boundary conditions. Finally, as an example of application, our technique is adopted for gear-shifting control in a novel MSTS for EVs, as illustrated in Section 7.4.

7.2 Modified Optimal Control Problem

In this section, a variational approach is applied to solve a modified optimal control problem for an over-actuated system, where, besides the final time and the final state, constraints on the final value of the control input arise. Furthermore, the control input is required to be smooth without any jump or discontinuity. To this end, assume that the functional, i.e., the performance index to be minimized, is defined as

$$J(\mathbf{u}) = \int_{t_0}^{t_f} g(\mathbf{x}(t), \mathbf{u}(t), \dot{\mathbf{u}}(t), t)dt \tag{7.1}$$

subject to the state-space equation

$$\dot{\mathbf{x}}(t) = \mathbf{f}(\mathbf{x}(t), \mathbf{u}(t), t) \tag{7.2}$$

where the initial time t_0, state $\mathbf{x}(t_0) = \mathbf{x}_0$ and control input $\mathbf{u}(t_0) = \mathbf{u}_0$, as well as the final time t_f and state $\mathbf{x}(t_f) = \mathbf{x}_f$ are specified, while the final control input $\mathbf{u}(t_f) = \mathbf{u}_f$ is free. Note that the performance index includes a new term compared to the classical optimal control formulation, i.e., the time derivative of the control input $\dot{\mathbf{u}}(t)$. The problem consists in finding a smooth admissible control $\mathbf{u}(t)$, $t \in [t_0, t_f]$, that makes system (7.2) track a desired trajectory $\mathbf{r}(t)$, $t \in [t_0, t_f]$, while minimizing the performance index (7.1).

Adopting Lagrange multipliers $\mathbf{p}(t) \in \mathbb{R}^n$ to include the constraints (7.2) in the performance index (7.1) leads to

$$J_a(\mathbf{u}) = \int_{t_0}^{t_f} \left\{ g(\mathbf{x}(t), \mathbf{u}(t), \dot{\mathbf{u}}(t), t) + \mathbf{p}^T(t) \left[\mathbf{f}(\mathbf{x}(t), \mathbf{u}(t), t) - \dot{\mathbf{x}}(t) \right] \right\} dt \tag{7.3}$$

or, equivalently,

$$J_a(\mathbf{u}) = \int_{t_0}^{t_f} g_a(\mathbf{x}(t), \dot{\mathbf{x}}(t), \mathbf{u}(t), \dot{\mathbf{u}}(t), \mathbf{p}(t), t)dt \tag{7.4}$$

with

$$g_a(\mathbf{x}(t), \dot{\mathbf{x}}(t), \mathbf{u}(t), \dot{\mathbf{u}}(t), \mathbf{p}(t), t) \equiv g(\mathbf{x}(t), \mathbf{u}(t), \dot{\mathbf{u}}(t), t) + \mathbf{p}^T(t) \left[\mathbf{f}(\mathbf{x}(t), \mathbf{u}(t), t) - \dot{\mathbf{x}}(t) \right] \tag{7.5}$$

To find the variation of J_a, we first introduce the variations[1] $\delta\mathbf{x}$, $\delta\dot{\mathbf{x}}$, $\delta\mathbf{u}$, $\delta\dot{\mathbf{u}}$ and $\delta\mathbf{p}$. Hence,

$$\begin{aligned}\delta J_a(\mathbf{u}) = \int_{t_0}^{t_f} \Bigg\{ & \left[\frac{\partial g_a}{\partial \mathbf{x}}(\mathbf{x}(t), \dot{\mathbf{x}}(t), \mathbf{u}(t), \dot{\mathbf{u}}(t), \mathbf{p}(t), t)\right]^T \delta\mathbf{x}(t) \\ & + \left[\frac{\partial g_a}{\partial \dot{\mathbf{x}}}(\mathbf{x}(t), \dot{\mathbf{x}}(t), \mathbf{u}(t), \dot{\mathbf{u}}(t), \mathbf{p}(t), t)\right]^T \delta\dot{\mathbf{x}}(t) \\ & + \left[\frac{\partial g_a}{\partial \mathbf{u}}(\mathbf{x}(t), \dot{\mathbf{x}}(t), \mathbf{u}(t), \dot{\mathbf{u}}(t), \mathbf{p}(t), t)\right]^T \delta\mathbf{u}(t) \\ & + \left[\frac{\partial g_a}{\partial \dot{\mathbf{u}}}(\mathbf{x}(t), \dot{\mathbf{x}}(t), \mathbf{u}(t), \dot{\mathbf{u}}(t), \mathbf{p}(t), t)\right]^T \delta\dot{\mathbf{u}}(t) \\ & + \left[\frac{\partial g_a}{\partial \mathbf{p}}(\mathbf{x}(t), \dot{\mathbf{x}}(t), \mathbf{u}(t), \dot{\mathbf{u}}(t), \mathbf{p}(t), t)\right]^T \delta\mathbf{p}(t) \Bigg\} dt = 0 \end{aligned} \tag{7.6}$$

On the other hand, since $\delta\dot{\mathbf{x}}(t) = d(\delta\mathbf{x}(t))/dt$ and $\delta\dot{\mathbf{u}}(t) = d(\delta\mathbf{u}(t))/dt$, using integration by parts, we obtain

$$\begin{aligned} & \int_{t_0}^{t_f} \left\{ \left[\frac{\partial g_a}{\partial \dot{\mathbf{x}}}(\mathbf{x}(t), \dot{\mathbf{x}}(t), \mathbf{u}(t), \dot{\mathbf{u}}(t), \mathbf{p}(t), t)\right]^T \delta\dot{\mathbf{x}}(t) + \left[\frac{\partial g_a}{\partial \dot{\mathbf{u}}}(\mathbf{x}(t), \dot{\mathbf{x}}(t), \mathbf{u}(t), \dot{\mathbf{u}}(t), \mathbf{p}(t), t)\right]^T \delta\dot{\mathbf{u}}(t) \right\} dt \\ & = \left[\frac{\partial g_a}{\partial \dot{\mathbf{u}}}(\mathbf{x}(t_f), \dot{\mathbf{x}}(t_f), \mathbf{u}(t_f), \dot{\mathbf{u}}(t_f), \mathbf{p}(t_f), t_f)\right]^T \delta\mathbf{u}(t_f) \\ & \quad - \int_{t_0}^{t_f} \Bigg\{ \frac{d}{dt}\left[\frac{\partial g_a}{\partial \dot{\mathbf{x}}}(\mathbf{x}(t), \dot{\mathbf{x}}(t), \mathbf{u}(t), \dot{\mathbf{u}}(t), \mathbf{p}(t), t)\right]^T \delta\mathbf{x}(t) \\ & \quad + \frac{d}{dt}\left[\frac{\partial g_a}{\partial \dot{\mathbf{u}}}(\mathbf{x}(t), \dot{\mathbf{x}}(t), \mathbf{u}(t), \dot{\mathbf{u}}(t), \mathbf{p}(t), t)\right]^T \delta\mathbf{u}(t) \Bigg\} dt \end{aligned} \tag{7.7}$$

Note that since t_0, $\mathbf{x}(t_0)$, $\mathbf{u}(t_0)$, t_f and $\mathbf{x}(t_f)$ are fixed, $\delta\mathbf{x}(t_0) = \mathbf{0}$, $\delta\mathbf{u}(t_0) = \mathbf{0}$ and $\delta\mathbf{x}(t_f) = \mathbf{0}$. Next, substituting Eq. (7.7) into Eq. (7.6), and applying the relations

$$\delta\mathbf{u}(t_f) = \delta\mathbf{u}_f - \dot{\mathbf{u}}(t_f)\delta t_f, \quad \delta t_f = 0 \tag{7.8}$$

the variation of the performance index becomes

[1] Note that the final time t_f is fixed, i.e., $\delta t_f = 0$.

$$\delta J_a(\mathbf{u}) = \left[\frac{\partial g_a}{\partial \dot{\mathbf{u}}}(\mathbf{x}(t_f), \dot{\mathbf{x}}(t_f), \mathbf{u}(t_f), \dot{\mathbf{u}}(t_f), \mathbf{p}(t_f), t_f)\right]^T \delta \mathbf{u}_f$$
$$+ \int_{t_0}^{t_f} \left\{ \left[\left[\frac{\partial g_a}{\partial \mathbf{x}}(\mathbf{x}(t), \dot{\mathbf{x}}(t), \mathbf{u}(t), \dot{\mathbf{u}}(t), \mathbf{p}(t), t)\right]^T - \frac{d}{dt}\left[\frac{\partial g_a}{\partial \dot{\mathbf{x}}}(\mathbf{x}(t), \dot{\mathbf{x}}(t), \mathbf{u}(t), \dot{\mathbf{u}}(t), \mathbf{p}(t), t)\right]^T \right] \delta \mathbf{x}(t) \right.$$
$$+ \left[\left[\frac{\partial g_a}{\partial \mathbf{u}}(\mathbf{x}(t), \dot{\mathbf{x}}(t), \mathbf{u}(t), \dot{\mathbf{u}}(t), \mathbf{p}(t), t)\right]^T - \frac{d}{dt}\left[\frac{\partial g_a}{\partial \dot{\mathbf{u}}}(\mathbf{x}(t), \dot{\mathbf{x}}(t), \mathbf{u}(t), \dot{\mathbf{u}}(t), \mathbf{p}(t), t)\right]^T \right] \delta \mathbf{u}(t)$$
$$\left. + \left[\frac{\partial g_a}{\partial \mathbf{p}}(\mathbf{x}(t), \dot{\mathbf{x}}(t), \mathbf{u}(t), \dot{\mathbf{u}}(t), \mathbf{p}(t), t)\right]^T \delta \mathbf{p}(t) \right\} dt \tag{7.9}$$

Note that $\dot{\mathbf{p}}(t)$ does not appear in the foregoing relations. Using Eq. (7.5), the integral term in Eq. (7.9) can be written as

$$\int_{t_0}^{t_f} \left\{ \left[\left[\frac{\partial g}{\partial \mathbf{x}}(\mathbf{x}(t), \dot{\mathbf{x}}(t), \mathbf{u}(t), \dot{\mathbf{u}}(t), t)\right]^T + \mathbf{p}^T(t) \left[\frac{\partial \mathbf{f}}{\partial \mathbf{x}}(\mathbf{x}(t), \mathbf{u}(t), t)\right] - \frac{d}{dt}\left[-\mathbf{p}(t)\right]^T \right] \delta \mathbf{x}(t) \right.$$
$$+ \left[\left[\frac{\partial g}{\partial \mathbf{u}}(\mathbf{x}(t), \dot{\mathbf{x}}(t), \mathbf{u}(t), \dot{\mathbf{u}}(t), t)\right]^T + \mathbf{p}^T(t) \left[\frac{\partial \mathbf{f}}{\partial \mathbf{u}}(\mathbf{x}(t), \mathbf{u}(t), t)\right] \right.$$
$$\left. \left. - \frac{d}{dt}\left[\frac{\partial g}{\partial \dot{\mathbf{u}}}(\mathbf{x}(t), \dot{\mathbf{x}}(t), \mathbf{u}(t), \dot{\mathbf{u}}(t), t)\right]^T \right] \delta \mathbf{u}(t) + \left[\mathbf{f}(\mathbf{x}(t), \mathbf{u}(t), t) - \dot{\mathbf{x}}(t)\right]^T \delta \mathbf{p}(t) \right\} dt \tag{7.10}$$

Since on an extremal, regardless of the end conditions, the integral should vanish, the coefficient of each independent variation $\delta\mathbf{x}$, $\delta\mathbf{u}$ and $\delta\mathbf{p}$ must be zero. The latter yields the equations [70, 71]:

$$\dot{\mathbf{x}}(t) = \mathbf{f}(\mathbf{x}(t), \mathbf{u}(t), t) \tag{7.11a}$$
$$\dot{\mathbf{p}}(t) = -\left[\frac{\partial g}{\partial \mathbf{x}}(\mathbf{x}(t), \dot{\mathbf{x}}(t), \mathbf{u}(t), \dot{\mathbf{u}}(t), t)\right] - \left[\frac{\partial \mathbf{f}}{\partial \mathbf{x}}(\mathbf{x}(t), \mathbf{u}(t), t)\right]^T \mathbf{p}(t) \tag{7.11b}$$
$$\frac{d}{dt}\left[\frac{\partial g}{\partial \dot{\mathbf{u}}}(\mathbf{x}(t), \dot{\mathbf{x}}(t), \mathbf{u}(t), \dot{\mathbf{u}}(t), t)\right] = \left[\frac{\partial g}{\partial \mathbf{u}}(\mathbf{x}(t), \dot{\mathbf{x}}(t), \mathbf{u}(t), \dot{\mathbf{u}}(t), t)\right] + \left[\frac{\partial \mathbf{f}}{\partial \mathbf{u}}(\mathbf{x}(t), \mathbf{u}(t), t)\right]^T \mathbf{p}(t) \tag{7.11c}$$

where Eqs. (7.11a) and (7.11b) denote the state $\mathbf{x}(t)$ and co-state $\mathbf{p}(t)$ equations, respectively. Moreover, the term outside of the integral in Eq. (7.9) must also vanish. Therefore, using Eq. (7.5), we obtain

$$\left[\frac{\partial g}{\partial \dot{\mathbf{u}}}(\mathbf{x}(t_f), \dot{\mathbf{x}}(t_f), \mathbf{u}(t_f), \dot{\mathbf{u}}(t_f), t_f)\right]^T \delta \mathbf{u}_f = 0 \tag{7.12}$$

Based on Eq. (7.12), if the final control input $\mathbf{u}(t_f)$ is fixed, $\delta\mathbf{u}_f = \mathbf{0}$, while the free-end control input leads to

$$\frac{\partial g}{\partial \dot{\mathbf{u}}}(\mathbf{x}(t_f), \dot{\mathbf{x}}(t_f), \mathbf{u}(t_f), \dot{\mathbf{u}}(t_f), t_f) = \mathbf{0} \tag{7.13}$$

Next, defining the *Hamiltonian* as

$$\mathcal{H}(\mathbf{x}(t), \mathbf{u}(t), \dot{\mathbf{u}}(t), \mathbf{p}(t), t) = g(\mathbf{x}(t), \mathbf{u}(t), \dot{\mathbf{u}}(t), t) + \mathbf{p}^T(t)\mathbf{f}(\mathbf{x}(t), \mathbf{u}(t), t) \tag{7.14}$$

relations (7.11)–(7.12) can be rewritten as

$$\dot{\mathbf{x}}(t) = \frac{\partial \mathcal{H}}{\partial \mathbf{p}}(\mathbf{x}(t), \mathbf{u}(t), \dot{\mathbf{u}}(t), \mathbf{p}(t), t) \tag{7.15a}$$

$$\dot{\mathbf{p}}(t) = -\frac{\partial \mathcal{H}}{\partial \mathbf{x}}(\mathbf{x}(t), \mathbf{u}(t), \dot{\mathbf{u}}(t), \mathbf{p}(t), t) \tag{7.15b}$$

$$\frac{d}{dt}\left[\frac{\partial \mathcal{H}}{\partial \dot{\mathbf{u}}}(\mathbf{x}(t), \mathbf{u}(t), \dot{\mathbf{u}}(t), \mathbf{p}(t), t)\right] = \frac{\partial \mathcal{H}}{\partial \mathbf{u}}(\mathbf{x}(t), \mathbf{u}(t), \dot{\mathbf{u}}(t), \mathbf{p}(t), t) \tag{7.15c}$$

$$\left[\frac{\partial \mathcal{H}}{\partial \dot{\mathbf{u}}}(\mathbf{x}(t_f), \dot{\mathbf{x}}(t_f), \mathbf{u}(t_f), \dot{\mathbf{u}}(t_f), t_f)\right]^T \delta\mathbf{u}_f = 0 \tag{7.15d}$$

7.3 Modified Linear Quadratic Tracking (LQT)

This section is devoted to an important class of optimal control problems using the results of Section 7.2, i.e., the control of linear time-varying (LTV) systems applying LQT.

Consider an LTV system described by

$$\dot{\mathbf{x}}(t) = \mathbf{A}(t)\mathbf{x}(t) + \mathbf{B}(t)\mathbf{u}(t) \tag{7.16}$$

and the performance index to be minimized given as

$$J(\mathbf{u}) = \frac{1}{2}\int_{t_0}^{t_f} \left\{ [\mathbf{x}(t) - \mathbf{r}(t)]^T \mathbf{Q}(t) [\mathbf{x}(t) - \mathbf{r}(t)] + \mathbf{u}^T(t)\mathbf{R}(t)\mathbf{u}(t) + \dot{\mathbf{u}}^T(t)\mathbf{N}(t)\dot{\mathbf{u}}(t) \right\} dt \tag{7.17}$$

where $\mathbf{r}(t)$ denotes the desired value of the state vector $\mathbf{x}(t)$. As well, $\mathbf{Q}(t)$, $\mathbf{R}(t)$ and $\mathbf{N}(t)$ are the weighting matrices.

Using Eq. (7.14), the Hamiltonian is given by

$$\begin{aligned}\mathcal{H}(\mathbf{x}(t), \mathbf{u}(t), \dot{\mathbf{u}}(t), \mathbf{p}(t), t) = \frac{1}{2}\Big\{ &[\mathbf{x}(t) - \mathbf{r}(t)]^T \mathbf{Q}(t) [\mathbf{x}(t) - \mathbf{r}(t)] + \mathbf{u}^T(t)\mathbf{R}(t)\mathbf{u}(t) \\ &+ \dot{\mathbf{u}}^T(t)\mathbf{N}(t)\dot{\mathbf{u}}(t) \Big\} + \mathbf{p}^T(t)\mathbf{A}(t)\mathbf{x}(t) + \mathbf{p}^T(t)\mathbf{B}(t)\mathbf{u}(t)\end{aligned} \tag{7.18}$$

Hence, applying Eqs. (7.15a)–(7.15c), the normality conditions are

$$\dot{\mathbf{x}}(t) = \mathbf{A}(t)\mathbf{x}(t) + \mathbf{B}(t)\mathbf{u}(t) \tag{7.19a}$$

$$\dot{\mathbf{p}}(t) = -\mathbf{Q}(t)\mathbf{x}(t) - \mathbf{A}^T(t)\mathbf{p}(t) + \mathbf{Q}(t)\mathbf{r}(t) \tag{7.19b}$$

$$\frac{d}{dt}\left[\mathbf{N}(t)\dot{\mathbf{u}}(t)\right] = \mathbf{R}(t)\mathbf{u}(t) + \mathbf{B}^T(t)\mathbf{p}(t) \tag{7.19c}$$

Moreover, fixed-end control input $\mathbf{u}(t_f)$ requires $\delta\mathbf{u}_f = \mathbf{0}$, while, based on Eq. (7.15d), the free-end control input yields:

$$\mathbf{N}(t_f)\dot{\mathbf{u}}(t_f) = \mathbf{0} \tag{7.20}$$

Hence,

$$\dot{\mathbf{u}}(t_f) = \mathbf{0} \quad \text{or} \quad \dot{\mathbf{u}}(t_f) \in \mathcal{N}(\mathbf{N}(t_f)) \tag{7.21}$$

7.4 Case Study: Gear-shifting in EVs

In this section, we investigate an important application of the developed approach, i.e., gear-shifting control in MSTS for EVs.

7.4.1 Gear-shifting problem

Consider a novel modular MSTS designed for EVs, comprising two planetary gear sets, as depicted in Fig. 7.1. The output shaft is connected to the common carrier for both planetary gear sets. As well, the same input shaft is attached to the sun gears. When one of the ring gears is engaged, the corresponding gear ratio is reached. The gear-shifting problem includes disengaging the fixed ring gear, while engaging the other one.

Applying the Lagrangian method, the mathematical model of the transmission can be expressed as

$$A_0\dot{\omega}_s + B_0\dot{\omega}_c = \tau_d - c_s\omega_s - \frac{r_{s_1}}{r_{r_1}}\tau_{r_1} - \frac{r_{s_2}}{r_{r_2}}\tau_{r_2} \tag{7.22a}$$

$$B_0\dot{\omega}_s + C_0\dot{\omega}_c = \tau_l - c_c\omega_c + \frac{2r_c}{r_{r_1}}\tau_{r_1} + \frac{2r_c}{r_{r_2}}\tau_{r_2} \tag{7.22b}$$

with all the above variables defined below:

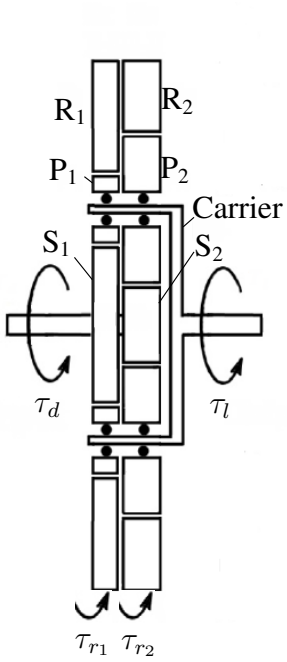

Figure 7.1: A two-speed transmission designed for EVs

A_0, B_0, C_0: generalized inertia terms;
ω_c, ω_s: angular velocities of the carrier and the sun gears;
c_c, c_s: generalized damping coefficients;
τ_d: drive torque of the electric motor applied to the input shaft;
τ_l: external load applied to the output shaft;
τ_{r_1}, τ_{r_2}: torques applied to the first and the second ring gears;
r_{s_1}, r_{s_2}, r_{r_1}, r_{r_2}: pitch radii of the sun and the ring gears of the two planetary sets;
r_c: radius of the carrier.

Let $x_1(t) = \omega_c(t)$ and $x_2(t) = \omega_s(t)$ be the states of the transmission. Under no external load applied to the output shaft, the state-space model can be written as

$$\dot{\mathbf{x}}(t) = \mathbf{A}\mathbf{x}(t) + \mathbf{B}\mathbf{u}(t) \tag{7.23}$$

where $\mathbf{u}(t) = \begin{bmatrix} \tau_{r_1}(t) & \tau_{r_2}(t) & \tau_d(t) \end{bmatrix}^T$ denotes the control input. Also, $\mathbf{A} \in \mathbb{R}^{2\times 2}$ and $\mathbf{B} \in \mathbb{R}^{2\times 3}$ are constant matrices, i.e., the system is linear time-invariant (LTI).

As an example, consider that we want to switch from the first gear ratio to the second one. For this case, at t_0, i.e., the start of gear-shifting, the first ring gear is fully engaged and the second one disengaged completely, namely,

$$\omega_{r_1}(t_0) = 0, \quad \tau_{r_2}(t_0) = 0 \tag{7.24}$$

At t_f, i.e., the end of gear-shifting, the second ring gear should be completely engaged, while the first one fully disengaged, i.e.,

$$\omega_{r_2}(t_f) = 0, \quad \tau_{r_1}(t_f) = 0 \tag{7.25}$$

Based on Eqs. (7.24) and (7.25), there are terminal conditions on the control input in the gear-shifting problem. To achieve a smooth, swift gear-shifting, constant output angular velocity $\omega_c(t)$ is required during shifting. Furthermore, to assure the angular velocity, acceleration and jerk continuity at the ends, the input angular velocity $\omega_s(t)$ must track the 3-4-5 *blending polynomial* [74], i.e.,

$$\omega_{5s}(t) = \Delta\omega \left(6\theta^5 - 15\theta^4 + 10\theta^3\right) + \omega_{s_0}, \quad \theta \equiv \frac{t - t_0}{t_f - t_0}, \quad \Delta\omega \equiv \omega_{s_f} - \omega_{s_0} \tag{7.26}$$

where $\omega_{s_0} = \omega_s(t_0)$ and $\omega_{s_f} = \omega_s(t_f)$. In fact, it can be concluded that the desired state vector is $\mathbf{r}(t) = [\omega_{c_0} \quad \omega_{5s}(t)]^T$, where ω_{c_0} is the carrier angular velocity before gear-shifting.

7.4.2 Simulation Results

The simulation results, obtained with the proposed LQT for gear-shifting in a two-speed transmission system designed for EVs, are reported in this subsection.

As discussed in Subsection 7.4.1, the desired state vector is $\mathbf{r}(t) = [\omega_{c_0} \quad \omega_{5s}(t)]^T$. Assuming $t \,\epsilon\, [0, 0.1]$, $\omega_{c_0} = 10$ rad/s, and the gear ratios are 4 and $8/3$, we have

$$\omega_s(t_0) = 40 \text{ rad/s}, \quad \omega_s(t_f) = \frac{80}{3} \text{ rad/s} \tag{7.27}$$

which leads to $\mathbf{x}_0 = \begin{bmatrix} 10 & 40 \end{bmatrix}^T$ and $\mathbf{x}_f = \begin{bmatrix} 10 & 80/3 \end{bmatrix}^T$. Also,

$$\omega_{r_1}(t_0) = 0, \quad \tau_{r_2}(t_0) = 0, \quad \omega_{r_2}(t_f) = 0, \quad \tau_{r_1}(t_f) = 0 \tag{7.28}$$

Note that, as mentioned in Section 7.2, the initial control input before gear-shifting, i.e., $\mathbf{u}(t_0) = \mathbf{u}_0$, is assumed to be specified. Thus, while finding the control input, for a seamless shift, this condition should be satisfied.

The command signals and the output values for the angular velocities of the carrier and the sun gears, as well as the angular velocities of the ring gears, are depicted in Figs. 7.2(a) and (b), respectively. According to these figures, the outputs follow the desired values quite closely; $\omega_c(t)$ remaining constant during gear-shifting, while $\omega_s(t)$, $\omega_{r_1}(t)$ and $\omega_{r_2}(t)$ following the 3-4-5 polynomial.[2] Also, at $t = t_0$ and $t = t_f$, respectively, ω_{r_1} and ω_{r_2} vanish.

[2]Note that, based on the kinematic relations, $\omega_{r_1}(t)$ and $\omega_{r_2}(t)$ also follow the 3-4-5 blending polynomial.

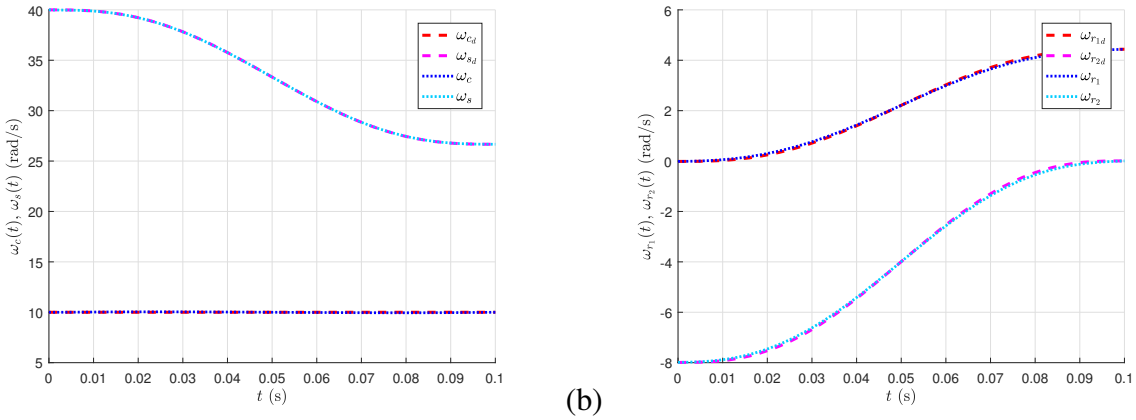

Figure 7.2: The angular velocities during gear-shifting: (a) the carrier and the sun gears; and (b) the ring gears

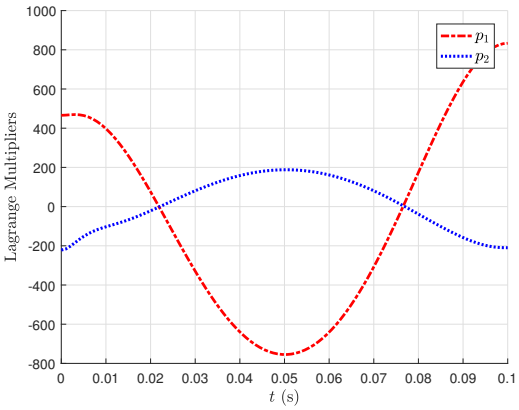

Figure 7.3: The Lagrange multipliers

The Lagrange multipliers are plotted in Fig 7.3. As well, the optimal control inputs during gear-shifting are indicated in Fig. 7.4. As observed in this figure, the torque τ_{r_2} is zero at $t = t_0$, while at $t = t_f$, the torque τ_{r_1} vanishes. Note that, as the initial control input before gear-shifting is specified, i.e., $\mathbf{u}_0 = \begin{bmatrix} 0.15 & 0 & 0.85 \end{bmatrix}^T$, this condition is satisfied. Further, since only one of the control inputs is fixed at t_f, i.e., $\tau_{r_1}(t_f) = 0$, for the terminal constraints of the other two inputs, assuming $\mathbf{N}(t_f)$ is diagonal, Eq. (7.21) leads to $\dot{\tau}_{r_2}(t_f) = 0$ and $\dot{\tau}_d(t_f) = 0$. In other words, although the control inputs change considerably during gear-shifting, all constraints are met at both ends.

To evaluate the performance of the proposed approach, an unknown external disturbance is assumed to be applied to the MSTS. The results for the states and the corresponding control inputs are depicted in Figs. 7.5(a) and (b), respectively. Simulations illustrate that our scheme provides encouraging results for the optimal control of over-actuated systems applying smooth control inputs with constraints on the initial and final values. Note that in the absence of an over-actuated system,

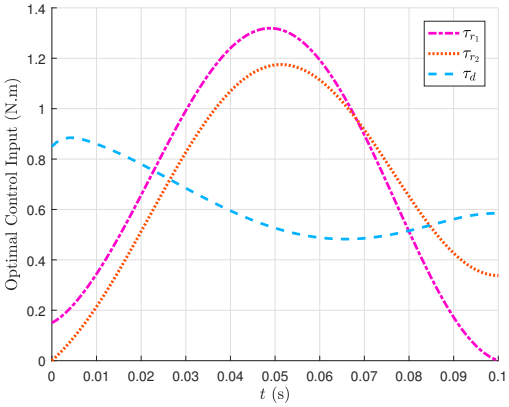

Figure 7.4: The optimal control inputs during gear-shifting

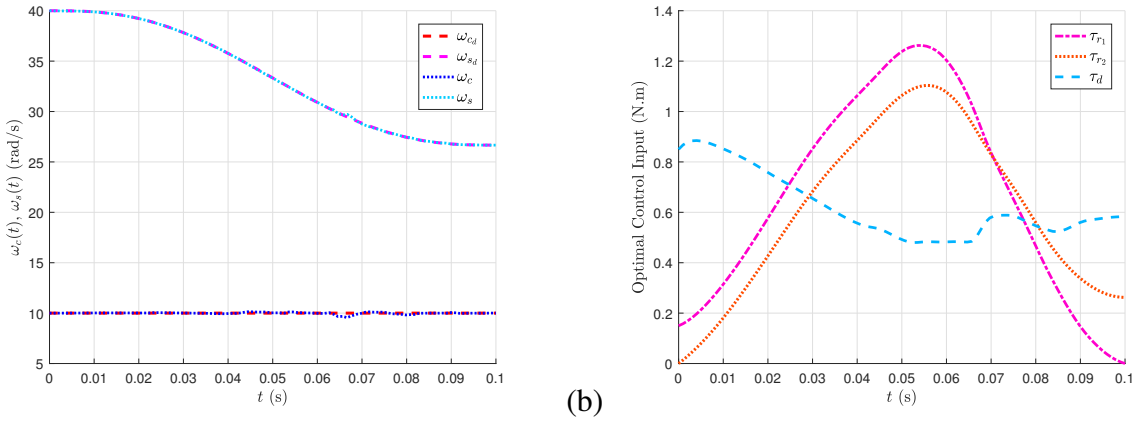

(a) (b)

Figure 7.5: The results in the presence of an external disturbance: (a) the states; and (b) the optimal control inputs

the method can still be applied, if the terminal conditions are feasible.

7.5 Conclusions

Employing a variational approach, the necessary conditions of optimality were found for the smooth optimal control of over-actuated systems, while applying boundary constraints on the control input. As well, the scheme was limited to the well-known LQT problem for LTV systems with the same end-point conditions. Afterwards, the necessary conditions were applied for optimal control of a modern over-actuated system with terminal state and control constraints, namely, the gear-shifting control in a novel MSTS for EVs. It was observed that the states followed the reference signals acceptably. Moreover, the state and control end conditions were satisfied precisely. Results demonstrate that the proposed scheme can be adopted for the seamless optimal control of over-actuated systems with

control and state boundary conditions. Future research will target the elimination of the blending trajectories, i.e., the command signals, in such optimization problems.

Chapter 8

Gear-shifting Control in Electric Vehicles with Multi-speed Transmissions via Dynamic Programming

Abstract

One way to enhance the efficiency of electric vehicles (EVs) is to apply multi-speed transmissions (MSTs), with a swift and seamless gear-shifting. A gear-shifting control scheme is proposed in this paper for a novel modular MST designed for EVs. After establishing the dynamics model of the designed MST and defining the gear-shifting problem, the proposed control methodology is formulated. From a control standpoint, the problem leads to an over-actuated system, with terminal constraints on both states and control inputs. Accordingly, a control algorithm is required, to meet all end control and state conditions, while leading to the optimum solution. To this end, Bellman's dynamic programming is applied to solve this specific optimal control problem. Simulation results are conducted for various performance indices to demonstrate the effectiveness of the proposed control approach.

8.1 Introduction

Increasing the efficiency of electric vehicles (EVs) is the motivation behind this paper, especially in light of the current limited storage capacity of batteries. One step in this direction is the application of multi-speed transmissions (MSTs) in EVs [1, 5, 6, 7]. By doing this, the desired power is transmitted in more than one way, since several gear ratios are included. Thus, by appropriate gear-shifting, a higher efficiency can be attained.

Various types of transmission systems can be used in EVs, such as automated manual transmissions (AMTs) [16, 21, 22], automatic transmissions (ATs) [10, 27, 28], dual-clutch transmissions (DCTs) [30, 37, 85], and continuously variable transmissions (CVTs) [40, 50]. These MSTs are applied in internal-combustion-engine vehicles (ICEVs). Nonetheless, since the control of the engine speed is extremely complicated in ICEVs, for a seamless shift, the engine should be disconnected from the transmission during gear-shifting, by means of a clutch or a torque converter. Conversely, as the electric motors (EMs) are speed-controllable in an extensive range, such clutches or torque converters can be omitted in MSTs designed for EVs. Indeed, for a smooth gear-shifting in EVs, the drive torque supplied by the EM can be adopted as an autonomous control input [9]. Since gear-shifting influences passenger comfort and vehicle drivability, the main objectives are smoothness, swiftness, and cancellation of output-torque interruption [58, 65, 66, 67].

There has been an intensive effort on the design, modelling, and gear-shifting control and estimation of MSTs [33]. For instance, besides finding the optimal gear-shifting instants, the optimal gear ratios and the optimal control inputs, the hybrid minimum principle was applied to achieve a certain speed in minimum time [59, 60]. Combining a PID and a robust controller, Meng et al. [86] proposed an optimal control algorithm for gear-shifting. Additionally, Rahimi et al. [76, 62, 63] estimated the unavailable states and inputs of a transmission system for EVs. The same authors established an observer-based back-stepping controller to achieve a smooth shift [64]. To enhance the gear-shifting transient response in DCTs, a new strategy was introduced by Walker et al. [36], based on the control of the engine and the clutches. Design, modelling and estimation of the unknown loads and states of a modular MST was studied using the Kalman filter, the Luenberger observer and neural networks (NNs) [81, 87]. In addition, based on blending polynomials, the optimal trajectory for gear-shifting was found, which assures velocity, acceleration and jerk continuity [74]. Applying a piecewise affine (PWA) feedback law, the engagement of a synchromesh system in a clutchless AMT for EVs was also investigated [128]. Considering the vehicle operation constraints, the optimal control of hybrid EVs during mode transition was studied, which ensures drivability [129]. A two-phase control algorithm was recently proposed for gear-shifting in MSTs for EVs [92].

The authors propose here a gear-shifting control algorithm for a novel modular MST designed for EVs. Firstly, the mathematical model of the designed MST is derived applying the Lagrange

methodology. Subsequently, after the formulation of the gear-shifting problem, the proposed control approach for a smooth, swift shift is clarified. From a control viewpoint, the transmission system under study is over-actuated, as the number of control inputs is greater than the number of states to be controlled. Additionally, there are end constrains on some control inputs and states. Accordingly, to find the optimum trajectory, while satisfying both terminal control and state constraints, a control scheme is suggested based on Bellman's dynamic programming (DP). Simulation results for different performance indices illustrate that the proposed control method is highly encouraging for gear-shifting in the designed MST, since all conditions are adequately met.

An outline of the paper follows. In Section 8.2, the dynamics model of the designed MST for EVs is established. Also, the gear-shifting problem is clearly explained in the same section. Section 8.3 is devoted to the proposed gear-shifting control algorithm based on DP. Simulation results are provided in Section 8.4.

8.2 The Proposed MST Designed for EVs

In the first subsection, applying the Lagrange approach, the dynamics model of the MST of interest is formulated. The gear-shifting problem is defined is Subsection 8.2.2.

8.2.1 Dynamics Model

In the proposed MST, designed for EVs, the sun gears are attached to the same shaft and the planetary gear sets share the same carrier, as illustrated in Fig. 8.1. The desired speed ratio is achieved by fixing the corresponding ring gear. Gear-shifting occurs upon releasing the fixed ring gear and engaging the other one. The key benefits of the designed MST are simplicity and modularity [81, 87].

With $\mathbf{q}$, T, V, L, Π and Δ indicating the vector of generalized coordinates, the kinetic energy, the potential energy, the Lagrangian, the power supplied and the dissipation function, respectively, the dynamics model is based on the equation below:

$$\frac{d}{dt}\left(\frac{\partial L}{\partial \dot{\mathbf{q}}}\right) - \frac{\partial L}{\partial \mathbf{q}} = \frac{\partial}{\partial \dot{\mathbf{q}}}\left(\Pi - \Delta\right), \quad L = T - V \tag{8.1}$$

If T_c, T_s, T_r and T_p denote the kinetic energies of the carrier, the sun, the ring and the planet gears, respectively, and n the number of planet gears in each set, then the kinetic energy of the transmission is given by

$$T = T_c + T_s + T_r + nT_p \tag{8.2}$$

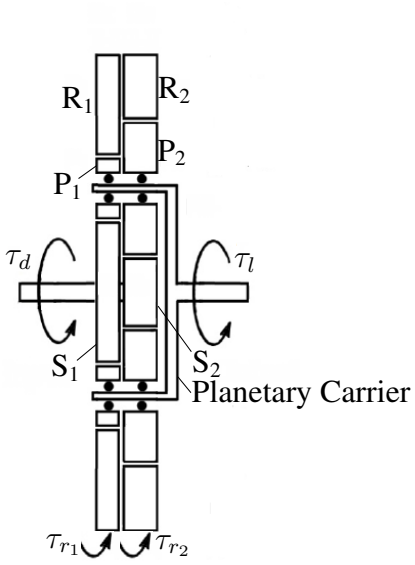

Figure 8.1: A two-stage planetary gear set designed for EVs

with

$$T_c = \frac{1}{2} I_c \omega_c^2, \quad T_s = \frac{1}{2} \left(I_{s_1} + I_{s_2} \right) \omega_s^2, \quad T_r = \frac{1}{2} I_{r_1} \omega_{r_1}^2 + \frac{1}{2} I_{r_2} \omega_{r_2}^2 \tag{8.3a}$$

$$T_p = \frac{1}{2} m_{p_1} v_{p_1}^2 + \frac{1}{2} I_{p_1} \omega_{p_1}^2 + \frac{1}{2} m_{p_2} v_{p_2}^2 + \frac{1}{2} I_{p_2} \omega_{p_2}^2, \quad v_{p_1} = v_{p_2} = r_c \omega_c \tag{8.3b}$$

where I_{s_1}, I_{s_2}, I_{r_1}, I_{r_2}, I_{p_1}, and I_{p_2} indicate the moments of inertia of the sun, the ring, and the planet gears of the first and the second gear sets, respectively, and I_c that of the carrier. Furthermore, m_{p_1}, m_{p_2}, v_{p_1} and v_{p_2} denote the masses and the speeds of the centers of mass of each planet gear. Moreover, ω_s, ω_c, ω_{r_1} and ω_{r_2} denote the angular velocities of the sun, carrier, and the first and the second ring gears, respectively, while r_c the radius of the carrier. In the ensuing derivation it is assumed that all components are statically and dynamically balanced rigid bodies. Thus, the potential energy of the system remains constant, and hence, plays no role in the model under formulation.

The power supplied to the system and the dissipation function are displayed below:

$$\Pi = \tau_d \omega_s + \tau_l \omega_c + \tau_{r_1} \omega_{r_1} + \tau_{r_2} \omega_{r_2}, \quad \Delta = \frac{1}{2} c_c \omega_c^2 + \frac{1}{2} c_s \omega_s^2 \tag{8.4}$$

with τ_d, τ_l, τ_{r_1} and τ_{r_2} denoting the drive torque applied to the input shaft by an EM, the external load applied to the output shaft, and the torques applied to the first and the second ring gears, respectively, as shown in Fig. 8.1. Additionally, c_c and c_s, including the effects of the bearings and friction, indicate the generalized damping coefficients. Substituting Eqs. (8.2)–(8.4) into Eq. (8.1),

the mathematical model of the transmission can be expressed as

$$A_0\dot{\omega}_s + B_0\dot{\omega}_c = \tau_d - c_s\omega_s - \frac{r_{s_1}}{r_{r_1}}\tau_{r_1} - \frac{r_{s_2}}{r_{r_2}}\tau_{r_2} \tag{8.5a}$$

$$B_0\dot{\omega}_s + C_0\dot{\omega}_c = \tau_l - c_c\omega_c + \frac{2r_c}{r_{r_1}}\tau_{r_1} + \frac{2r_c}{r_{r_2}}\tau_{r_2} \tag{8.5b}$$

where

$$A_0 = I_{s_1} + I_{s_2} + \left(\frac{r_{s_1}}{r_{r_1}}\right)^2 I_{r_1} + \left(\frac{r_{s_2}}{r_{r_2}}\right)^2 I_{r_2} + n\left(\left(\frac{r_{s_1}}{r_{p_1}}\right)^2 I_{p_1} + \left(\frac{r_{s_2}}{r_{p_2}}\right)^2 I_{p_2}\right) \tag{8.6a}$$

$$B_0 = -4r_c\left(\frac{r_{s_1}}{r_{r_1}^2}I_{r_1} + \frac{r_{s_2}}{r_{r_2}^2}I_{r_2}\right) - 2nr_c\left(\frac{r_{s_1}}{r_{p_1}^2}I_{p_1} + \frac{r_{s_2}}{r_{p_2}^2}I_{p_2}\right) \tag{8.6b}$$

$$C_0 = I_c + 4r_c^2\left(\frac{I_{r_1}}{r_{r_1}^2} + \frac{I_{r_2}}{r_{r_2}^2}\right) + nr_c^2\left(m_{p_1} + m_{p_2} + \frac{I_{p_1}}{r_{p_1}^2} + \frac{I_{p_2}}{r_{p_2}^2}\right) \tag{8.6c}$$

with r_{s_1}, r_{s_2}, r_{r_1}, r_{r_2}, r_{p_1} and r_{p_2} indicating the pitch radius of the sun, the ring, and the planet gears of the planetary sets.

8.2.2 Gear-shifting Problem

If $x_1(t) = \omega_c(t)$ and $x_2(t) = \omega_s(t)$ indicate the states, based on Eqs. (8.5) with no external load, the state-space equations take the form

$$\dot{\mathbf{x}}(t) = \mathbf{A}\mathbf{x}(t) + \mathbf{B}\mathbf{u}(t) \tag{8.7}$$

where $\mathbf{u}(t) = \begin{bmatrix}\tau_{r_1}(t) & \tau_{r_2}(t) & \tau_d(t)\end{bmatrix}^T$ denotes the control input. The entries of $\mathbf{A} \in \mathbb{R}^{2\times 2}$ and $\mathbf{B} \in \mathbb{R}^{2\times 3}$ depend on the system parameters in Eqs. (8.5) and (8.6), such as the damping coefficients, the radii of the components and the generalized inertia terms. As an example, in the case of switching from the first gear ratio to the second one, at the beginning ($t = t_0$) and the end ($t = t_f$) of gear-shifting we have

$$\omega_{r_1}(t_0) = 0, \quad \tau_{r_2}(t_0) = 0, \quad \omega_{r_2}(t_f) = 0, \quad \tau_{r_1}(t_f) = 0 \tag{8.8}$$

which means that at $t = t_0$, the first ring gear is engaged and the second one released, while at the end, it is the other way around.

Note that, based on Eqs. (8.8), there are initial and final constraints on some control inputs. Moreover, the system is over-actuated; there are only two states to be controlled, while three control

inputs. These properties make the gear-shifting problem complicated. A control algorithm for gear-shifting is developed in Section 8.3.

8.3 Gear-shifting Control Scheme

This section is devoted to the proposed gear-shifting control method in the designed MST based on DP. In the first subsection an outline of DP is provided for quick reference. Applying DP for gear-shifting in multi-speed EVs is discussed in Subsection 8.3.2.

8.3.1 Dynamic Programming

In this subsection, the fundamentals of DP, as introduced by R. E. Bellman in the late 1950s [102], is briefly described. DP can be employed to solve an extensive range of optimal control problems, including nonlinear and/or time-varying systems.

Bellman's DP is based on the *principle of optimality*, namely,

> *An optimal policy has the property that no matter what the previous decisions were, the remaining decisions must constitute an optimal policy with regard to the current state obtained from those previous decisions.*

Based on the above-mentioned principle, any portion of an optimal trajectory is optimum. Hence, DP implies that the optimal control inputs can be found backward-in-time, from the final stage. The main advantage of DP is reducing the number of required calculations dramatically, as the number of decisions at each stage is restricted. In other words, instead of trying all admissible trajectories leading from each state to the final state and selecting the one with the lowest cost, which is an exhaustive and time-consuming search, the principle of optimality is applied in DP. In fact, for the N-stage process, DP involves $N^2/2 + N$ additions, while the direct enumeration requires $(N-1)N!/((N/2)!(N/2)!)$ additions. For instance, for $N = 20$, DP requires only 220 additions, while enumeration involves more than three million additions. Another advantage of DP is applying constraints on the control inputs and state variables readily.

Consider a nonlinear system

$$\mathbf{x}_{k+1} = \mathbf{f}_k(\mathbf{x}_k, \mathbf{u}_k),\ k = i, i+1, ..., N-1 \tag{8.9}$$

which implies that $[i, N]$ is the interval of interest. Let us assume that the performance index is

$$J_i(\mathbf{x}_i) = \phi(N, \mathbf{x}_N) + \sum_{k=i}^{N-1} L_k(\mathbf{x}_k, \mathbf{u}_k) \tag{8.10}$$

The problem consists now in finding the optimal control inputs $\mathbf{u}_{k_i}^{N-1}$ which minimize the performance index (8.10) subject to constraints (8.9), based on the principle of optimality.

Assume that $J_{k+1}^*(\mathbf{x}_{k+1})$ indicates the optimal cost from stage $k+1$ to the final stage N for all possible states $\mathbf{x}_{k+1}$. This optimal cost is obtained when the optimal control inputs $\mathbf{u}_{k+1}^*$, $\mathbf{u}_{k+2}^*$, ..., $\mathbf{u}_{N-1}^*$ are applied to the system with the state $\mathbf{x}_{k+1}$. Now, by applying an arbitrary control $\mathbf{u}_k$ at stage k, the new cost can be written as

$$J_k(\mathbf{x}_k) = L_k(\mathbf{x}_k, \mathbf{u}_k) + J_{k+1}^*(\mathbf{x}_{k+1}) \tag{8.11}$$

Based on Bellman's principle of optimality, the optimal cost from stage k can be expressed as

$$J_k^*(\mathbf{x}_k) = \min_{\mathbf{u}_k}(L_k(\mathbf{x}_k, \mathbf{u}_k) + J_{k+1}^*(\mathbf{x}_{k+1})) \tag{8.12}$$

which is called the functional equation of DP. In other words, the optimal control input $\mathbf{u}_k^*$ at the kth stage is the control input $\mathbf{u}_k$ that minimizes the performance index (8.12). This equation can be used for implementation of DP while moving backward from the final stage.

Note that, in using DP, additional constraints and/or limits can be applied on the states and control inputs. Therefore, in implementing DP, all values must satisfy the constraints and stay within the admissible region. The main advantages of DP are summarized below.

- The solution found by DP is the global minimum, as the functional equation (8.12) is solved using a direct search. Since, instead of trying all admissible control inputs, the ones that satisfy the principle of optimality are considered, the direct search is feasible by DP.
- DP leads to the optimal control inputs in a closed-loop form, i.e., the optimal inputs are known for all admissible states. Hence, even if we deviate from the optimal trajectory, the new optimal path from the current state to the target can be readily determined.
- The number of calculations required to find the optimal control policy is reduced significantly, since DP employs the principle of optimality [70, 130].

8.3.2 The Control Algorithm Using DP

As mentioned in Subsection 8.2.2, for switching from the first to the second gear ratio, at the beginning and at the end of gear-shifting, the conditions

$$\omega_{r_1}(t_0) = 0, \quad \tau_{r_2}(t_0) = 0, \quad \omega_{r_2}(t_f) = 0, \quad \tau_{r_1}(t_f) = 0 \tag{8.13}$$

must be satisfied, which represent initial and final constraints on both the states and the control inputs. Approximating $\dot{\mathbf{x}}(t_{k+1}) \approx (\mathbf{x}_{k+1} - \mathbf{x}_k) \,/\, T$, where T indicates the sampling time, the discrete-time

state-space model of Eq. (8.7) is given by

$$\mathbf{x}_{k+1} = \mathbf{F}_k \mathbf{x}_k + \mathbf{G}_k \mathbf{u}_k \tag{8.14}$$

with $\mathbf{F}_k = \mathbf{1} + T\mathbf{A}$ and $\mathbf{G}_k = T\mathbf{B}$, where $\mathbf{1}$ denotes the identity matrix. Hence, assuming the process has N stages ($k = 0, 1, ..., N-1$), the conditions (8.13) change to

$$\omega_{r_1}(0) = 0, \quad \tau_{r_2}(0) = 0, \quad \omega_{r_2}(N) = 0, \quad \tau_{r_1}(N-1) = 0 \tag{8.15}$$

For a smooth shift, during gear-shifting, the output angular velocity ω_c should remain constant—$\omega_c(k) = \omega_{c_0}$, where ω_{c_0} denotes the output angular velocity before gear-shifting. Hence, assuming that the desired final value of ω_s is ω_{s_f}, the performance index is defined as[1]

$$\begin{aligned} J = c_1(k)(\omega_s(N) - \omega_{s_f})^2 + \sum_{k=0}^{N-1} \big[& c_2(k)(\omega_c(k) - \omega_{c_0})^2 \\ & + (\mathbf{x}_{k+1} - \mathbf{x}_k)^T \mathbf{C}_3(k)(\mathbf{x}_{k+1} - \mathbf{x}_k) + (\mathbf{u}_{k+1} - \mathbf{u}_k)^T \mathbf{C}_4(k)(\mathbf{u}_{k+1} - \mathbf{u}_k) \big] \end{aligned} \tag{8.16}$$

where the last two terms indicate the degree of smoothness of the states and the inputs during shifting, with the weighting matrices $\mathbf{C}_3(k)$ and $\mathbf{C}_4(k)$ assumed symmetric and positive definite. Similarly, $c_1(k) > 0$ and $c_2(k) > 0$ denote the weighting numbers for the first two terms in J.

Additionally, the input angular velocity ω_s should stay within its admissible region in all stages, i.e., assuming its initial value is ω_{s_0}, with $\omega_{s_f} < \omega_{s_0}$, the condition $\omega_{s_f} < \omega_s(k) < \omega_{s_0}$ must be met during gear-shifting. Note that, due to the limitations of the power supply, there are limitations on the control inputs, too.

Eventually, the problem consists in finding the control inputs $\mathbf{u}_k$ that minimize the performance index (8.16) subject to constraints (8.14), with the conditions below:[2]

$$\omega_s(0) = \omega_{s_0}, \quad \tau_{r_2}(0) = 0, \quad \tau_{r_1}(N-1) = 0, \quad \omega_{s_f} < \omega_s(k) < \omega_{s_0} \tag{8.17}$$

while the control inputs must stay within the predefined limits.

8.4 Simulation Results

Simulation results obtained with the foregoing scheme are reported in this section.

Assuming $t \in [0, 0.1]$, $N = 10$ (a ten-stage process)[3] and $\omega_{c_0} = 10$ rad/s, while the gear ratios are 4 and $8/3$, we have

[1] Note that if $\omega_c(N) = \omega_{c_0}$ and $\omega_s(N) = \omega_{s_f}$, then $\omega_{r_2}(N) = 0$, based on kinematic relations.

[2] Note that, based on the kinematic relations, if $\omega_c(0) = \omega_{c_0}$ and $\omega_s(0) = \omega_{s_0}$, then $\omega_{r_1}(0) = 0$.

[3] This is just an example to show that the algorithm works. In fact, depending on the control objectives and the precision required, the time interval and the number of stages can be changed.

$$\omega_s(0) = 40 \text{ rad/s}, \quad \omega_s(10) = \frac{80}{3} \text{ rad/s} \tag{8.18}$$

Hence, based on Eq. (8.17),

$$\omega_s(0) = 40 \text{ rad/s}, \quad \tau_{r_2}(0) = 0, \quad \tau_{r_1}(9) = 0, \quad \frac{80}{3} \text{ rad/s} < \omega_s(k) < 40 \text{ rad/s} \tag{8.19}$$

As well, the limits of the control inputs are assumed to be

$$0.4 \text{ N.m} < \tau_d(k) < 0.9 \text{ N.m}, \quad 0 < \tau_{r_1}(k) < 1.5 \text{ N.m}, \quad 0 < \tau_{r_2}(k) < 1.5 \text{ N.m} \tag{8.20}$$

In order to end up with a feasible number of computations, the number of calculations must be limited. Thus, the admissible state and control values must be quantized when implementing DP. However, to achieve more precise results at a relatively low computational cost, the admissible state and control values should be quantized into small intervals. Depending on the weighting numbers and matrices in the performance index (8.16), the optimum solution can vary. As the first example, suppose that the objective is to have smoother changes in the angular velocities rather than control inputs, i.e., the Frobenius norm of $\mathbf{C}_3(k)$ is greater than that of $\mathbf{C}_4(k)$. For this case, the optimum results using DP are illustrated in Figs. 8.2 and 8.3. The angular velocities of the input and output shafts, ω_s and ω_c, are indicated in Fig. 8.2(a), while the angular velocities of the ring gears, ω_{r_1} and ω_{r_2}, are represented in Fig. 8.2(b). As expected, the output angular velocity does not change during gear-shifting. As well, the initial and final conditions on ω_s are satisfied. Furthermore, at $t = t_0$, the first ring gear is fixed, i.e., ω_{r_1} is zero, while at the end, ω_{r_2} is zero, i.e., the second ring gear is fixed. Note that the angular velocities change remarkably smoothly.

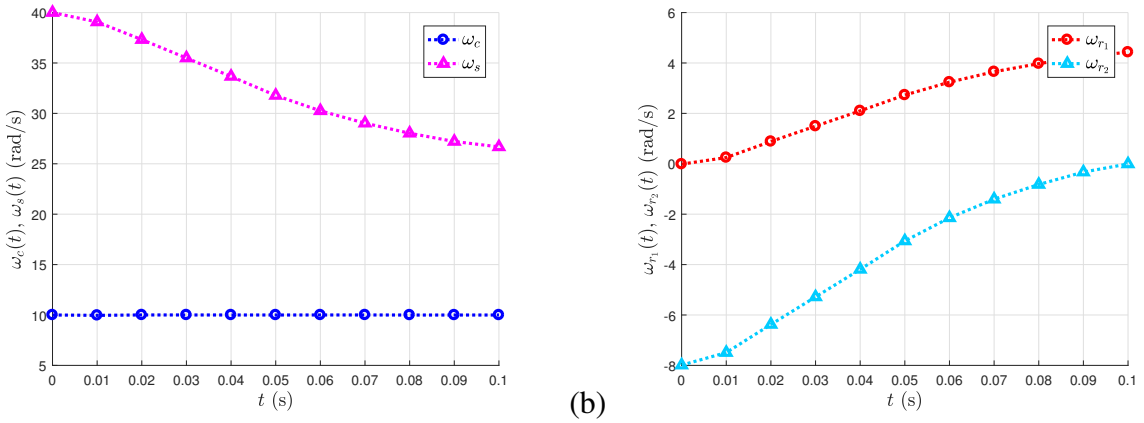

(a) (b)

Figure 8.2: Ex. 1. The smooth changes of the angular velocities during gear-shifting: (a) the input and output shafts; and (b) the ring gears

The optimal control inputs obtained during gear-shifting are depicted in Fig. 8.3. As represented in the figure, in the first stage, $\tau_{r_2} = 0$, i.e., the second planetary gear set is completely disengaged, while in the last stage, the first planetary gear set is completely released, i.e., $\tau_{r_1} = 0$. Note that all input values remain within their limits during gear-shifting.

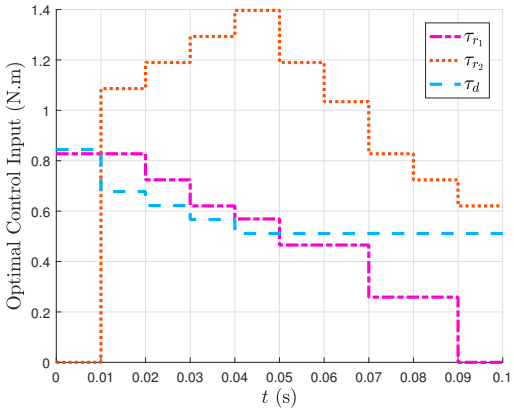

Figure 8.3: Ex. 1. The control inputs during gear-shifting for smooth changes of the states

As a second example, assume that the Frobenius norm of $\mathbf{C}_4(k)$ is greater than that of $\mathbf{C}_3(k)$, i.e., smoother control inputs are desired. As indicated in the results shown in Figs. 8.4 and **??**, the control inputs change more smoothly compared to the previous example. Note that, as in the first example, all terminal conditions are met. Besides, the angular velocities and the control inputs vary within their predefined bounds. However, as expected, the angular velocities do not change as smoothly as in the previous example.

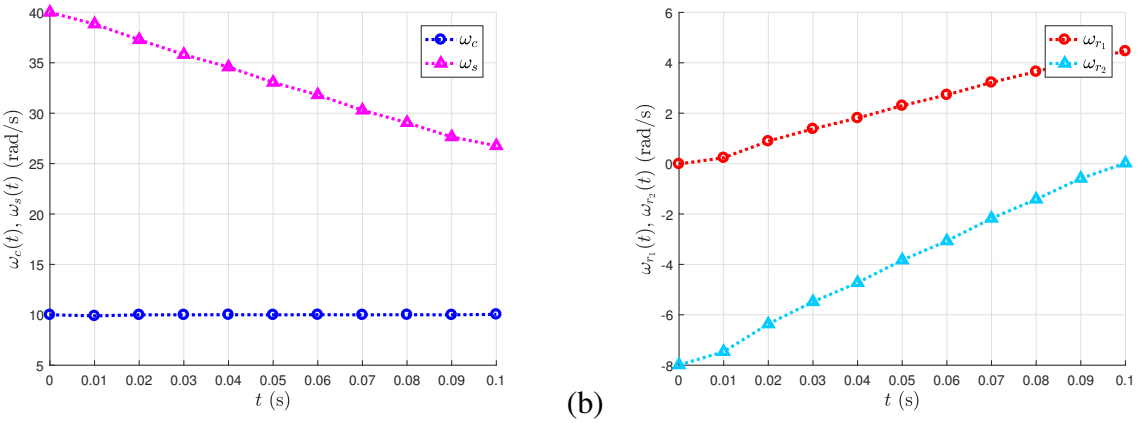

(a) (b)

Figure 8.4: Ex. 2. The angular velocities while applying smoother inputs: (a) the input and output shafts; and (b) the ring gears

Simulation results illustrate that the proposed scheme is quite promising for gear-shifting control in MSTs for EVs, which is an over-actuated system with terminal constraints on the states and

control inputs. In fact, depending on the control objectives, various performance indices with different weighting numbers/matrices can be defined to solve the optimization problem and find the optimal control inputs.

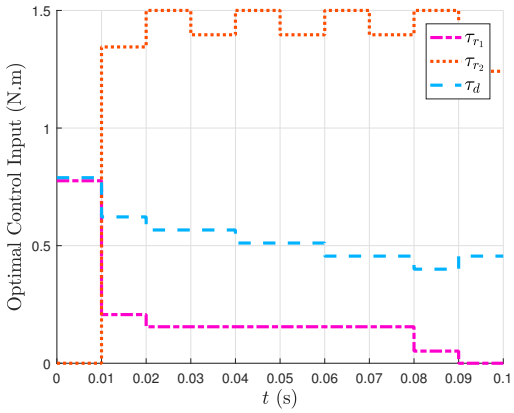

Figure 8.5: Ex. 2. The smoother control inputs during gear-shifting

8.5 Conclusions

Application of MSTs, with a smooth and swift gear-shifting, can lead to improved efficiency in EVs. Based on the dynamics model developed, a gear-shifting control methodology was established for the proposed modular MST designed for EVs. From a control viewpoint, besides having an over-actuated system, the problem includes end-constraints on some of the control inputs and states. Consequently, to find the optimal control inputs, while satisfying terminal control and state constraints, Bellman's DP was invoked. Simulation results for different performance indices, defined according to the control objectives, verify the performance of the proposed control scheme, as all initial and final conditions on the controls and states were appropriately met. Further, the states and the control inputs remained within their predefined limits.

Chapter 9

Closing Remarks

Because of the problems with ICEVs, mainly pollution, we need to find a proper substitute. HEVs and EVs, with a much lower impact on the environment, appear as appropriate substitutes for ICEVs. Nonetheless, due to the current limited storage-capacity of electric batteries, it is required to improve the efficiency of EVs. One step in this direction, adopting MSTs in EVs and developing suitable control algorithms for gear-shifting, is reported here. In this way, the EM can operate in the high-efficiency region for longer periods, given that a multi-speed EM can transmit the desired power to the wheels through various gear ratios and, therefore, enhance the efficiency of EVs via proper gear-shifting.

Various kinds of MSTs can be applied in EVs, such as AMTs, ATs, DCTs and CVTs, which were initially designed for ICEVs. However, compared to ICEVs, EMs are controllable in an extensive range of speed and torque. Accordingly, it is not required to disconnect the EM from the MST during gear-shifting. In fact, to make smooth gear-shifting feasible, the torque applied by the EM can be employed as an independent control input in MSTs designed for EVs. Since gear-shifting affects passenger comfort, efficiency and vehicle drivability, the main objectives are seamlessness, swiftness and continuous output-torque, which were given due attention. This study focused on establishing several algorithms for gear-shifting in the proposed MST for EVs, with the advantages of simplicity and modularity, while developing the appropriate controllers to adequately meet the shifting targets. The summary of the results and the main conclusions of this research work are included in Section 9.1. Section 9.2 includes recommendations for future work.

9.1 Results and Conclusions

The mathematical model of the proposed MST was established using a Lagrangian formulation. Next, based on the process and measurement models, the Kalman-filter, the Luenberger observer and neural networks were utilized for the estimation of the states, the unknown arbitrary disturbance and the unknown clutch torque applied to the MST. To assess the estimation algorithms, different disturbances were applied to the transmission, such as linear, parabolic, sinusoidal, and arbitrary. Results showed that the Kalman filter outperforms the two other methods. In fact, since the Kalman filter is based on a mathematical model, not the case of neural networks, it is more effective. Further, compared to the Luenberger observer, the Kalman filter considers the covariance of the noise of both the process and the measurement models. Also, according to the error covariance, the Kalman gain is updated during the estimation, while the Luenberger gain remains constant.

Considering the optimum performance under functional constraints, the gear-shifting in the proposed transmission was investigated. Firstly, based on the kinematic relations, the gear-shifting problem was stated in the space of angular velocities. Next, employing variational calculus and polynomial transition functions to find the optimum trajectory, the schedules of the angular velocities during gear-shifting were determined, for a swift, smooth operation. After comparing the results obtained with the suggested functions, 2-3, 3-4-5 and 4-5-6-7 polynomials, while considering the limits on the power supply, it was concluded that the 3-4-5 polynomial offers the optimum performance. In a 3-4-5 polynomial, the continuity of the angular velocity, acceleration and jerk are guaranteed. Based on the inverse dynamics of the system, the corresponding input torques of the EM and the clutches were also found.

From a control standpoint, in the gear-shifting problem, the number of control inputs is greater than the number of outputs, thereby leading to an over-actuated system. Besides, conditions on the end values of some control inputs and states are imposed. Consequently, to meet all terminal control and state constraints, while following the desired trajectory to ensure swiftness and seamlessness, several control algorithms were developed for this specific problem.

The first proposed scheme includes the approaching phase and the coasting phase. In the former, the goal is to shift the gears without engaging the free clutch; in the latter, the free clutch starts engaging. Using trial-and-error and genetic algorithms, various PID controllers were tuned and compared to find the appropriate control inputs for each phase of the proposed gear-shifting algorithm. Depending on the phase and the gear ratio values, a supervisory controller was applied to choose the suitable PID gains, i.e., PID gain-scheduling. Due to the motor limitations, in order to implement the schedule on a physical prototype, saturation was included for the control inputs. Results showed that the genetic algorithm scheme led to a controller with both a much shorter shifting time and a better performance in the presence of unknown external disturbances. Further,

the desired trajectories were tracked plausibly, while all end-point conditions were satisfied.

In the second method, to guarantee velocity, acceleration and jerk continuity while meeting the input terminal constraints, one input was suggested to be changed autonomously, based on a 2-3 blending polynomial. Subsequently, the new fully-actuated system was controlled using an LQI controller, an extension of the LQR for tracking problems. Some parameters, such as the mass of the vehicle, the vehicle speed, the forces between road and tires, the road slope and the aerodynamic drag force, affect considerably the size of the EMs employed and the ranges of power and torque applied in a real EV. Accordingly, to evaluate the performance of the proposed algorithm and include the effects of all parameters mentioned above, unknown external disturbances and external loads were assumed to be applied to the MST during gear-shifting. Compared to the first approach, this strategy was less sophisticated for implementation on a real MST. Besides, the inputs changed more seamlessly than when the first method was used.

In addition to the first two algorithms, two different novel, non-standard optimal control problems were formulated to find the continuous, seamless optimal control effort for this specific over-actuated system, with end control and state constraints. In fact, compared to classical approaches, which only include end-time and state conditions in formulating optimal control problems, in our proposed schemes, besides the seamlessness and continuity of the control inputs in the given time interval, one can apply a set of soft or hard boundary conditions on the controls too. In other words, in finding the necessary conditions for optimality, in the first approach, a modified terminal penalty term consisting of the terminal control input was included in defining a general Lagrange variational problem. In the second approach, however, the time-derivative of the control input was included in the functional. The results were narrowed to find control allocation in an over-actuated LQT problem for LTV systems, applicable to the gear-shifting problem in MSTs for EVs. Nonetheless, the results can be applied to various optimal control problems with initial and final control and/or state constraints, where the smoothness of the system operation is required over extended periods. If the constraints at the ends are reasonable and a solution exists, the proposed schemes can also be used for either fully-actuated systems or in the presence of external disturbances.

Finally, Bellman's DP and the principle of optimality were adopted to solve this specific optimal control problem. Indeed, to find the optimum trajectory for the states, while meeting both control and state boundary conditions, a control method was proposed based on DP. The solution found this way is the global minimum, as the functional equation is solved using a direct search. Since, instead of trying all admissible control inputs, the ones that satisfy the principle of optimality are considered, the direct search is feasible for DP. This way, the computational complexity required to find the optimal control policy was also reduced significantly. Furthermore, DP leads to the optimal control inputs in a closed-loop form, i.e., the optimal inputs are known for all admissible states. Hence, even if we deviate from the optimal trajectory, the new optimal path from the current state to the target

can be readily determined. To find the optimal state trajectory and control input using DP, depending on the control objectives, various performance indices with different weights can be defined.

9.2 Future Work

Based on the current study, several recommendations for future research are mentioned below.

- A more detailed, realistic mathematical model of the proposed transmission designed for EVs should be derived. In other words, in the model derivation, one should consider all the nonlinearities, energy sinks and flexibility, i.e., stiffness and dissipation, of all components, including gears, planet-carrier and shafts. That is, Coulomb and viscous friction between different elements of the transmission in contact and bearings should be considered.

- For estimation of the unavailable states, the unknown external disturbances and the unknown inputs applied to the transmission system, assuming a nonlinear model, the model-based extended Kalman filter (EKF) should be employed. In fact, EKF is an extension of the Kalman filter for nonlinear systems, which, compared to other algorithms, provides much better results with the least errors. Moreover, for comparison of the results, adaptive approaches based on the steepest-descent and heuristic fuzzy logic systems should be adopted.

- In order to develop a more comprehensive gear-shifting control algorithm that can readily be implemented on a physical EV, the dynamics models of all elements and actuators of the transmission system, including the clutches and the EMs, should be considered in designing/tuning controllers.

- Depending on the market feedback and the customer's need, after implementation of the proposed gear-shifting algorithms on a real EV, various performance indices should be considered in defining the optimization problems and finding the optimum trajectory of the angular velocities for gear-shifting.

- To overcome uncertainty, noise and disturbances, adaptive schemes, such as a model-reference adaptive controller (MRAC) or a model predictive controller (MPC), robust H_∞ controllers, and nonlinear controllers, e.g., different versions of sliding-mode controllers, should be employed for gear-shifting.

- New gear-shifting algorithms should be established based on optimal control where, instead of tracking a predefined blending trajectory, the optimum state trajectory and control input are determined directly, while considering the gear-shifting objectives and satisfying the boundary conditions.

- To evaluate the performance of all the proposed gear-shifting algorithms, these algorithms should be implemented on a physical EV. This way, the schemes can be tested and modified in the real world.

Appendix

As per Section 1.4, when formulating the gear-shifting control algorithms in EVs, the clutches are considered *active*. In other words, regardless of the angular velocity direction, they are capable of applying the required torques in either directions. As an example, a mechanism for such operation is described below.

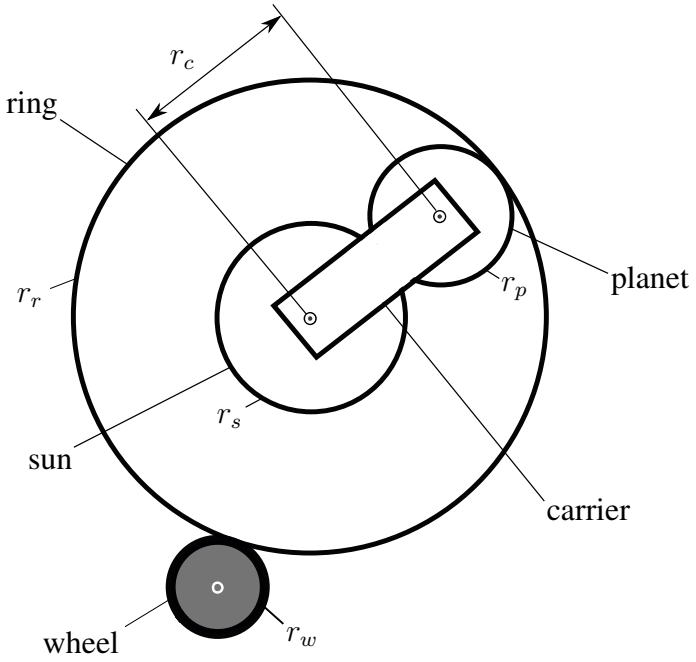

A: The mechanism for applying active torques

In the proposed mechanism, a metal wheel surrounded by rubber, to provide high friction, is employed to control the motion of the ring gear, as illustrated in Fig. A. As shown in the figure, the wheel connected to the motor shaft is in direct contact with the ring gear. By activating the EM, as an independent control input, the required torque can be applied to the ring gear in both directions.

However, the speed and torque ratios depend on the radii of the ring gear and the wheel, i.e., r_r and r_w. In other words, assuming that ω_r and ω_w indicate the angular velocities of the ring gear and the wheel, respectively, and τ_r and τ_w denote the corresponding torques, we have

$$\frac{\omega_r}{\omega_w} = \frac{\tau_w}{\tau_r} = \frac{r_w}{r_r}$$

A similar mechanism can be developed for this operation where the wheel is replaced by a gear installed on the motor shaft to drive the ring gear. Note that, in this case, the ring gear must have teeth on the outer surface as well [131, 132].

On the other hand, a passive clutch applies a dissipative force. In fact, the torque of a passive clutch can only be applied in the opposite direction of the ring gear angular velocity, i.e.,

$$\begin{aligned}\tau_{r_1} &= -|\tau_{r_1}|\text{sgn}(\omega_{r_1}), \quad \text{for } \omega_{r_1} \neq 0\\ \tau_{r_2} &= -|\tau_{r_2}|\text{sgn}(\omega_{r_2}), \quad \text{for } \omega_{r_2} \neq 0\end{aligned}$$

where $\text{sgn}(\cdot)$ denotes the sign function. For passive clutches, the dynamics model of the transmission system can be expressed as

$$\begin{aligned}A_0\dot{\omega}_c(t) + B_0\dot{\omega}_s(t) &= \tau_d - c_s\omega_s + \left(\frac{r_{s_1}}{r_{r_1}}\right)|\tau_{r_1}|\text{sgn}(\omega_{r_1}) + \left(\frac{r_{s_2}}{r_{r_2}}\right)|\tau_{r_2}|\text{sgn}(\omega_{r_2})\\ C_0\dot{\omega}_c(t) + D_0\dot{\omega}_s(t) &= \tau_l - c_c\omega_c - \left(\frac{2r_c}{r_{r_1}}\right)|\tau_{r_1}|\text{sgn}(\omega_{r_1}) - \left(\frac{2r_c}{r_{r_2}}\right)|\tau_{r_2}|\text{sgn}(\omega_{r_2})\end{aligned}$$

As an example, assuming $\omega_{c_0} = 10$ rad/s, for switching from the second to the first gear ratio, at the beginning,

$$\omega_{r_1}(t_0) = 40/9\ \text{rad/s}, \quad \omega_{r_2}(t_0) = 0, \quad \tau_{r_1}(t_0) = 0$$

while at the end,

$$\omega_{r_1}(t_f) = 0, \quad \omega_{r_2}(t_f) = -8\ \text{rad/s}, \quad \tau_{r_2}(t_f) = 0$$

Hence, during gear-shifting $\omega_{r_1} \geq 0$ and $\omega_{r_2} \leq 0$, which implies that $\tau_{r_1} \leq 0$ and $\tau_{r_2} \geq 0$. At the beginning of the gear-shifting, the second clutch is engaged. According to Subsection 3.4.1, if this clutch is released based on a 2-3 blending polynomial, the continuity of the angular velocity, acceleration and jerk are guaranteed, while the control terminal conditions are also met. The other two inputs can be found by solving the inverse dynamics or using a proper controller. The results are represented in Fig. B.

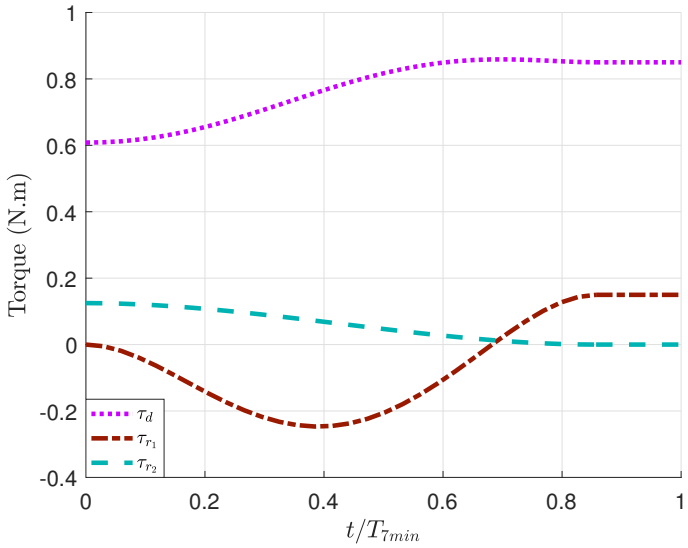

B: The input torques during gear-shifting using passive clutches

As indicated in Fig. B, the second clutch is disengaged using a 2-3 polynomial, while satisfying $\tau_{r_2} \geq 0$. The first clutch also engages while meeting $\tau_{r_1} \leq 0$ until τ_{r_2} is zero. When the second clutch is released and $\omega_{r_1} = 0$, the direction of the torque applied by this clutch changes, since the first ring gear tends to rotate in the negative direction although its angular velocity is zero. Note that an engaged clutch always applies a torque to resist the motion of the ring gear, even if its angular velocity is zero.

Bibliography

[1] P. D. Walker, S. A. Rahman, B. Zhu, and N. Zhang, "Modelling, simulations, and optimisation of electric vehicles for analysis of transmission ratio selection," *Advances in Mechanical Engineering*, vol. 5, pp. 340435–340448, jan 2015.

[2] T. Holdstock, A. Sorniotti, M. Everitt, M. Fracchia, S. Bologna, and S. Bertolotto, "Energy consumption analysis of a novel four-speed dual motor drivetrain for electric vehicles," in *Vehicle Power and Propulsion Conference (VPPC), 2012 IEEE*, pp. 295–300, IEEE, 2012.

[3] A. Sorniotti, S. Subramanyan, A. Turner, C. Cavallino, F. Viotto, and S. Bertolotto, "Selection of the optimal gearbox layout for an electric vehicle," *SAE International Journal of Engines*, vol. 4, no. 2011-01-0946, pp. 1267–1280, 2011.

[4] Q. Ren, D. A. Crolla, and A. Morris, "Effect of transmission design on electric vehicle (ev) performance," in *2009 IEEE Vehicle Power and Propulsion Conference*, pp. 1260–1265, Sept 2009.

[5] X. Zhou, P. Walker, N. Zhang, B. Zhu, and J. Ruan, "Numerical and experimental investigation of drag torque in a two-speed dual clutch transmission," *Mechanism and Machine Theory*, vol. 79, pp. 46–63, sep 2014.

[6] B. Gao, Q. Liang, Y. Xiang, L. Guo, and H. Chen, "Gear ratio optimization and shift control of 2-speed i-AMT in electric vehicle," *Mechanical Systems and Signal Processing*, vol. 50-51, pp. 615–631, jan 2015.

[7] M. S. R. Mousavi, A. Pakniyat, T. Wang, and B. Boulet, "Seamless dual brake transmission for electric vehicles: Design, control and experiment," *Mechanism and Machine Theory*, vol. 94, pp. 96–118, dec 2015.

[8] M. S. Rahimi Mousavi *et al.*, "Modeling, simulation and control of a seamless two-speed automated transmission for electric vehicles," in *American Control Conference (ACC)*, pp. 3826–3831, IEEE, 2014.

[9] M. S. R. Mousavi, A. Pakniyat, and B. Boulet, "Dynamic modeling and controller design for a seamless two-speed transmission for electric vehicles," in *Control Applications (CCA), 2014 IEEE Conference on*, pp. 635–640, IEEE, 2014.

[10] H. Naunheimer, B. Bertsche, J. Ryborz, and W. Novak, *Automotive transmissions: fundamentals, selection, design and application*. Springer Science & Business Media, 2010.

[11] J. Ruan, P. D. Walker, J. Wu, N. Zhang, and B. Zhang, "Development of continuously variable transmission and multi-speed dual-clutch transmission for pure electric vehicle," *Advances in Mechanical Engineering*, vol. 10, no. 2, pp. 1–15, 2018.

[12] G. Lucente, M. Montanari, and C. Rossi, "Modelling of an automated manual transmission system," *Mechatronics*, vol. 17, pp. 73–91, mar 2007.

[13] A. Ge, H. Jin, and Y. Lei, "Engine constant speed control in starting and shifting process of automated mechanical transmission (AMT)," in *FISITA World Automotive Congress, Seoul*, 2000.

[14] J. Zhang, L. Chen, and G. Xi, "System dynamic modelling and adaptive optimal control for automatic clutch engagement of vehicles," *Proceedings of the Institution of Mechanical Engineers, Part D: Journal of Automobile Engineering*, vol. 216, pp. 983–991, jan 2002.

[15] R. Heath and A. Child, "Zeroshift automated manual transmission (AMT)," *SAE paper*, no. 2007-26-061, 2007.

[16] L. Miao, X. Cheng, Z. Liu, X. Li, and X. Liu, "Optimal control of gearshift in automatic mechanical transmission," in *2015 International Conference on Automation, Mechanical Control and Computational Engineering*, Atlantis Press, 2015.

[17] C.-H. Yu, C.-Y. Tseng, and C.-P. Wang, "Smooth gear-change control for EV clutchless automatic manual transmission," in *2012 IEEE/ASME International Conference on Advanced Intelligent Mechatronics (AIM)*, jul 2012.

[18] X. Zhu, H. Zhang, J. Xi, J. Wang, and Z. Fang, "Optimal speed synchronization control for clutchless AMT systems in electric vehicles with preview actions," in *American Control Conference*, IEEE, jun 2014.

[19] A. Sorniotti, G. L. Pilone, F. Viotto, S. Bertolotto, M. Everitt, R. Barnes, and I. Morrish, "A novel seamless 2-Speed transmission system for electric vehicles: Principles and simulation results," *SAE International Journal of Engines*, vol. 4, pp. 2671–2685, jun 2011.

[20] Q. Liang, B. Z. Gao, and H. Chen, "Gear shifting control for pure electric vehicle with inverse-AMT," *AMM*, vol. 190-191, pp. 1286–1289, jul 2012.

[21] B. Gao, Y. Xiang, H. Chen, Q. Liang, and L. Guo, "Optimal trajectory planning of motor torque and clutch slip speed for gear shift of a two-speed electric vehicle," *J. Dyn. Sys., Meas., Control*, vol. 137, p. 061016, feb 2015.

[22] G. Wu and Z. Dong, "Design, analysis and modeling of a novel hybrid powertrain system based on hybridized automated manual transmission," *Mechanical Systems and Signal Processing*, vol. 93, pp. 688 – 705, 2017.

[23] L. Li, K. He, X. Wang, and Y. Liu, "Sensor fault-tolerant control for gear-shifting engaging process of automated manual transmission," *Mechanical Systems and Signal Processing*, vol. 99, pp. 790 – 804, 2018.

[24] J. Liang, H. Yang, J. Wu, N. Zhang, and P. D. Walker, "Power-on shifting in dual input clutchless power-shifting transmission for electric vehicles," *Mechanism and Machine Theory*, vol. 121, pp. 487 – 501, 2018.

[25] G.-H. Jung, B.-H. Cho, and K.-I. Lee, "Dynamic analysis and closed-loop shifting control of ef-automatic transmission with proportional control solenoid valves," in *FISITA World Automotive Congress, Seoul, Korea*, pp. 12–15, 2000.

[26] A. Haj-Fraj and F. Pfeiffer, "Dynamic modeling and analysis of automatic transmissions," in *Advanced Intelligent Mechatronics, 1999. Proceedings. 1999 IEEE/ASME International Conference on*, pp. 1026–1031, IEEE, 1999.

[27] C. Lazar, C. F. Caruntu, and A. E. Balau, "Modelling and predictive control of an electro-hydraulic actuated wet clutch for automatic transmission," in *Industrial Electronics (ISIE), 2010 IEEE International Symposium on*, pp. 256–261, IEEE, 2010.

[28] H. A. Asl, N. L. Azad, and J. McPhee, "Modeling torque converter characteristics in automatic drivelines: lock-up clutch and engine braking simulation," in *ASME 2012 International Design Engineering Technical Conferences and Computers and Information in Engineering Conference*, pp. 359–367, 2012.

[29] M. Kulkarni, T. Shim, and Y. Zhang, "Shift dynamics and control of dual-clutch transmissions," *Mechanism and Machine Theory*, vol. 42, pp. 168–182, feb 2007.

[30] E. Galvagno, M. Velardocchia, and A. Vigliani, "Dynamic and kinematic model of a dual clutch transmission," *Mechanism and Machine Theory*, vol. 46, pp. 794–805, jun 2011.

[31] Y. Zhang, X. Chen, X. Zhang, H. Jiang, and W. Tobler, "Dynamic modeling and simulation of a dual-clutch automated lay-shaft transmission," *Journal of Mechanical Design*, vol. 127, no. 2, pp. 302–307, 2005.

[32] M. Goetz, M. Levesley, and D. Crolla, "Integrated powertrain control of gearshifts on twin clutch transmissions," tech. rep., SAE Technical Paper, 2004.

[33] M. Goetz, M. C. Levesley, and D. A. Crolla, "Dynamics and control of gearshifts on twin-clutch transmissions," *Proceedings of the Institution of Mechanical Engineers, Part D: Journal of Automobile Engineering*, vol. 219, pp. 951–963, jan 2005.

[34] Y. Liu, D. Qin, H. Jiang, and Y. Zhang, "A systematic model for dynamics and control of dual clutch transmissions," *Journal of Mechanical Design*, vol. 131, no. 6, p. 061012, 2009.

[35] R. Ahlawat, H. K. Fathy, B. Lee, J. L. Stein, and D. Jung, "Modelling and simulation of a dual-clutch transmission vehicle to analyse the effect of pump selection on fuel economy," *Vehicle System Dynamics*, vol. 48, pp. 851–868, jul 2010.

[36] P. D. Walker, N. Zhang, and R. Tamba, "Control of gear shifts in dual clutch transmission powertrains," *Mechanical Systems and Signal Processing*, vol. 25, pp. 1923–1936, aug 2011.

[37] B. Zhu, N. Zhang, P. Walker, W. Zhan, X. Zhou, and J. Ruan, "Two-speed DCT electric powertrain shifting control and rig testing," *Advances in Mechanical Engineering*, vol. 5, pp. 323917–323927, jan 2015.

[38] M. Golkani, M. Steinberger, M. Bachinger, J. Rumetshofer, M. Stolz, and M. Horn, "Optimal gear shift strategy for dual clutch transmissions," *IFAC-PapersOnLine*, vol. 50, no. 1, pp. 4800 – 4805, 2017. 20th IFAC World Congress.

[39] S. Kim and S. Choi, "Control-oriented modeling and torque estimations for vehicle driveline with dual-clutch transmission," *Mechanism and Machine Theory*, vol. 121, pp. 633 – 649, 2018.

[40] N. Srivastava and I. Haque, "A review on belt and chain continuously variable transmissions (CVT): Dynamics and control," *Mechanism and Machine Theory*, vol. 44, pp. 19–41, jan 2009.

[41] G. Carbone, L. Mangialardi, B. Bonsen, C. Tursi, and P. Veenhuizen, "CVT dynamics: Theory and experiments," *Mechanism and Machine Theory*, vol. 42, pp. 409–428, apr 2007.

[42] G. Carbone, L. Mangialardi, and G. Mantriota, "The influence of pulley deformations on the shifting mechanism of metal belt CVT," *Journal of Mechanical Design*, vol. 127, no. 1, pp. 103–113, 2005.

[43] K. Narita and M. Priest, "Metal-metal friction characteristics and the transmission efficiency of a metal v-belt-type continuously variable transmission," *Proceedings of the Institution of Mechanical Engineers, Part J: Journal of Engineering Tribology*, vol. 221, pp. 11–26, jan 2007.

[44] N. Srivastava and I. Haque, "Transient dynamics of the metal v-belt CVT: Effects of pulley flexibility and friction characteristic," *Journal of Computational and Nonlinear Dynamics*, vol. 2, no. 1, pp. 86–97, 2007.

[45] N. Srivastava and I. Haque, "Transient dynamics of metal v-belt CVT: Effects of band pack slip and friction characteristic," *Mechanism and Machine Theory*, vol. 43, pp. 459–479, apr 2008.

[46] N. Srivastava and I. Haque, "Clearance and friction-induced dynamics of chain CVT drives," *Multibody System Dynamics*, vol. 19, pp. 255–280, jul 2007.

[47] N. Srivastava and I. U. Haque, "Dynamics of chain cvt drives: effects of friction characteristic," in *ASME 2007 International Design Engineering Technical Conferences and Computers and Information in Engineering Conference*, pp. 1089–1097, American Society of Mechanical Engineers, 2007.

[48] N. Srivastava, Y. Miao, and I. U. Haque, "Influence of clearance on the dynamics of chain cvt drives," in *ASME 2006 International Mechanical Engineering Congress and Exposition*, pp. 163–175, American Society of Mechanical Engineers, 2006.

[49] N. Srivastava and I. Haque, "Influence of friction characteristic on the performance of chain cvt drives," *Journal of KONES Powertrain and Transport*, vol. 13, no. 2, pp. 405–419, 2006.

[50] N. Srivastava and I. Haque, "Nonlinear dynamics of a friction-limited drive: Application to a chain continuously variable transmission (CVT) system," *Journal of Sound and Vibration*, vol. 321, pp. 319–341, mar 2009.

[51] A. Yildiz, A. Piccininni, F. Bottiglione, and G. Carbone, "Modeling chain continuously variable transmission for direct implementation in transmission control," *Mechanism and Machine Theory*, vol. 105, pp. 428 – 440, 2016.

[52] B. Bonsen, R. Pulles, S. Simons, M. Steinbuch, and P. Veenhuizen, "Implementation of a slip controlled cvt in a production vehicle," in *Control Applications, 2005. CCA 2005. Proceedings of 2005 IEEE Conference on*, pp. 1212–1217, IEEE, 2005.

[53] B. Bonsen, T. Klaassen, R. Pulles, S. Simons, M. Steinbuch, and P. Veenhuizen, "Performance optimisation of the push-belt cvt by variator slip control," *International journal of vehicle design*, vol. 39, no. 3, pp. 232–256, 2005.

[54] W. Ryu, J. Nam, Y. Lee, and H. Kim, "Model based control for a pressure control type cvt," *International Journal of Vehicle Design*, vol. 39, no. 3, pp. 175–188, 2005.

[55] M. Pesgens, B. Vroemen, B. Stouten, F. Veldpaus, and M. Steinbuch, "Control of a hydraulically actuated continuously variable transmission," *Vehicle System Dynamics*, vol. 44, no. 5, pp. 387–406, 2006.

[56] K. Adachi, Y. Ochi, and K. Kanai, "Development of cvt control system and its use for fuel-efficient operation of engine," *Asian journal of control*, vol. 8, no. 3, pp. 219–226, 2006.

[57] M. A. Fernandes, "Fuzzy controller applied to electric vehicles with continuously variable transmission," *Neurocomputing*, vol. 214, pp. 684–691, 2016.

[58] N. Zhang, A. Crowther, D. Liu, and J. Jeyakumaran, "A finite element method for the dynamic analysis of automatic transmission gear shifting with a four-degree-of-freedom planetary gearset element," *Proceedings of the Institution of Mechanical Engineers, Part D: Journal of Automobile Engineering*, vol. 217, no. 6, pp. 461–473, 2003.

[59] A. Pakniyat and P. E. Caines, "Time optimal hybrid minimum principle and the gear changing problem for electric vehicles," *IFAC-PapersOnLine*, vol. 48, no. 27, pp. 187–192, 2015.

[60] A. Pakniyat and P. E. Caines, "The gear selection problem for electric vehicles: An optimal control formulation.," in *ICARCV*, pp. 1261–1266, 2014.

[61] M. S. Rahimi Mousavi and B. Boulet, "Dynamical modeling and optimal state estimation using kalman-bucy filter for a seamless two-speed transmission for electric vehicles," in *Control and Automation (MED), 2015 23th Mediterranean Conference on*, pp. 76–81, IEEE, 2015.

[62] M. S. R. Mousavi and B. Boulet, "Estimation of the state variables and unknown input of a two-speed electric vehicle driveline using fading-memory Kalman filter," *IEEE Transactions on Transportation Electrification*, pp. 1–11, 2016.

[63] H. V. Alizadeh, M. Mousavi, and B. Boulet, "Synchromesh torque estimation in an electric vehicle's clutchless automated manual transmission using unknown input observer," in *Vehicle Power and Propulsion Conference (VPPC), 2015 IEEE*, pp. 1–5, IEEE, 2015.

[64] M. S. R. Mousavi, A. Pakniyat, M. K. Helwa, and B. Boulet, "Observer-based backstepping controller design for gear shift control of a seamless clutchless two-speed transmission for electric vehicles," in *Vehicle Power and Propulsion Conference (VPPC), 2015 IEEE*, pp. 1–6, IEEE, 2015.

[65] A. Sorniotti, T. Holdstock, G. L. Pilone, F. Viotto, S. Bertolotto, M. Everitt, R. J. Barnes, B. Stubbs, and M. Westby, "Analysis and simulation of the gearshift methodology for a novel two-speed transmission system for electric powertrains with a central motor," *Proceedings of the Institution of Mechanical Engineers, Part D: Journal of Automobile Engineering*, pp. 915–929, 2012.

[66] S. Hong, S. Ahn, B. Kim, H. Lee, and H. Kim, "Shift control of a 2-speed dual clutch transmission for electric vehicle," in *Vehicle Power and Propulsion Conference (VPPC), 2012 IEEE*, pp. 1202–1205, IEEE, 2012.

[67] J. Xu, X. Xu, X. Su, and X. Guo, "Design of automatic shifting controller for electric vehicle with five speed transmission," in *Strategic Technology (IFOST), 2013 8th International Forum on*, vol. 1, pp. 294–297, IEEE, 2013.

[68] S. Kim, J. Oh, and S. Choi, "Gear shift control of a dual-clutch transmission using optimal control allocation," *Mechanism and Machine Theory*, vol. 113, no. Supplement C, pp. 109 – 125, 2017.

[69] G. Li and D. Görges, "Optimal control of the gear shifting process for shift smoothness in dual-clutch transmissions," *Mechanical Systems and Signal Processing*, vol. 103, pp. 23 – 38, 2018.

[70] D. E. Kirk, *Optimal control theory: an introduction*. Courier Corporation, 2012.

[71] D. S. Naidu, *Optimal control systems*. CRC press, 2002.

[72] G. Tao, M. Wu, and F. Meng, "Online performance evaluation of a heavy-duty automatic transmission launching process," *Mechatronics*, vol. 38, pp. 143–150, 2016.

[73] P. Walker, B. Zhu, and N. Zhang, "Powertrain dynamics and control of a two speed dual clutch transmission for electric vehicles," *Mechanical Systems and Signal Processing*, vol. 85, pp. 1–15, 2017.

[74] M. Roozegar and J. Angeles, "The optimal gear-shifting for a multi-speed transmission system for electric vehicles," *Mechanism and Machine Theory*, vol. 116, pp. 1 – 13, 2017.

[75] Y.-H. Liu, T. Li, Y.-Y. Yang, X.-W. Ji, and J. Wu, "Estimation of tire-road friction coefficient based on combined APF-IEKF and iteration algorithm," *Mechanical Systems and Signal Processing*, vol. 88, pp. 25–35, 2017.

[76] M. S. R. Mousavi, H. V. Alizadeh, and B. Boulet, "Estimation of synchromesh frictional torque and output torque in a clutchless automated manual transmission of a parallel hybrid electric vehicle," *IEEE Transactions on Vehicular Technology*, vol. 66, pp. 5531–5539, July 2017.

[77] J. J. Oh, S. B. Choi, and J. Kim, "Driveline modeling and estimation of individual clutch torque during gear shifts for dual clutch transmission," *Mechatronics*, vol. 24, no. 5, pp. 449–463, 2014.

[78] R. Rajamani, *Vehicle Dynamics and Control*. Springer US, 2012.

[79] R. Andrzejewski and J. Awrejcewicz, *Nonlinear Dynamics of a Wheeled Vehicle*. Springer-Verlag, 2005.

[80] D. E. Rumelhart and J. L. McClelland, *Learning Internal Representations by Error Propagation*, pp. 318–362. MIT Press, 1987.

[81] M. Roozegar, Y. Setiawan, and J. Angeles, "Design, modelling and estimation of a novel modular multi-speed transmission system for electric vehicles," *Mechatronics*, vol. 45, pp. 119 – 129, 2017.

[82] J. Angeles, *Fundamentals of Robotic Mechanical Systems*. Springer International Publishing, 2014.

[83] A. Gasparetto and V. Zanotto, "A technique for time-jerk optimal planning of robot trajectories," *Robotics and Computer-Integrated Manufacturing*, vol. 24, pp. 415–426, jun 2008.

[84] J. Angeles, A. Alivizatos, and P. Zsombor-Murray, "The synthesis of smooth trajectories for pick-and-place operations," *IEEE Transactions on Systems, Man, and Cybernetics*, vol. 18, no. 1, pp. 173–178, 1988.

[85] Z. Zhao, L. He, Y. Yang, C. Wu, X. Li, and J. K. Hedrick, "Estimation of torque transmitted by clutch during shifting process for dry dual clutch transmission," *Mechanical Systems and Signal Processing*, vol. 75, pp. 413–433, jun 2016.

[86] F. Meng, G. Tao, T. Zhang, Y. Hu, and P. Geng, "Optimal shifting control strategy in inertia phase of an automatic transmission for automotive applications," *Mechanical Systems and Signal Processing*, vol. 60-61, pp. 742–752, aug 2015.

[87] Y. D. Setiawan, M. Roozegar, T. Zou, and J. Angeles, "A mathematical model of multi-speed transmissions in electric vehicles in the presence of gear-shifting," *IEEE Transactions on Vehicular Technology*, vol. PP, no. 99, pp. 1–13, 2017.

[88] M. Roozegar and M. J. Mahjoob, "Modelling and control of a non-holonomic pendulum-driven spherical robot moving on an inclined plane: simulation and experimental results," *IET Control Theory & Applications*, vol. 11, no. 4, pp. 541–549, 2016.

[89] J. H. Holland, *Adaptation in natural and artificial systems: an introductory analysis with applications to biology, control, and artificial intelligence*. MIT press, 1992.

[90] M. Mitchell, *An introduction to genetic algorithms*. MIT press, 1998.

[91] C.-T. Chen, *Linear system theory and design*. Oxford University Press, Inc., 1995.

[92] M. Roozegar and J. Angeles, "A two-phase control algorithm for gear-shifting in a novel multi-speed transmission for electric vehicles," *Mechanical Systems and Signal Processing*, vol. 104, pp. 145 – 154, 2018.

[93] P. C. Young and J. C. Willems, "An approach to the linear multivariable servomechanism problem†," *International Journal of Control*, vol. 15, no. 5, pp. 961–979, 1972.

[94] D. Luong and T. C. Tsao, "Linear quadratic integral control of an organic rankine cycle for waste heat recovery in heavy-duty diesel powertrain," in *2014 American Control Conference*, pp. 3147–3152, June 2014.

[95] Y. Ebihara, T. Hagiwara, and M. Araki, "Sequential tuning methods of LQ/LQI controllers for multivariable systems and their application to hot strip mills," *International Journal of Control*, vol. 73, no. 15, pp. 1392–1404, 2000.

[96] M. Roozegar and J. Angeles, "Gear-shifting in a novel modular multi-speed transmission for electric vehicles using linear quadratic integral control," *Mechanism and Machine Theory*, vol. 128, pp. 359–367, 2018.

[97] M. Giaquinta and S. Hildebrandt, *Calculus of Variations I*, vol. 310. Springer Science & Business Media, 2013.

[98] M. Giaquinta and S. Hildebrandt, *Calculus of variations II*, vol. 311. Springer Science & Business Media, 2013.

[99] A. E. Bryson and Y.-C. Ho, *Applied optimal control: optimization, estimation and control*. CRC Press, 1975.

[100] M. Athans and P. L. Falb, *Optimal control: an introduction to the theory and its applications*. Courier Corporation, 2013.

[101] L. D. Berkovitz, *Optimal control theory*, vol. 12. Springer Science & Business Media, 2013.

[102] R. Bellman, *Dynamic programming*. Courier Corporation, 2013.

[103] E. B. Lee and L. Markus, "Foundations of Optimal Control Theory," tech. rep., Minnesota Univ Minneapolis Center for Control Sciences, 1967.

[104] H. J. Sussmann, "A Nonsmooth Hybrid Maximum Principle," in *Stability and Stabilization of Nonlinear Systems* (D. Aeyels, F. Lamnabhi-Lagarrigue, and A. van der Schaft, eds.), pp. 325–354, Springer London, 1999.

[105] R. Vinter, *Optimal control*. Springer Science & Business Media, 2010.

[106] F. Taringoo and P. E. Caines, "On the Optimal Control of Impulsive Hybrid Systems on Riemannian Manifolds," *SIAM Journal on Control and Optimization*, vol. 51, no. 4, pp. 3127–3153, 2013.

[107] S. Dharmatti and M. Ramaswamy, "Hybrid Control Systems and Viscosity Solutions," *SIAM Journal on Control and Optimization*, vol. 44, no. 4, pp. 1259–1288, 2005.

[108] A. Pakniyat and P. E. Caines, "On the Relation between the Minimum Principle and Dynamic Programming for Classical and Hybrid Control Systems," *IEEE Transactions on Automatic Control*, vol. 62, no. 9, pp. 4347–4362, 2017.

[109] A. Pakniyat and P. E. Caines, "Hybrid Optimal Control of an Electric Vehicle with a Dual-Planetary Transmission," *Nonlinear Analysis: Hybrid Systems*, vol. 25, pp. 263–282, 2017.

[110] P. Pisu and G. Rizzoni, "A comparative study of supervisory control strategies for hybrid electric vehicles," *IEEE Transactions on Control Systems Technology*, vol. 15, no. 3, pp. 506–518, 2007.

[111] F. R. Salmasi, "Control strategies for hybrid electric vehicles: Evolution, classification, comparison, and future trends," *IEEE Transactions on vehicular technology*, vol. 56, no. 5, pp. 2393–2404, 2007.

[112] J. Gao, F. Sun, H. He, G. G. Zhu, and E. G. Strangas, "A comparative study of supervisory control strategies for a series hybrid electric vehicle," in *Power and Energy Engineering Conference, 2009. APPEEC 2009. Asia-Pacific*, pp. 1–7, IEEE, 2009.

[113] J. A. Saglia, N. G. Tsagarakis, J. S. Dai, and D. G. Caldwell, "A high-performance redundantly actuated parallel mechanism for ankle rehabilitation," *The International Journal of Robotics Research*, vol. 28, no. 9, pp. 1216–1227, 2009.

[114] J. Zhou, L. Fiorentini, M. Canova, and A. Serrani, "Dynamic steady-state allocation for over-actuated turbocharged diesel engines," in *Decision and Control (CDC), 2013 IEEE 52nd Annual Conference on*, pp. 6843–6848, IEEE, 2013.

[115] D. Costantinescu and E. Croft, "Smooth and time-optimal trajectory planning for industrial manipulators along specified paths," *Journal of robotic systems*, vol. 17, no. 5, pp. 233–249, 2000.

[116] N. Takagi, M. Oya, T. Kobayashi, and Q. Wang, "Adaptive control scheme achieving smooth control input in the presence of input saturation," *International Journal of Advanced Mechatronic Systems*, vol. 2, no. 4, pp. 225–235, 2010.

[117] K. Tanaka, M. Iwasaki, and H. O. Wang, "Switching control of an r/c hovercraft: stabilization and smooth switching," *IEEE Transactions on Systems, Man, and Cybernetics, Part B (Cybernetics)*, vol. 31, no. 6, pp. 853–863, 2001.

[118] B. Lu, Y. Fang, and N. Sun, "A new sliding-mode like nonlinear controller for overhead cranes with smooth control inputs," in *American Control Conference (ACC)*, pp. 252–257, IEEE, 2016.

[119] A. K. Naskar, S. Patra, and S. Sen, "New control allocation algorithms in fixed point framework for overactuated systems with actuator saturation," *International Journal of Control*, vol. 90, no. 2, pp. 348–356, 2017.

[120] O. Härkegård and S. T. Glad, "Resolving actuator redundancy—optimal control vs. control allocation," *Automatica*, vol. 41, no. 1, pp. 137–144, 2005.

[121] L. Zaccarian, "Dynamic allocation for input redundant control systems," *Automatica*, vol. 45, no. 6, pp. 1431–1438, 2009.

[122] M. Chen and B. Jiang, "Adaptive control and constrained control allocation for overactuated ocean surface vessels," *International Journal of Systems Science*, vol. 44, no. 12, pp. 2295–2309, 2013.

[123] S. M. Roberts and J. S. Shipman, *Two-point boundary value problems: shooting methods*. New York, American Elsevier Pub. Co., 1972.

[124] M. Roozegar, J. Angeles, and H. Michalska, "Optimal control problems with terminal control constraints and over-actuation," in *American Control Conference (ACC) 2018*, pp. 4129–4134, IEEE Proceedings, 2018.

[125] A. Casavola and E. Garone, "Fault-tolerant adaptive control allocation schemes for over-actuated systems," *International Journal of Robust and Nonlinear Control*, vol. 20, no. 17, pp. 1958–1980, 2010.

[126] S. Tohidi, A. Khaki Sedigh, and D. Buzorgnia, "Fault tolerant control design using adaptive control allocation based on the pseudo inverse along the null space," *International Journal of Robust and Nonlinear Control*, vol. 26, no. 16, pp. 3541–3557, 2016.

[127] J. J. Oh, J. S. Eo, and S. B. Choi, "Torque observer-based control of self-energizing clutch actuator for dual clutch transmission," *IEEE Transactions on Control Systems Technology*, vol. 25, no. 5, pp. 1856–1864, 2017.

[128] H. V. Alizadeh, M. K. Helwa, and B. Boulet, "Modeling, analysis and constrained control of wet cone clutch systems: A synchromesh case study," *Mechatronics*, vol. 49, pp. 92–104, 2018.

[129] G. Wu, X. Zhang, and Z. Dong, "Optimal control for ensured drivability of paralell hevs/phevs during mode transition," tech. rep., SAE Technical Paper, 2014.

[130] F. L. Lewis, D. Vrabie, and V. L. Syrmos, *Optimal control*. John Wiley & Sons, 2012.

[131] N. Sclater and N. P. Chironis, *Mechanisms and mechanical devices sourcebook*. McGraw-Hill New York, 2007.

[132] R. L. Norton, *Design of machinery: an introduction to the synthesis and analysis of mechanisms and machines*. McGraw-Hill Boston, 2008.